FORMULATION AND DELIVERY OF DRUGS FOR MACULAR EDEMA AND RETINOBLASTOMA; SYNTHESIS AND *IN VITRO* CHARACTERIZATION OF DOXORUBICIN LOADED SURFACE MODIFIED NANOPARTICLES USING PLGA-PEG-FOL POLYMER

A DISSERTATION IN

Pharmaceutical Science
and
Chemistry

Presented to the faculty of the University
of Missouri-Kansas City in partial fulfillment of
the requirements for the degree

DOCTOR OF PHILOSOPHY

by
SAI HANUMAN SAGAR BODDU,

M. Pharm. University of Pune, 2005

Kansas City, Missouri
2010

FORMULATION AND DELIVERY OF DRUGS FOR MACULAR EDEMA AND RETINOBLASTOMA; SYNTHESIS AND *IN-VITRO* CHARACTERIZATION OF DOXORUBICIN LOADED SURFACE MODIFIED NANOPARTICLES USING PLGA-PEG-FOL POLYMER

Sai H.S. Boddu, Candidate for the Doctor of Philosophy Degree

University of Missouri-Kansas City, 2010

ABSTRACT

Macular edema (ME) is caused by central extravascular swelling of the macula resulting in a significant loss of visual activity. Corticosteroids are widely used in the treatment of ME. In this project, nanoparticles of dexamethasone (DEX), hydrocortisone acetate (HA) and prednisolone acetate (PA) were developed and characterized for size, shape, polydispersity, and *in vitro* release. Further the effect of PLGA-PEG-PLGA thermosensitive gel on the release mechanisms of steroids from PLGA nanoparticles was also studied. Release from nanoparticles suspended in thermosensitive gels followed zero-order kinetics with no apparent burst effect. *Ex vivo* permeability studies further confirmed sustained release of DEX from nanoparticles suspended in thermosensitive gels. Retinoblastoma (RB) represents a common form of intraocular malignancy affecting the retina. Recent work has explored the systemic/intravitreal administration of topotecan, etoposide, carboplatin and vincristine for the treatment of RB. However, the current therapy is associated with non-specific toxicity and patient non-compliance. An attempt was made to develop and evaluate a novel folate receptor targeted and sustained

drug delivery system for RB cells using doxorubicin (DOX) as a model drug. Uptake of DOX was approximately four times higher with DOX-loaded PLGA-PEG-FOL micelles (DOXM) than DOX in Y-79 cells over-expressing folate receptors. Dispersion of DOXM in PLGA-PEG-PLGA gel sustained drug release over a period of two weeks.

Nanoparticles are colloidal particulate systems widely employed in targeted delivery of drugs to cancer cells. In this project, a novel strategy was proposed for the synthesis of folate conjugated nanoparticles for both hydrophilic and hydrophobic drug molecules using PLGA-PEG-FOL polymer. Nanoparticles were evaluated for the entrapment efficiency, morphology, particle size and *in vitro* release. Presence of folate on the nanoparticle surface was confirmed by using ^{1}HNMR and TEM studies. Quantitative uptake and cell viability studies were carried out in folate receptor-positive ovarian cancer (SKOV3) cells. Folate conjugated nanoparticles (size ~200 nm) were successfully prepared using single (O/W) and double emulsion (W/O/W) methods. Folate conjugated nanoparticles exhibited higher uptake and cytotoxicity in SKOV3 cells in comparison with the pure DOX and unmodified nanoparticles.

The faculty listed below, appointed by the Dean of School of Graduate Studies, have examined a dissertation titled, "Formulation and Delivery of Drugs for Macular Edema and Retinoblastoma; Synthesis and *In Vitro* Characterization of Doxorubicin Loaded Surface Modified Nanoparticles Using PLGA-PEG-FOL Polymer" presented by Sai Hanuman Sagar Boddu, candidate for the Doctor of Philosophy degree, and certify that in their opinion it is worthy of acceptance.

Supervisory Committee

Ashim K. Mitra, Ph.D.
School of Pharmacy

Bi-Botti C. Youan, Ph.D.
School of Pharmacy

Kun Cheng, Ph.D.
School of Pharmacy

David Van Horn, Ph.D.
Department of Chemistry

Andrew J. Holder, Ph.D.
Department of Chemistry

Marcus Iszard, Ph.D.
Division of Pharmacology

CONTENTS

ILLUSTRATIONS

Figure Page

TABLES

Table Page

ACKNOWLEDGEMENTS

My sincere acknowledgment goes to my advisor Dr. Ashim K. Mitra who has been very influential in ensuring my academic and professional well being ever since I joined the PhD program. He is a great mentor, whose constructive feedback and unfailing support always motivated me to excel in my research. I am also thankful to Drs. Youan, Cheng, Van Horn, Holder and Iszard for serving on my supervisory committee and for their encouragement and timely support. It's a great honor to have such outstanding researchers in the committee. Their constructive feedback at various levels has significantly helped me in shaping my dissertion up to completion.

I am very thankful to Dr. Dhananjay Pal for his timely professional and emotional support during various stages of my PhD. His kind words have always been a source of strength to hold on to. I owe a big thanks to Mrs. Ranjana Mitra for her cheerful encouragement and help throughout my stay at UMKC. It is my pleasure to extend my gratitude to Drs. Janoira and Gunda for their constant support, time, and scientific input into my research. Thanks are due to Ravi Vaishya, Jwala Jwala, Ripal Gaudana, Deep Kwatra and all my other lab mates for their help, understanding and constant input in my research and for making my stay at UMKC a memorable one. I also sincerely thank Joyce Johnson, Sharon Self, and Rodger Palmer at School of Pharmacy and Connie Mahone, Nancy Hover at School of Graduate Studies for their help at various stages.

I would like to express my profound gratitude to my family for their love, emotion and moral support.

DEDICATED TO MY FAMILY

CHAPTER 1

INTRODUCTION

1.1. Structure of the Eye: Anatomy and Physiology

The eye is primarily divided into anterior and posterior segments (Kaplan, 2007). Both the compartments are protected by various anatomical and biological barriers. These barriers along with the complex structure of the globe result in poor ocular bioavailability (Gaudana et al., 2009). The topical route is the most common mode of drug administration for targeting the anterior segment diseases (Gaudana et al., 2009; Lee and Robinson, 1986). However, following topical administration, a large fraction of the instilled dose is washed away due to tear turn over (0.5-2.2 μL/min) and rapid blinking (6-15times/min) within 2-5 minutes. These non productive processes result in poor ocular bioavailability, generally less than 5% (Janoria et al., 2007; Kearns and Williams, 2009; Lee and Robinson, 1979). Anterior segment bioavailability is further diminished by the presence of various barriers such as nasolachryimal drainage, impermeable corneal epithelium and blood ocular barriers. The cornea is mainly composed of 5 different layers, i.e., epithelium, Bowman's membrane, stroma, Descemet's membrane and endothelium (Dingeldein and Klyce, 1988). The corneal epithelium acts as a hurdle to the absorption of hydrophilic drugs while the stroma acts as a barrier for the passage of hydrophobic drugs (Huang et al., 1983; Prausnitz and Noonan, 1998). Therefore compounds with an optimum oil to water partition will exhibit maximum corneal penetration (Prausnitz and Noonan, 1998). Topical formulations consisting of penetration enhancers and mucoadhesives can also significantly enhance the

ocular bioavailability. Incorporation of mucoadhesive and viscosity enhancers such as carbopols, polyacrylic acids and chitosan in the topical formulations helps in increasing the residence time of drugs in the cul-de-sac and thereby improving ocular absorption (Anumolu et al., 2009). Penetration enhancers (surfactants, calcium chelators) disrupt tight epithelial junctions on the cornea in a reversible manner and thereby facilitating drug penetration (Kaur and Smitha, 2002; Saha et al., 1998). Recent studies (Karla et al., 2009b) have identified various efflux transporters (MRPs) on human corneal epithelium and demonstrated that these transporters can significantly lower permeability of anti-glaucoma and anti-viral agents.

Drug delivery to the posterior segment is further challenging due to the presence of unique anatomical and physiological barriers (Lee and Robinson, 2009). Intravitreal injection is primarily employed as a drug delivery strategy for the treatment of retinal diseases such as age related macular degeneration, proliferative vitreoretinopathy, diabetic retinopathy, diabetic macular edema, retinoblastoma, and cytomegalovirus retinitis (Janoria et al., 2007). Although intravitreal injections deliver molecules directly to the neural retina; adverse effects such as endophthalmitis, retinal detachment and hemorrhage, often result in poor patient compliance (Baum et al., 1982; Velez and Whitcup, 1999). Entry of xenobiotics following systemic or periocular (subconjunctival, retrobulbar, peribulbar and sub-tenon) administration is hindered by the blood retinal barrier (BRB) (Cunha-Vaz, 1997). Remarkable modifications have been observed in the arena of ocular drug delivery over the past two decades. This section briefly describes the ocular anatomy, pathology of various

retinal diseases and various novel drug delivery systems designed for treatment of the diseases.

1.1.1. Definition and Development of the Eye

The eye can be considered as a photoreceptor which is shielded by a shading pigment on one side. This pigment helps with recognition of the light source direction (Gehring and Ikeo, 1999). Eyes can be broadly classified into two categories-simple or compound eyes. Simple eyes are found in unicellular organisms and help to distinguish between bright and dark surroundings that are sufficient enough in following circadian rhythms. The simplest form of the eye, which is found in algae and flatworm, consists of just one photoreceptor and pigment cell (Arendt and Wittbrodt, 2001; Fernald, 1997; Plachetzki et al., 2005). Compound eyes consist of thousands of photoreception units and can distinguish shapes and colors (the human eye can distinguish ~ 10 million colors) (Judd and Wyszecki, 1975). Moreover, they have the capacity to detect fast movements and view very large angles compared to simple eyes.

Six stages are involved in the development of eye. These include: a) growth of photoreceptor cells, b) depressed/folded area allowing limited directional sensitivity of light, c) formation of the pinhole, increasing directional sensitivity and imaging, d) formation of transparent humor enclosed in a chamber, e) development of a distinct lens, and f) development of the iris and cornea (Fernald, 1997, 2004, 2006). Early stages are marked by the formation of "eyespots" which are simple patches of photoreceptor cells. These eyespots can only distinguish bright light from the dim light. The eyespots gradually depress into a

shallow cup granting the ability to slightly discriminate directional brightness. This cup deepens into a pit over time resulting in the formation of an effective pinhole camera. The photoreceptor cells gradually grow in number and increase the capability of distinguishing dim shapes (Land and Fernald, 1992). Thin transparent cells, which are originally formed to prevent damage to the eyespot, segregate into a transparent humor. This has the property of color filtering and improving eye refractive index. An increase in the concentration of crystalline proteins inside these cells result in the formation of the lens (Doolittle, 1988). A nontransparent (iris) and a transparent (cornea) layer split in front of the lens in an independent fashion. Separation of these two layers by aqueous humor increases refractive power and eases circulatory problems. Six extraocular muscles which include the medial rectus, lateral rectus, superior rectus, inferior rectus, superior oblique, and inferior oblique control the vertical and horizontal movement of the eye. Various functions of the muscle are shown in Table 1 (Newell, 1982).

Table 1. Function of various orbit muscles**.**

Muscle	**Functions of the muscle**	Innervations
Medial rectus	adduction or movement of the eye inward	cranial nerve III or Oculomotor
Lateral rectus	abduction or movement of the eye outward	cranial nerve VI or Abducens
Superior rectus	elevation or upward movement of the eye intorsion or rotates the top portion of the eye towards the nose adduction or inward movement of the eye	cranial nerve III or Oculomotor
Inferior rectus	depression or downward movement of the eye extorsion or movement of the eye away from the nose adduction or inward movement of the eye	cranial nerve III or Oculomotor
Superior oblique	intorsion or rotates the top of the eye towards the nose depression or downward movement of the eye abduction or outward movement of the eye	cranial nerve IV or Trochlear
Inferior oblique	extorsion or movement of the eye away from nose elevation or upward movement of the eye abduction or outward movement of the eye	cranial nerve III or Oculomotor

The eyeball diameter in a newborn is ~1.8 cm which gradually increases to about 2.54 cm in adulthood. The eye is a two piece system consisting of cornea (smaller unit) and sclera (larger unit). The cornea and sclera are connected by a ring called the limbus. The eye attains its full size at the age of thirteen years. The volume of a fully grown eye is approximately 6.5 mL and weighs 7.5 gm. The eye wall is made of 3 major layers. The outermost layer is fibrous tunica consisting of cornea, sclera, and corneoscleral limbus. The intermediate vascular layer is pigmented tunica consisting of choroid, ciliary body and iris. The innermost layer is nervous tunica consisting of retina, photoreceptor cells, modulator cells, transmitter cells, and supporting cells. Aqueous humor, lens, and vitreous humor are responsible for light refraction. The sclera is a white protective coat lining the entire eyeball except the cornea. It consists of dense interlacing white fibrous tissue which guards the subtle structures and prevents injury of the eye. Various parts of the eye are shown Fig 1. The complete description of anatomy and physiology of ocular structures is beyond the scope of this work and, hence we have curtailed our discussion to some of the major ocular tissues starting with the anterior segment, Fig 2.

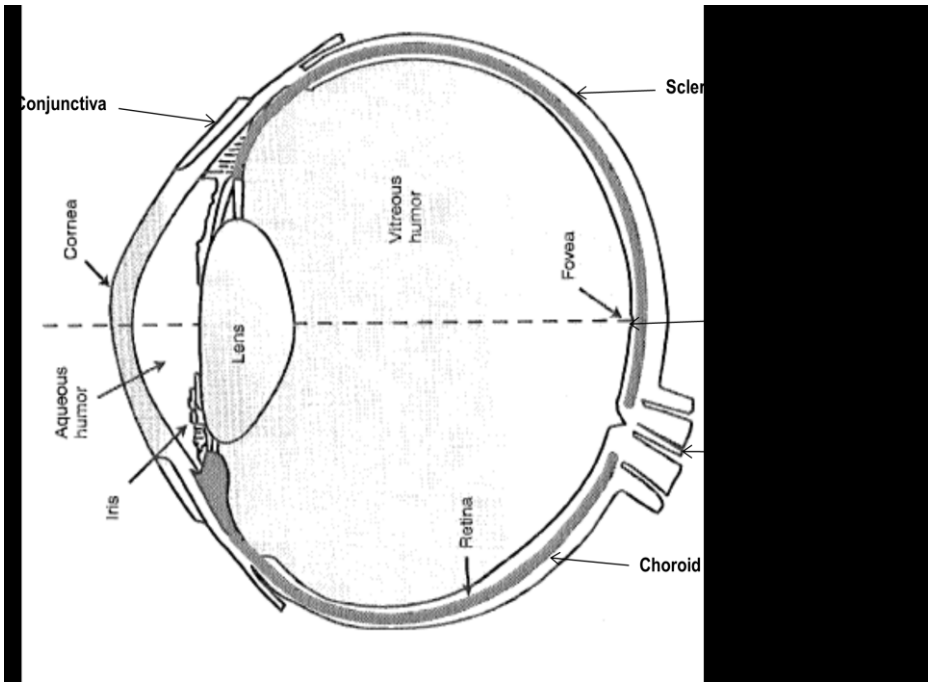

Fig. 1. Structure of the eye (Reused with permission, (Dey and Mitra, 2005)

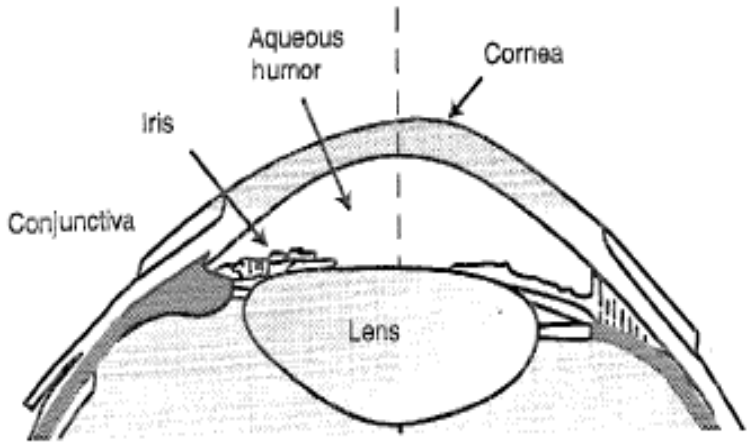

Fig. 2. Anterior segment of the eye (Reused with permission, (Dey and Mitra, 2005)

1.1.2. Conjunctiva

It is a mucous membrane composed of non-keratinizing squamous epithelium that covers the external surface of the eye and inner surface of the eyelids. The former is defined as the bulbar conjunctiva and the latter as the palpebral conjunctiva. The bulbar conjunctiva moves freely and blends with Tenon's capsule and anteriorly it inserts into the limbus (Martini et al., 2003). The conjunctiva located in the fornices is referred to as the fornical conjunctiva. The majority of the conjunctiva is made up of specialized stratified squamous cells. Goblet cells are interspersed within this epithelium assisting in production of mucin. This helps in nourishing the cornea and decreasing the friction and drying of the opposing palpebral and bulbar conjunctiva. In addition to goblet cells, the conjunctiva also contains lymphatic vessels, plasma cells, macrophages, and mast cells. There is a lymphoid layer that exists from the bulbar conjunctiva to the subtarsal folds of the lids which contain specialized aggregations of conjunctiva-associated lymphoid tissue (CALT) responsible for antigen processing. Furthermore, conjunctiva is innervated by free nerve endings derived from the ophthalmic division of cranial nerve five. It contains no specialized sensory receptors. The bulbar conjunctiva is supplied by the anterior ciliary arteries, anterior conjunctival arteries, and posterior conjunctival arteries. The marginal arcades of the eyelids supply the palpebral conjunctiva (Martini et al., 2003).

1.1.3. Cornea

The cornea is a transparent and avascular structure continuous with the sclera. It is composed of five layers and joins the sclera at the limbus region. From the anterior to posterior surface

of the cornea these layers are: surface epithelium, Bowman's layer, stroma, Descemet's membrane, and endothelium, Fig 3. Given its avascularity, the anterior surface epithelial cells obtain oxygen and nutrients from the tears whereas the posterior corneal endothelium depends on the aqueous humor (Dey and Mitra, 2005; Trotter, 1968). The cornea is the most sensitive portion of the eye and is innervated by free nerve endings (Gray and Carter, 1991; Martini et al., 2003). The surface epithelium is derived from the surface ectoderm and consists of nonkeratinized, stratified squamous epithelium continuous with the bulbar conjunctiva (Gray and Carter, 1991; Martini et al., 2003). Bowman's layer is located just beneath the basal lamina of the epithelial layer, consisting of collagen fibrils that are not restored if injured, resulting in scar formation (Gray and Carter, 1991). The stroma is the largest portion of the cornea, and is ~90% of the total thickness. It is anchored to the epithelium by type VII collagen and is otherwise primarily composed of types I, III, V, and VI collagen lamellae, produced by keratocytes. Interspersed with the collagen and keratocytes is ground substance. This layer allows for the cornea's transparency due to the oblique orientation of the collagen lamellae in the anterior one-third and the parallel lamellae in the posterior two-third (Gray and Carter, 1991; Martini et al., 2003). Descemet's membrane is a true basement membrane composed of type IV collagen. It is extremely thin and highly elastic with a tendency to curl up; furthermore, it is the basal lamina of the corneal endothelium and increases in thickness throughout life (Gray and Carter, 1991; Martini et al., 2003).

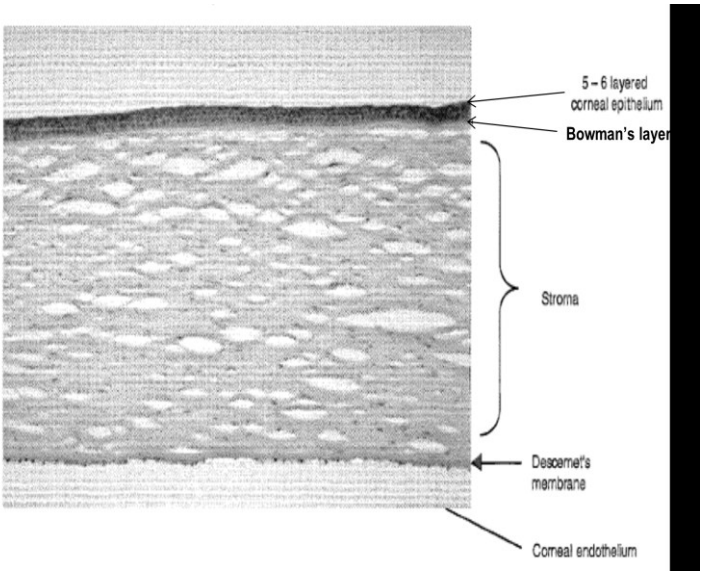

Fig. 3. Layers of the cornea (Reused with permission, (Dey and Mitra, 2005)

The endothelium is madeup of a single layer of polygonal, transparent nucleated cells whose primary function is to maintain corneal transparency through fluid balance within the stroma. The apical surfaces are in direct contact with the anterior chamber and its aqueous solution, while the basal surface is secured in Descemet's membrane. This structure and placement of the cells allow for active transport of ions and therefore the transfer of water from the corneal stroma into the anterior chamber. With age, the number of endothelial cells declines causing the residual cells to spread and enlarge to permit continuance of fluid balance (Gray and Carter, 1991; Martini et al., 2003). The cornea and crystalline lens are mainly responsible for the focusing of incident light entering the eye. The cornea contains the highest nerve fiber concentration (enter on the margins and branch out towards the center) making it extremely sensitive to pain. These fibers are mainly associated with very low threshold pain receptors.

1.1.4. Anterior Chamber and Aqueous Humor

The anterior chamber varies in depth and is surrounded anteriorly by the cornea and posteriorly by the pupil and iris diaphragm. It consists of aqueous humor formed by the ciliary epithelium in the posterior chamber. Aqueous humor is formed from the blood's plasma by mechanisms of diffusion, ultrafiltration, and active transport (Civan and Macknight, 2004). The rate of aqueous humor formation is ~ 2-3 μL/min with the total volume of the anterior chamber averaging 250 μL. Before entering into anterior chamber, the aqueous humor flows through the posterior chamber with a small resistance from the posterior iris and the anterior lens, Fig 4. The production of aqueous humor decreases with sleep, age, uveitis, retinal detachment and ciliochoroidal detachment. The fluid enters the

chamber via the pupil and exits mainly through the trabecular meshwork into Schlemm's canal along the periphery of the iris, Fig 4. There is a non-trabecular passageway for drainage known as the uveoscleral drainage pathway. For this pathway, the aqueous humor crosses the ciliary body moving into the supraciliary space. Outflow is altered by contraction and relaxation of the ciliary muscles. Contraction leads to increased trabecular outflow while relaxation decreases it. These same actions lead to a decrease in uveoscleral outflow and increase respectively. The uveoscleral pathway is believed to be dependent upon the age of the person and may account for 50% of aqueous outflow in the younger population. Aqueous humor is continuously circulating as an important network for nutrient delivery to the avascular lens and cornea as well as for metabolic waste removal with turnover time averaging 1.5-2 hours. It is also important for maintenance of intraocular pressure and provides diopteric power to the cornea (Brubaker, 1991).

1.1.5. Iris

The iris is a circular shaped structure with a circular aperture, the pupil, located at its center. It is located in the aqueous humor anterior to the lens and behind the cornea. It is the part of the uveal tract continuous with the ciliary body. All irides, independent of color, have the same stromal structure composed of melanocytes, non-pigmented cells, collagen fibrils, and a matrix containing hyaluronic acid. The anterior border of the iris contains multiple crypts and crevices with variable sizes, shapes and depths through which the aqueous humor flows. The unique color of individuals' irides is dependent upon the amount of pigmentation in the

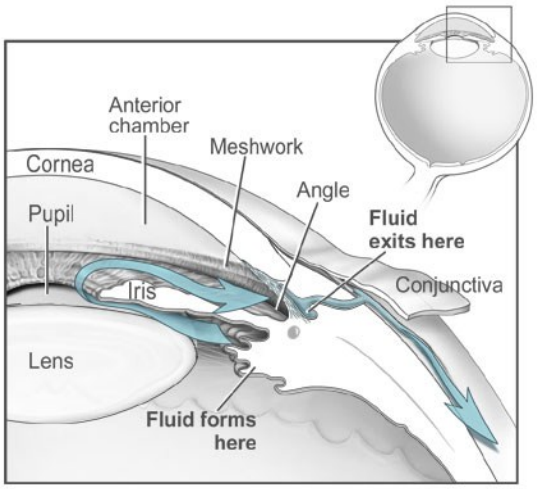

Fig. 4. Flow of aqueous humor (Courtesy of National Eye Institute and National Institutes of Health)

anterior border layer and the deep stroma. People with blue irides have a lightly pigmented stroma, whereas those with brown irides are densely pigmented leading to increased absorption of light. Albinos lack any pigmentation in their stroma (Gray and Carter, 1991). There are numerous blood vessels and nerves throughout the stroma. Of note, in a normal human iris, the anterior border layer is avascular with the remainder of the stroma being primarily composed of vasculature which arises and radiates from the major arterial circle to the pupil. At the thickest portion of the iris, the collarette, arteriovenous anastomoses form a minor vascular circle. Also found within the stroma are myelinated and non-myelinated nerve fibers. The majority of the stroma is composed from blood vessels that arise and radiate from the major arterial circle to the pupil. In addition, a normal anterior border layer of the iris in humans is avascular. Also found within the stroma are myelinated and non-myelinated nerve fibers. The posterior surface of the iris is densely pigmented and is known as the posterior pigmented layer. This layer is continuous with the non-pigmented epithelium of the ciliary body and thus with the neurosensory portion of the retina. While the basal surface of the pigmented layer borders the posterior chamber, the apical surface faces the stroma and adheres to the anterior pigmented layer (Gray and Carter, 1991). The pupil is capable of changing size through the activity of the iris sphincter and dilator muscles both derived from the neuroectoderm. The sphincter muscle is composed of smooth muscle fibers circumferentially located in the deep stroma near the pupillary margin, anterior to the pigment epithelium on the posterior surface of the iris (Gray and Carter, 1991). Innervation is primarily from parasympathetic nerve fibers that originate from cranial nerve III which leads

to contraction of the muscle fibers and constriction of the pupil (Gray and Carter, 1991; Imesch et al., 1997; Martini et al., 2003). Pharmacologically, the sphincter muscles contract with muscarinic stimulation. The sphincter muscle does have sympathetic innervation, but an inhibitory action leads to relaxation of the muscle. The dilator muscles cause dilation with contraction, and its muscle fibers radiate from the iris' outer circumference toward the papillary margin on the posterior surface of the iris (Gray and Carter, 1991; Martini et al., 2003). The smooth muscle fibers are innervated by both the sympathetic and parasympathetic autonomic systems with sympathetic α1-adrenergic stimulation leading to contraction. The iris is mainly responsible for controlling the pupil diameter and size. Depending on the amount of light reaching the retina, iris muscles expand or contract the aperture at the pupil (center of the iris).

1.1.6. Lens

The lens is composed of concentric layers of cells which form a biconvex structure that functions to focus images on the retina. It is located directly behind the posterior chamber and pupil and is enclosed in a fibrous, elastic capsule suspended from the ciliary body by suspensory ligaments. The lens capsule is rich in type IV collagen and other matrix proteins as it is a basal lamina. Throughout life, the anterior lens capsule increases in thickness unlike the posterior capsule which remains constant. This is important because the thinness of the posterior capsule creates an increased risk of rupture during extracapsular cataract extraction. The lens has an inner nucleus and outer cortex. The nucleus component of the lens is a mass of fibers already formed at birth, whereas the cortex is formed by fibers postnatally. The

cytoplasm of the cell fibers is mostly homogeneous with few organelles permitting a high concentration of lens crystallins within the cytoplasm, and thus creates a high refractive index for the lens. The lens is positioned for distant vision at rest as the suspensory ligaments' tension causes the elastic capsule containing the lens to flatten. With accommodation, the ciliary muscle contracts and decreases tension in the suspensory ligaments leading the elastic lens to resume a curved shape (Gray and Carter, 1991). Accommodative power is steadily lost with age secondary to increased lens size and stiffness of the lens nucleus. The lens lacks innervation and blood supply leading to a much lower oxygen concentration than that found in other parts of the body (Kaufman et al., 2003). Metabolic activity for the majority of the lens is reliant on the glycolytic metabolism of glucose from the aqueous humor to produce the reducing equivalents and ATP necessary for energy production (Gray and Carter, 1991; Kaufman et al., 2003). There are also lens epithelial and superficial fiber cells which contain mitochondria and permit cells located at the surface of the lens to use oxidative pathways in addition to the glycolytic pathway for energy production (Henkind et al., 1979; Kirsch, 1975).

1.1.7. Sclera

Sclera is the opaque or white portion (except horses and lizards which can have black sclera) of eye which is fibrous in nature. The development and differentiation of the sclera starts in the sixth week of human embryonic stage from the neural crest and mesoderm region (Johnston et al., 1979; Trotter, 1968). It is fibrous and opaque tissue which forms the external protective coat (posterior five sixths of the connective tissue that coats the globe)

(Rada et al., 2006). Sclera is mainly composed of collagen (~28.8%), proteoglycans (~0.9%), elastin (~1-2%), proteins and cellular components (~3%), and water (~68%) (Sandberg-Lall et al., 2000). Recent studies demonstrated the presence of types III, IV, V, VI, VIII, XII, XIII, and XVIII collagen in addition to type I (Rada et al., 2006; Watson and Young, 2004). Each subtype of collagen acts in a unique manner providing a robust framework which supports the visual apparatus of the inner eye. Table 2 presents the type and function of various collagens present in the sclera.

Table 2. Type and function of collagen present in the sclera

Collagen	Function
Type I	Interacts with Type V collagen and helps in maintaining fibril diameter during fibrillogenesis (Norton and Rada, 1995)
Type III	Present in the major D-periodic interstitial fibrils along with Type I collagen (Marshall et al., 1993)
Type V	Present at the fibril perimeter (Marshall et al., 1993)
Type VI	Assembles into filamentous structure between fiber bundles (Marshall et al., 1993)
Type VIII	Responsible for the formation of hexagonal lattice in Descemet's membrane (Sawada et al., 1990)
Type XII	Mediates interfibrillar interactions and development of ocular connective tissues (Shaw and Olsen, 1991)
Type XVIII	Collagen gene has been implicated in the development of high myopia and is known to be expressed in the human eye

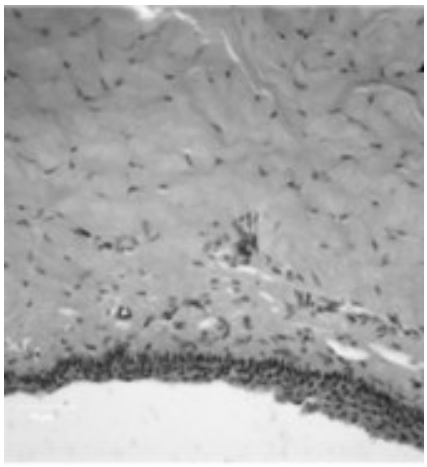

Fig. 5. Histology of the sclera

Elastin fibers consist of microfibrillar and amorphous components which support the collagen framework in sclera. These fibers are synthesized by scleral fibroblasts and are mainly present in the inner layers of stroma and lamina fusca, Fig. 5 (Marshall, 1995).

1.1.8. Retina

The retina is the innermost layer of the eye and consists of a multi-layered sensory tissue (Fig 6). It contains millions of rod and cone cells, also known as photoreceptors. The photoreceptors are present in the macula which is the retinal portion and mainly responsible for central vision. The retina is mainly divided into two layers: retinal pigment epithelium (outer layer) and neural retina (inner layer).These 2 layers are separated by the fluid filled subretinal space (Thomas, 1989). The neural retina is a multi-layered and highly organized membrane which consists of rods, cones, bipolar cells, and ganglionic cells. Light rays entering the eye converge at the cornea and the crystalline lens makes them intersect at a point just behind the lens (in the vitreous humor). These rays again pass through nine layers and diverge back to the outermost retinal layer (pigmented epithelium) which is reflected back to the rods and cones. Rods are responsible for night vision. Rod and cone cells capture light rays and translate them into electrical impulses. These impulses reach the brain via optic nerve and get converted into images.

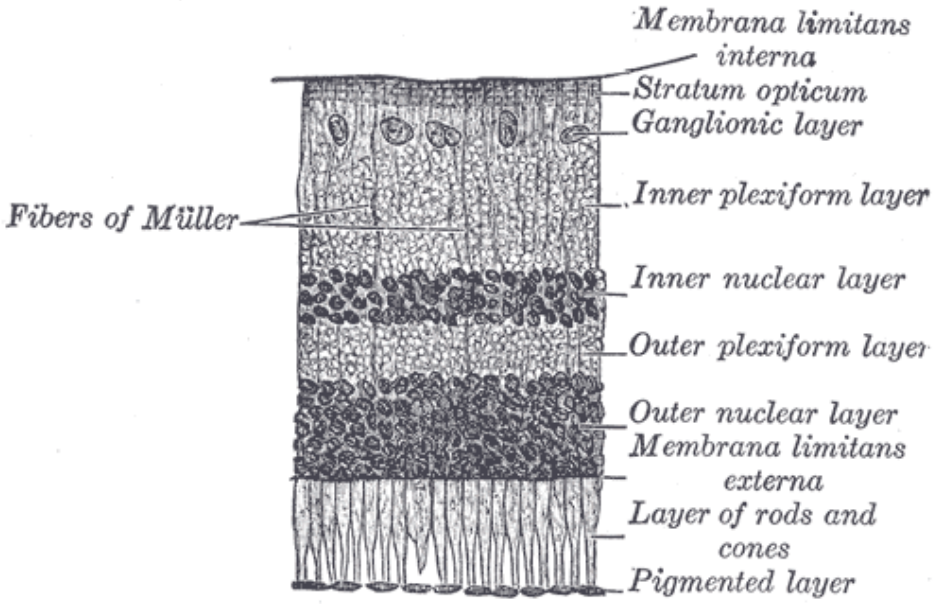

Fig. 6. Structure of the retina. This diagram has been reproduced from Gray's Anatomy 20th US edition (public domain)

The bipolar cells synapse with the ganglionic cells whose axons course horizontally forming the optic nerve. Ganglionic cells conduct the signals from the retina to the brain. Retinal pigment epithelium (RPE) is a non visual portion located between the neural portion of the retina and choroid. It consists of a layer of melanin-containing epithelial cells (except in albinos). Melanin helps in absorption of stray light rays entering the eyeball and hence prevents the reflection of scattering of light (Tortora and Derrickson, 2009). The RPE forms the outer blood–retinal barrier and has tight junctions that enable the epithelium to form a barrier by connecting the neighboring cells (Rizzolo, 2007). RPE cells are well differentiated and polarized on both the apical and basolateral portions. These cells regulate the trans-epithelial transport of various molecules similar to other epithelia and endothelia. This is facilitated by apical tight junctions (retards diffusion through the paracellular spaces) and asymmetric distribution of proteins (regulates vectorial transport) (Rizzolo, 1997; Williams and Rizzolo, 1997). Numerous microvilli are found on the apical or neural retinal portion while small convoluted infoldings are present on the basolateral or choroid facing portion. This helps in the absorption of various nutrients and thereby maintains the viability of the neural retina. RPE expresses numerous efflux transporters which prevent the entry of xenobiotics into the retina.

1.1.9. Formation of an Image on the Retina

Light rays tend to diverge in all directions from the source and hence the set of rays from all the points in space that reach the pupil should be focused. Refraction of light by the cornea and lens results in focusing the image on the photoreceptor cells of the retina. The cornea is

responsible for the major portion of refraction while the lens has considerably less refractive power. However, refraction by the lens can be adjusted according to convenience but refraction of the cornea cannot be adjusted. This adjusting property of the lens is responsible for bringing objects situated at various distances from the eye on to the surface of retina. This dynamic change in the refractive power of the lens is known as accommodation**.** While distant objects are being viewed, the lens becomes comparatively thin and flat, and in this position, the lens has the least refractive power. While viewing near objects, the lens becomes more thick and round relative to its earlier position and has the most refractive power. While distant objects are being viewed, the lens becomes comparatively thin and flat, and in this position, it has the least refractive power. The lens becomes thicker and round when viewing near objects requiring high refractive power. These changes are facilitated by the ciliary muscles surrounding the lens. The circular opening in the iris, which is referred to as pupil, undergoes adjustment in its size. This contributes immensely to the clarity of images which are formed on the retina. Images generated by the eye are affected by chromatic and spherical aberrations which blur the retinal image. These aberrations occur most in the light rays which are farthest from the center of the lens. When the pupil is narrowed, these aberrations are minimized and thus the image quality is improved. This is similar to the closure of the iris diaphragm on a camera lens which enhances the sharpness of a photograph. Light rays falling on the photoreceptor cells of the retina generate electrical signals that are passed on to the brain via the optic nerve. The photoreceptor cells consist of rods and cones which communicate with three distinct layers of cells via junctions known as synapses. In

fact, the actual image formed on the retina is inverted and small; nevertheless, the brain interprets the image and it becomes upright.

1.1.10. Optic Nerve

It is known as cranial nerve two. It is responsible for the conduction of visual information from the retina to the brain. It is composed of ~1.2 million myelinated axons of retinal ganglion cells of a single retina and has a varying diameter (1-10 μm).

It is located within the orbit, and it extends from the eyeball to the optic foramen. The length of the optic nerve varies from 20-30 mm with a diameter of ~5 mm, Fig 7.

The fibers of the optic nerve are made of the retinal ganglionic and Portort cells. These fibers are covered with three meningeal layers (dura, arachnoid, and pia mater) produced by oligodendrocytes. Within the ocular bulb, the fibers converge to the optic papilla where they are accumulated into a rounded bundle known as the optic nerve. The nerve pierces the choroid and sclerotic coats and enters the orbital fat present in the back of the eye towards the optic foramen. Later, it enters the middle fossa of the cranium and joins its fellow nerve from the other side forming the optic chiasma. The optic nerve can be classified under four subdivisions for convenience

1. Intraocular portion: It is less than 1mm in length and consists of the optic nerve head, optic disc, and the optic papilla

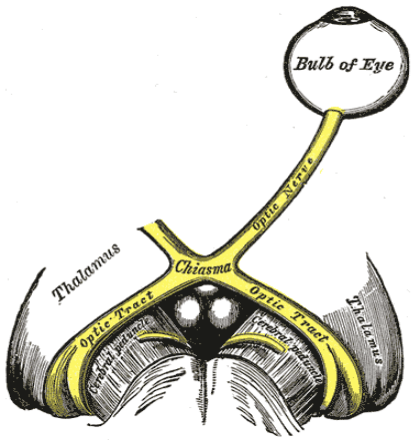

Fig. 7. The left optic nerve and optic tracts. This diagram has been reproduced from Gray's Anatomy 20th US edition (public domain)

2. Intraorbital portion: It emerges from the sclera ~3 mm below and extends into the medial side of the posterior pole of the bulbus. It is ~25 mm long and passes in the backward and medial direction up to the optic foramen. This tissue is surrounded by the posterior part of the fascia bulbi (tenon's capsule) and orbital fat.
3. Intracanalicular portion: It is ~5 mm in length and is located within the optic canal. The tissue receives blood supply from the pial plexus.
4. Intracranial portion: It is ~10 mm in length and runs backward, upward, and medially and merges into the optic chiasm present in the subarachnoid space (Snell and Lemp, 1989).

Fiber tracks are incapable of regeneration, and hence optic nerve damage results in irreversible blindness. Functionally, the optic nerve begins in the retinal ganglion cells. The axons which arise at these cells move toward the exit of the optic nerve from the eye, while the axons arising from the nasal side go towards the head of optic nerve. The axons which arise from around the fovea (in the macular region) form a spindle-shaped papillomacular bundle which enters the temporal sector of the optic nerve head. The fovea is usually situated underneath the middle of the nerve head. The papillomacular bundle makes its entry into the optic disc inferior to its equator. Axons from the remaining retinal region take a curved route around the papillomacular bundle to make entry into the optic nerve head at the superior and inferior poles. The layer of retinal nerve fiber is thickest in these curved bundles as they near the upper and lower sector of the optic disc.

1.1.11. Vitreous Humor

Nearly 80% of the volume of the eye is made up of a clear gel-like substance known as vitreous humor. This fluid fills up the room between the lens and the retina. Vitreous humor consists of water (~99%), hyalocytes, hyaluronic acid, ascorbic acid, inorganic salts, sugar, and a network of collagen fibrils (Sebag, 1989). The network of non-branching collagen fibers with hyaluronic acid imparts viscosity to the vitreous humor which is two to four times higher than pure water and has a refractive index of 1.336. Hyalocytes help in the removal of unwanted cellular debris. Vitreous humor is stagnant, while aqueous humor is continuously replenished (Tolentino, 1974). It is produced by certain retinal cells and has similar composition to the cornea. The vitreous humor is in continuous contact with the retina; nevertheless, it adheres to the retina only at three places: the macula, optic nerve disc, and fovea.

1.1.12. Macula

Macula is a Latin word which means “spot”. It is an oval-shaped, yellow spot which is highly pigmented and is present in the center of retina. It has a diameter of around 5 mm with two or more layers of ganglionic cells. The fovea is located at the center of the macula, and it has the largest cone cell concentration which is responsible for most visual acuity. The macular/foveal area is mainly responsible for color discrimination. Moreover, the yellow color of the macula helps in absorption of excess light entering the eye and thus acts as a natural form of protection.

1.2. Anatomical and Physiological Constraints to Ocular Drug Delivery

The anatomy and physiology of the eye presents unique challenges to ocular drug delivery. Topical administration of drugs is the most preferred route for the treatment of anterior segment diseases. Depending on the physico-chemical properties, the absorption of a drug following topical administration occurs by one or two pathways: corneal or non-corneal, Fig. 8. A major fraction of the drug absorbed through the cornea enters various anterior ocular tissues, while the non-corneal absorption process primarily results in systemic drainage via the nasolacrimal duct (Doane et al., 1978; Patton and Robinson, 1976). Drugs absorption across the corneal epithelium is mediated by either active or passive process, Fig 9. Passive transport involves simple diffusion of drug molecules in the direction of concentration gradient while the active transport involves uptake of drug molecules by transmembrane proteins. Trans-corneal absorption mainly depends on the ocular contact time and permeability of the drug. The lipophilic corneal epithelium layer provides maximum resistance to the penetration of hydrophilic drug molecules (Schoenwald, 1997). Non-corneal absorption route plays an important role in the entry of large hydrophilic drug molecules. The conjunctiva offers the least resistance to permeation of hydrophilic macromolecules relative to sclera and cornea. Ahmed and his co-workers observed that timolol maleate and inulin were absorbed into the intraocular tissues via the non-corneal route involving penetration across the conjunctiva/sclera (Ahmed and Patton, 1985). A normal eye accommodates a tear volume of 7–9 μL (Table 3).

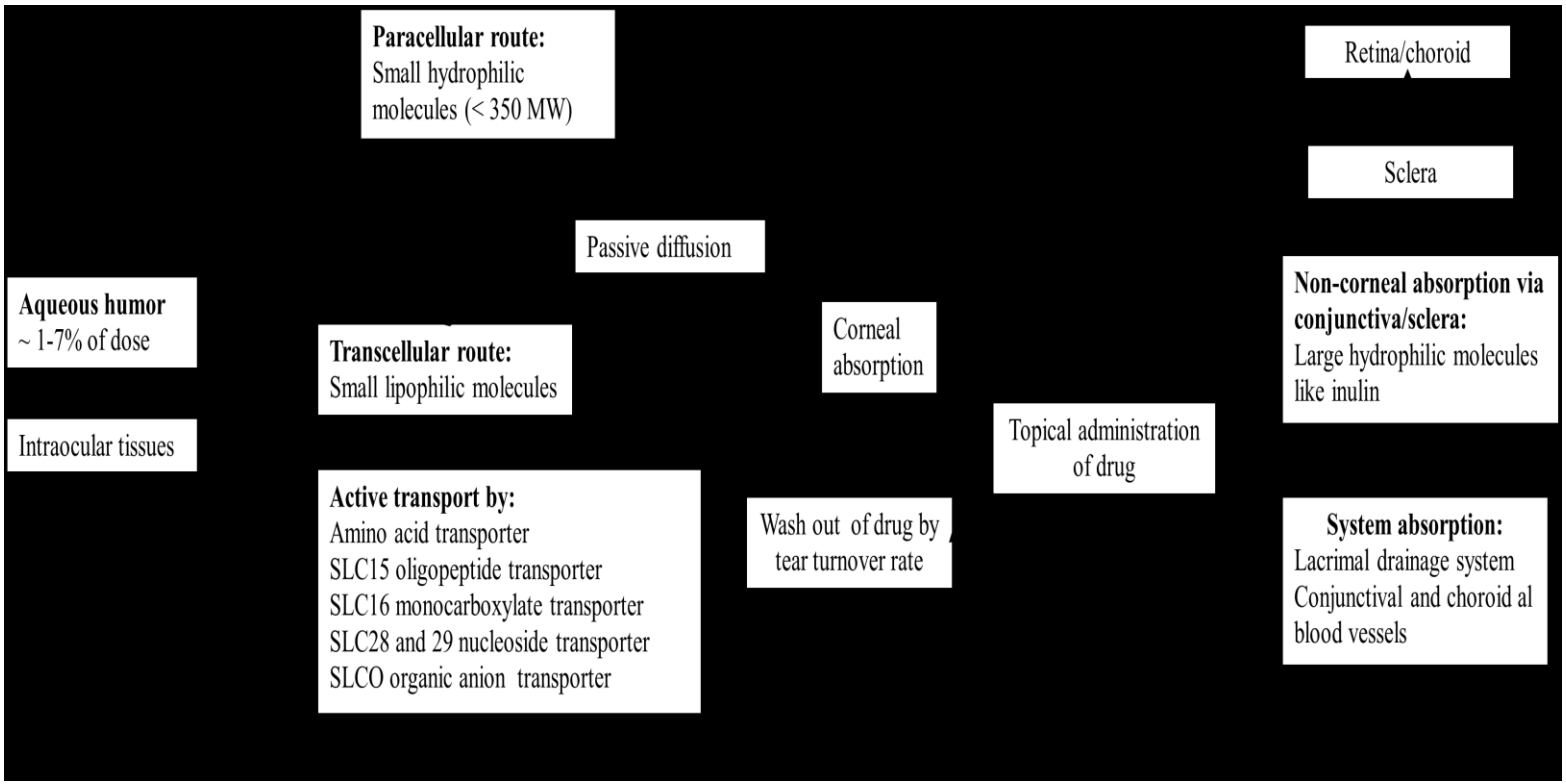

Fig. 8. Drug disposition following topical administration

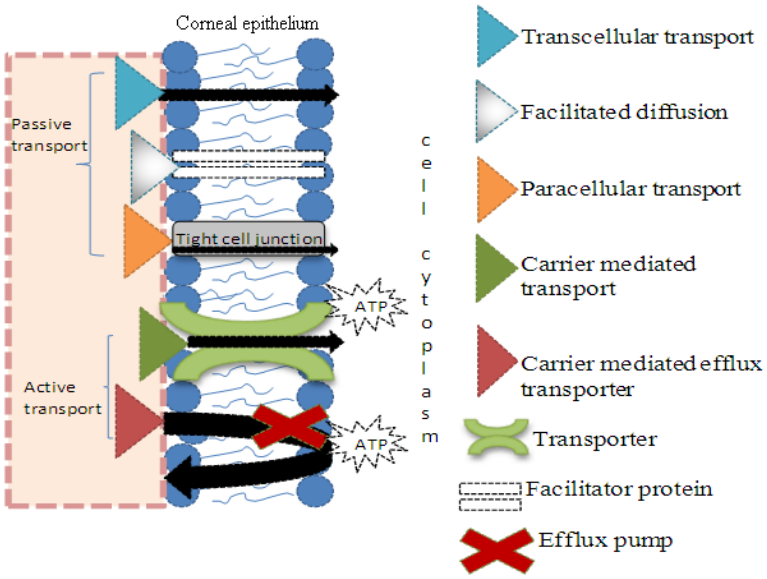

Fig. 9. Schematic of passive and active diffusion processes

Table 3. Various physiological factors in the human eye. Inspired from reference (Schoenwald, 1993)

Factors	**Values**
Tear volume	7–9 μL
Tear turnover rate	0.5–2.2 μL/min
Spontaneous blinking rate	6–15 times/min
Corneal thickness	0.52 mm
Corneal diameter	12 mm
Corneal surface area	1.04 cm^2
Conjunctival surface area	17 cm^2
Aqueous humor volume	0.1-0.25 mL
Aqueous humor turnover rate	2-3 μL/min

However, a typical eye drop volume ranges between 30–50 μL. Topical administration of an eye drop results in a rapid increase in the tear volume causing swift reflex blinking resulting in wash out of ~90% of applied dose within 5-10 mins. Furthermore, the impermeable nature of the cornea (~0.1 mm in thickness) prevents permeant entry into the eye. Absorption rate constant across the cornea ranges between 0.001-0.005 min^{-1}. Corneal cells are generated in the corneoscleral limbus and migrate towards the epithelial surface. These cells form tight junctions during the maturation phase and thus provide a strong diffusion barrier to drug absorption process (Maurice and Mishima, 1984). During the early 1980s, corneal permeability of agents with varying logD values were studied. It was observed that drugs with logD values between 2-3 exhibited optimal corneal permeability (Huang et al., 1983). Various strategies such as increase in drug retention time and inclusion of penetration enhancers have been adopted to render the drug absorption process efficient following topical administration. Penetration enhancers such as benzalkonium chloride, bile salts and acids, ethylenediaminetetraacetic acid, and lysophosphatidyl lipids transiently change the barrier properties of corneal epithelium and hence raise drug permeability (Grass et al., 1985; Green and Tonjum, 1971). Drug retention time in the cul-de-sac can be significantly enhanced by incorporating viscosity enhancing agents such as poly(vinyl alcohol), methylcellulose, hydroxypropylmethylcellulose, and hydroxyethyl cellulose (Schoenwald, 1997). Further use of various mucoadhesive polymers such as xanthane, carboxymethycellulose, carrageenan, and polyacrylic derivatives also promote drug absorption (Barar et al., 2008). More recently, various efflux transporters such as P-glycoprotein (P-gp) (Kawazu et al., 1999), multidrug

resistance protein-2 (MRP2) (Karla et al., 2007), and breast cancer resistance protein (BCRP) (Karla et al., 2009a) have been identified on the cornea and conjunctiva. Efflux transporters retard drug entry resulting in outward directed transport and hence play a significant role in the ocular distribution of drugs. Functional evidence of MRP2/P-gp and their role in drug efflux out of corneal epithelium was studied in rabbits (Hariharan et al., 2009). This report concluded that aqueous humor concentration of erythromycin, a substrate of MRP2 and P-gp can be significantly improved by co-administration of 6α-methyl prednisolone. The topical route fails miserably in the treatment of diseases affecting the choroid and retina. These diseases are treated by systemic, periocular, or intravitreal administration (Barar et al., 2008; Myles et al., 2005). Though systemic administration is most widely indicated, only 1–2% of the dose reaches the vitreous (Cunha-Vaz, 1997). Entry of therapeutic agents following systemic and periocular administration is challenging due to the presence of blood-ocular barriers (BOBs). Physiologically, these barriers prevent the entry of toxic substances and blood proteins into the aqueous/vitreous and thus maintain transparency (Cunha-Vaz, 1997). BOB is a physical barrier between the local blood vessels and ocular tissues. There are two types of BOBs:

a) Blood-aqueous barrier (BAB) consists of an epithelial barrier present on the non-pigmented ciliary epithelium layer and the posterior iridial epithelium, iridial vessels, and the endothelium (Cunha-Vaz, 1979). Under normal conditions, BAB maintains the composition of aqueous humor by preventing the transfer of high molecular weight proteins between the blood and ocular chambers. Moreover, BAB also affects

the metabolism of the cornea and lens and aids in the regulation of intraocular fluid volume (Cunha-Vaz, 1979).

b) Blood-retinal barrier (BRB) consists of tightly joined non-fenestrated capillaries between the blood and retina. This plays a major role in the pathophysiology of retinal drug delivery. It prevents the entry of large drug molecules from choriocapillaris into the retina (Vinores, 1995). BRB operates at two levels: (i) inner BRB or the endothelial membrane of retinal vessels and (ii) outer BRB or chorioepithelial interface or retinal pigment epithelium (Cunha-Vaz, 1976, 2004). BRB restricts inward movement following periocular or systemic drug administration and outward movement after intravitreal administration. These barriers exhibit mainly active transport processes. Minor alteration in the BRB results in the formation of vascular retinopathies, retinal edema, and pigment epitheliopathies. For treatment of retinal diseases, a significant amount of drugs must pass the BRB to have a therapeutic effect (Mannermaa et al., 2006). Several attempts have been made to increase permeability properties of BRB. Intracarotid infusion of hyperosmotic solution containing mannitol or arabinose for thirty seconds results in irreversible opening of the BRB. However, this technique is non-specific and may cause toxicity. Chemical modification of drugs is yet another widely utilized approach to increase BRB permeability of drugs. This can be accomplished by increasing the lipophilicity of drug molecules or by modifying the drugs to target the specific carrier systems present on the RPE.

1.3. Retinal Diseases

1.3.1. Age-Related Macular Degeneration (AMD)

AMD has remained as one of the major vision-threatening ocular diseases in elderly population (Hawkins et al., 1999). It occurs mainly in two forms, known as dry AMD (non-exudative) and wet AMD (exudative or neovascular). Age is considered as one of the major risk factor in AMD patients. Dry AMD occurs mostly in people with mean age of 56.8 years as compared to 70.5 years average for wet AMD. Apart from age, the other risk factors of AMD include smoking, obesity, race, gender and family history (Leibowitz et al., 1980). Dry AMD occurs more commonly compared to wet AMD. It is characterized by slow breakdown of photoreceptors, retinal pigment epithelium (RPE) and choriocapillaris leading to blurred central vision. At the initial stage this disease affects only one eye with the formation of small/medium sized drusen (yellow deposits formed under the retina) which gradually spreads to the other eye and finally results in loss of vision (Iu and Kwok, 2007; Sunness et al., 1997). The exact cause, mechanism and treatment of dry AMD is still not clear. Some studies suggest that specific high-dose formulations containing antioxidants, zinc and vitamin supplements can considerably delay the advancement of dry AMD. Wet AMD is characterized by growth of abnormal blood vessels behind the retina. These blood vessels are often fragile leading to leakage of blood beneath the macula. Other pathophysiological processes associated with wet AMD include deposition of drusen, disruption of Bruch's membrane and degeneration of RPE leading to complete loss of vision. Wet AMD patients are frequently characterized by high levels of vascular endothelial growth factor (VEGF)

which is a potent mitogen of vascular endothelial cells. VEGF is a homodimeric glycoprotein that is known to induce angiogenesis and vascular permeability. Various isoforms of VEGF have been identified in humans. The major isoforms include VEGF121, VEGF165, VEGF189, VEGF206 and minor isoforms include VEGF145, VEGF148, VEGF162, VEGF165b and VEGF183. Out of all these isoforms, VEGF165 is the most abundantly expressed and is mainly responsible for angiogenesis and endothelial cell growth (Spilsbury et al., 2000). Currently, wet AMD is treated using photodynamic therapy, laser treatment and intravitreal injection of anti-angiogenic agents. Photodynamic therapy involves the intravenous infusion of light activated drug vertiporfin (Schmidt-Erfurth et al., 2002). This agent has a tendency to accumulate in abnormal blood vessels present at back of the eye. Following accumulation, a low energy laser beam is used to activate the drug, which destroys the abnormal blood vessels. In laser treatment, a high energy laser beam is used to seal the tiny, leaky blood vessels (Virgili and Bini, 2007). This improves the vision only for a short period of time. Intravitreal injection of anti-VEGF agents has revolutionized the treatment of wet AMD. Anti-VEGF agents like ranibizumab, pegaptanib sodium salt, bevacizumab, and glucocorticoids have been widely administered as intravitreal injections. These agents act by blocking various isoforms of VEGF which are responsible for angiogenesis and vascular permeability (Costa et al., 2006).

1.3.2. Diabetic Macular Edema (DME)

DME mainly affects people with a history of diabetes mellitus. It is characterized by swelling of the retina within the macula gradually leading to leakage of fluids from blood vessels and

breakdown of blood-retinal barrier (Klein et al., 2009). Macula is a small structure present at the center of the retina which is rich in cones and specialized nerve endings. Apart from diabetes mellitus, hypertension may also lead to increase in hydrostatic pressure within blood capillaries resulting in expulsion of fluid into the retina. DME can be broadly classified into 2 types: focal or non-cystoid DME and diffuse or cystoid DME. Noncystoid edema is caused by small aberrations in retinal blood vessels followed by intraretinal leakage. Cystoid edema is associated with the formation of microcysts and dilation of retinal capillaries. Focal or grid lasers are currently being used in the treatment of DME. In focal laser treatment, leaky blood vessels are sealed while grid laser treatment is applied to dilated retinal capillaries (Bandello et al., 2003; Meyer, 2007). Failure of patients to completely recover following laser treatment has promoted vision scientists to develop better alternative strategies. More insight into pathophysiological processes of DME revealed that increase in retinal capillary permeability following the breakdown of the blood retinal barrier is partly mediated by VEGF (Aiello et al., 1997). A recent report had suggested that corticosteroids significantly inhibit the expression of a gene responsible for the production of VEGF (Nauck et al., 1997). This finding has generated considerable interest for the use of corticosteroids in the treatment of DME.

1.3.3. Proliferative Vitreoretinopathy (PVR)

PVR is the most common complication associated with retinal detachment surgery. It is characterized by simple scar formation and proliferation of cells in vitreous and retina. *"Proliferative"* refers to cell proliferation and *"Vitreoretinopathy"* as the problems involve

vitreous and retina. Proliferative vitreoretinopathy can be divided into multiple categories based on the inflammation (focal, diffuse, subretinal, circumferential and anterior displacement) of retina and location of the scar tissue (anterior and posterior). Currently, PVR is managed by surgery. Patients remain on adjunctive treatment after surgery so as to avoid relapses. A combination of 5-fluorouracil/steroids and low molecular weight heparin primarily aids in the treatment of patients who are at risk of developing PVR following retinal reattachment surgery (Asaria et al., 2001; Scheer et al., 2004).

1.3.4. Uveitis

Uveitis refers to inflammation occurring in the middle layer of eye also known as uvea (vascular layer present in between the retina and the sclera). The exact cause of uveitis is still not clear but studies indicate that viral (mumps and herpes), fungal (histoplasmosis) and bacterial (toxoplasmosis) infections may play an important role (Forrester, 1990). Based on the structures affected, uveitis can be categorized into anterior, intermediate, posterior and pan-uveitic forms. Anterior uveitis is the most common form of uveitis affecting iris and anterior chamber while posterior uveitis affects mainly retina and choroid. Intermediate uveitis is characterized by inflammation in the vitreous cavity while pan-uveitis affects all layers of uvea (Forrester, 2007). Currently uveitis is being treated with corticosteroids and immunosuppressive agents (Lightman, 1991).

1.3.5. Conjunctivitis

Conjunctivitis or “pink eye” involves inflammation of the conjunctiva resulting from allergy or bacterial or viral infections. Bacterial conjunctivitis is caused by common pus-producing

bacteria like *Chlamydia* and *Moraxella,* while viral conjunctivitis is caused by adenovirus and herpes simplex virus (Riva et al., 1992; Wickstrom, 2008). Conjunctivitis usually affects one eye and gradually spreads to the contralateral one. Based on the structures involved, conjunctivitis can be subdivided into blepharoconjunctivitis (inflammation of eyelids), keratoconjunctivitis (inflammation of the cornea) and episcleritis (inflammation between conjunctiva and sclera) (Kumar, 2009). All forms of conjunctivitis have certain common symptoms like redness, irritation, a feeling of grittiness, and watering of eyes. Conjunctivitis due to allergic infections is treated using anti-histamines and non-steroidal anti-inflammatory agents, while bacterial conjunctivitis is treated using antibiotics and corticosteroids (Sheikh and Hurwitz, 2001).

1.4. Delivery Routes

1.4.1. Conventional Delivery Routes

Conventionally, many ocular diseases are treated with either topical or systemic medications. Topical application of drug has remained the most preferred method due to ease of administration and low cost. Topical application is useful in the treatment of disorders affecting the anterior segment of the eye (Lee and Robinson, 1986). Anatomic and physiological barriers hinder drugs from reaching posterior segment of eye mainly choroid and retina. A major fraction of drug following topical administration is lost by lacrimation, tear dilution, and tear turnover. Such precorneal losses result in very low ocular bioavailability. Typically, less than 5% of the total administered dose reaches aqueous humor (Hughes et al., 2005). So, in order to maintain minimum inhibitory concentrations, the agents

need to be frequently dosed resulting in poor patient compliance. Upon topical instillation, drugs are absorbed either by a corneal route (cornea → aqueous humor → intraocular tissues) or a non-corneal route (conjunctiva → sclera → choroid/RPE). The preferred route depends mainly on the corneal permeability of drug molecule (Barar et al., 2008). Unlike topical administration, systemic dosing helps in the treatment of diseases affecting posterior segment of the eye. A major drawback associated with systemic administration is that only about 1-2% of administered drug reaches to vitreous cavity. The blood retinal barrier, which is selectively permeable to more lipophilic molecules mainly governs the entry of drug molecules into the posterior segment of the eye. This results in frequent administration of high amounts of drugs leading to systemic side effects (Duvvuri et al., 2003). Though topical and systemic routes are convenient, lack of adequate bioavailability and failure to deliver therapeutic amounts of drugs to the retina has prompted vision scientists to search for alternative routes of administration.

1.4.2. Novel Delivery Routes

1.4.2.1.Intravitreal Injections

Intravitreal injections have gained considerable momentum during the past two decades. This method involves injection of drug solution directly into vitreous via pars plana using a 30G needle. Unlike other routes, intravitreal injection offers higher drug concentrations in vitreous and retina. Elimination of drugs following intravitreal administration depends on their molecular weight. Linear and globular molecules with molecular weight greater than 40 or 70 kDa, respectively, tend to have longer retention in the vitreous humor (Marmor et al.,

1985). Though intravitreal administration offers high concentrations of drugs in the retina, it is associated with various short term complications such as retinal detachment, cataracts, glaucoma, an increase in intraocular presure, endophthalmitis, or intravitreal hemorrhages (Ausayakhun et al., 2005). Moreover, patients need to be carefully monitored following intravitreal injections.

1.4.2.2.Periocular Injection

Periocular route has been considered as the most promising and efficient route for administering drugs to posterior eye segment. Periocular refers to the region surrounding the eye. It is a broad term which includes peribublar, posterior juxtascleral, retrobulbar, sub-tenon, and subconjunctival routes Fig 10. Drug solutions are placed in close proximity to the sclera which results in high retinal and vitreal concentrations.

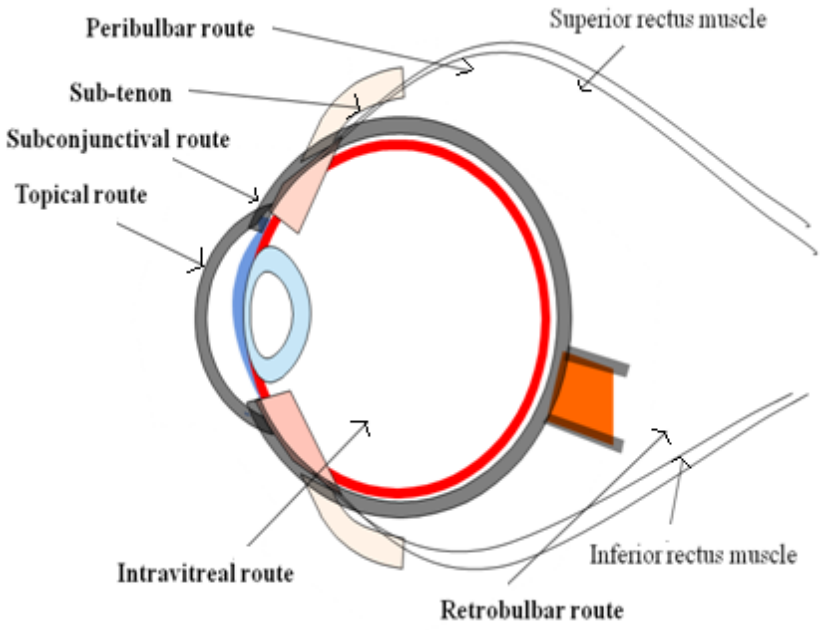

Fig. 10. Routes of drug administration to the eye

Sclera which is made up of fibrous tissue offers less resistance to permeability of drugs (Raghava, Hammond et al. 2004). Pharmacokinetics of sodium fluorescein following periocular administration was studied in rabbits. The study concluded that administration of drug via subtenon injection resulted in the highest and most sustained vitreous concentration of sodium fluorescein compared to retrobulbar and subconjunctival routes (Ghate et al., 2007). Anterior segment complications have been observed in some patients following periocular injections. These include rise in intraocular pressure, cataract, hyphema, strabismus and corneal decompensation (Castellarin and Pieramici, 2004).

1.4.2.2.1. Retrobulbar Injection

Retrobulbar injection involves deposition of drug solution into retrobulbar space within the muscle cone. This route is preferred when the medication needs to be in direct contact with macular region. Higher concentration of steroids was obsereved in the optic nerve after retrobulbar injection (Hyndiuk and Reagan, 1968). Such injections are usually given with a special 23 guage sharp 1.5 inch needle having rounded tip, bent 10^{o} outward away from the globe. The needle is inserted in the quadrant between the inferior and the lateral rectus muscles and moved posteriorly until orbital septum obstructs its penetration; the needle is directed toward the apex of the orbit and penetrated until it meets the resistance of the intermuscular septum. The needle tip penetrates into the retrobulbar space which can take up to 2 to 3 mL solution. Care should be taken to minimize needle movement so as to prevent possible laceration of the blood vessels. Pressure should be applied on the globe to distribute the anesthetic effect and to ensure haemostasis (Trivedi et al., 2003).

1.4.2.2.2. Peribulbar Injection

Peribulbar injection has been devised to lower the risk of injury to intraorbital structures associated with retrobulbar administration during cataract surgery. The injection is made in the inferiorlateral quadrant of the orbit using a 26G half inch disposable needle (Ebner et al., 2004). Unlike retrobulbar this technique is completely free from sight and life threatening complications. Peribulbar injections can be classified as circum-ocular (sub-tenon's, episcleral), peri-ocular (anterior, superficial); peri-conal (posterior, deep) and apical (ultra-deep) based on the depth of needle (van den Berg, 2004). Clinical efficacy of anesthesia following retrobulbar and peribulbar techniques was compared following ophthalmic surgery (Ripart et al., 2001). For placing the needle in the proper peribulbar space, the physician should watch for the movement of the lower lid until the needle hub touches the skin of eyelid. Approximately 8 mL of anaesthetic solution may be injected in both the sites, though peribulbar and retrobulbar injections are proven to be useful in analgesia, akinesia, control of intraocular pressure (Watkins et al., 2001) and postoperative analgesia but complications like diplopia, orbital haemorrhage, globe perforation, artery occlusion, brainstem anaesthesia, optic nerve trauma and ptosis have been reported (Davis and Mandel, 1994; Klein et al., 1982; Morgan and Clearkin, 2001; Roman et al., 1997; Wylie et al., 1994).

1.4.2.2.3. Sub-Tenon Injection

Tenon’s capsule is a fascial sheath of connective tissue sandwiched between conjunctiva and episcleral plexus. Episcleral or sub-tenon’s space is a void between tenon’s capsule and

sclera (Canavan et al., 2003). Sub-tenon injection places the drug in contact with sclera for longer periods due to its avascular nature. Drug solution administered by sub-tenon's injection has the disadvantages of decreased and difficult molecular penetration through the sclera and choroid. Moreover a rapid removal of the drug by the choroidal circulation can result in shortened duration of action. It is considered to be the most promising route for targeting posterior segment (Canavan et al., 2003).

1.4.2.2.4. Subconjunctival Injection

Conjunctiva is a membrane that covers sclera. A mucus layer secreted by the goblet cells of conjunctiva hydrates, lubricates, cleanses, and serves as a defense against pathogens. Injection of drug solution beneath the conjunctiva is considered a localized and minimally invasive drug delivery to the retina. About 500μL of a solution can be injected to the subconjunctival area (bulbar conjunctiva) using a 25/30 G needle, 30 mm long. Following a subconjunctival injection, molecules may directly diffuse through the sclera to reach the choroid (Kim et al., 2002). Significantly higher levels of bioactive protein was observed in the posterior segment of the rabbit eye following a subconjunctival infusion (Ambati et al., 2000). Prostaglandins are more permeable across the sclera relative to cornea (Bito and Baroody, 1981). High concentrations of dexamethasone were found in subretinal fluid of humans following subconjunctival injection compared to oral and peribulbar indicating that subconjunctival route may deliver greater amounts of drugs to the retina (Weijtens et al., 2000). Sustained delivery can be achieved in the posterior segment by using polymeric vehicles (Geroski and Edelhauser, 2001; Zignani et al., 2000). Many research articles

propound the use of subconjunctival injection for the posterior segment delivery because of its numerous advantages over other routes.

1.5. Novel Drug Delivery Systems

Drug delivery to the inner compartments of the eye is very challenging. Posterior segment access via non-invasive or minimal invasive techniques would be more patient compliant and will offer significant advantages in treating diseases like AMD, DME and PVR. Advancements in surgical techniques, chemical technologies, formulation strategies, and material science led to the development of novel drug delivery. This section briefly describes various novel delivery systems and their role in enhancing drug bioavailability in the posterior ocular segments.

1.5.1. Nanoparticles

Nanoparticles are colloidal systems with a size range of 10 to 1000 nm. They are classified into two types, nanospheres and nanocapsules. In nanospheres, drugs are either adsorbed or entrapped inside the polymeric matrix (Barratt, 2000). In nanocapsules, drugs are confined to the inner liquid core while the external surface of nanoparticles is covered by the polymeric membrane (Soppimath et al., 2001). They have been successfully employed as an alternative strategy for long term drug delivery to the posterior segment of eye. Pharmacokinetics and tolerance of dexamethasone loaded poly (lactic acid–co-glycolic acid) nanoparticles in rabbits following intravitreal injection was studied in rabbits (Zhang et al., 2009). They concluded that dexamethasone when encapsulated in nanoparticles exhibited sustained release for ~50 days and the release pattern was constant until 30 days with a concentration

of 3.85 mg/L. These results imply that intravitreal injection of dexamethasone nanoparticles may be utilized for sustained delivery of drugs for the treatment of posterior segment eye diseases (Zhang et al., 2009). Retinal levels of budenoside from PLA-nano/microparticles following subconjunctival administration was studied in Sprague-Dawley rats. They concluded that following subconjunctival injection both budesonide nanoparticles and microparticles produced sustained drug concentrations in various ocular tissues and the retina up to 1, 7, and 14 days (Kompella et al., 2003).

1.5.2. Microneedles

Microneedles are a novel strategy to deliver drugs into inner compartments by topical administration. This drug delivery strategy confers various advantages by reducing pain and tissue damage and results in more patient compliance. Moreover, due to the small needle size the device is predicted to avoid damage to nerves innervating tissues by injection (Jiang 2008).The microneedle as a drug delivery technique has been successfully demonstrated to deliver vaccines, polymer encapsulated drugs and peptides (insulin) via transdermal route (Gupta et al., 2009; Prausnitz et al., 2009; Wang et al., 2009). Studies by Jian and his co-workers have successfully demonstrated that macromolecules can be delivered employing microneedles to the inner ocular compartments via intra-scleral and intra-corneal routes (Jiang et al. AICHE Annual Meeting, Abstract 96395). *In vitro* experiments demonstrated that hollow microneedles can successfully deliver drugs in humans via intrascleral route. These experiments for the first time demonstrated that microneedles can efficiently deliver higher drug concentrations to inner ocular compartments in a minimally invasive manner

relative to traditional methods. *In vivo* studies using topical administration of drug loaded microneedles were also performed by Jiang et al. in rabbit model, which indicated a ~60 fold increase in fluorescein concentration in the anterior chamber compared to equivalent drug alone as control. Also, no cytotoxicity or tissue damage was observed in these studies.

1.5.3. Liposomes

Liposomes are lipid bilayer vesicular systems. They consist of one or more concentric lipid layers separated by a compartment consisting of aqueous buffer. Depending on the size, liposomes can be categorized into a) small unilamellar vesicles (10 – 100 nm), b) large unilamellar vesicles (0.1 – 10.0 μm) and c) large multilamellar vesicles (more than one lipid bilayer). Liposomes have been successfully employed as an alternative strategy for posterior segment delivery. Depending on this nature, hydrophilic or hydrophobic drugs can be suitably entrapped either in the aqueous phase or in the lipid phase (Mainardes and Silva, 2004). Liposomeswere used in the delivery of antivirals (Liu et al., 1987; Peyman et al., 1987), antibiotics (Fishman et al., 1986; Zeng et al., 1993), and cyclosporin (Alghadyan et al., 1988a; Alghadyan et al., 1988b) for retinal diseases. Liposomal delivery for the treatment of the back of the eye disease is known to improve drug efficacy and distribution and reduce their toxicity (Peyman and Ganiban, 1995). However, the commercial success of liposomes is limited by the short shelf life and difficulty in sterilization.

1.5.4. Dendrimers

Dendrimers are repeatedly branched synthetic macromolecules with a three dimensional nano-architecture (10 to 100 nm). They are highly versatile and can be controlled structurally

and compositionally by choosing different building blocks and surface functional groups during synthesis. A series of branches around an inner core create countless cavities within their structure which can hold therapeutic agents. High reactivity of dendrimers is mainly attributed to the presence of multiple functional groups on their surface such as amines, carboxylic acids or hydroxyl groups. These functional groups provide dendrimers an ability to conjugate multiple surface groups for biological recognition (Cheng et al., 2008). Wimmer and his colleagues have synthesized lipid–lysine dendrimers for improving the delivery of anti-VEGF ODN-1 into the nuclei of retinal cells. The oligonucleotide ODN1- dendrimers complexes showed good efficiency in transfecting human cells (D-407). *In vivo* studies in laser induced choroidal neovascularization (CNV) rat models revealed significant reduction in the severity of CNV. After intravitreal injection, these complexes remained active up to 2 months and maintained anti-CNV activity without any significant toxicity (Wimmer et al., 2002).

1.5.5. Implants

Although injectable drug delivery systems such as liposomes, micro- and nanoparticles are easy to administer but once injected it would be difficult to retract particles, in case of any complications such as toxic responses. Thus it could be advantageous to use implants instead, for controlling the rate and duration of drug release. Ocular implants can be removed as needed by surgical intervention. Ocular implants may be divided in to two broad categories depending on the polymer in the matrix:

- Nonbiodegradable implants (Musch et al., 1997; Sanborn et al., 1992): They are not metabolized to any significant extent and are not eroded *in vivo.*E.g. Ganciclovir nonbiodegradable implant for CMV retinitis, i.e., Vitrasert® (Chiron Vision).
- Biodegradable implants (Hashizoe et al., 1997; Kimura et al., 1994): They eventually degrade *in vivo* into soluble components by enzymatic and/or non-enzymatic processes. E.g. Dexamethasone implant for macular edema, i.e., Ozurdex™ (Allergan, Inc.)

Though implants overcome many of the disadvantages associated with intravitreal injections, surgical procedure and risk of drug precipitation due to poor solubility may cause side effects (Duvvuri et al., 2003)

1.5.6. Niosomes

Niosomes are bilayered non-ionic surfactant vesicles similar to liposomes. Niosomes are used in the entrapment of both hydrophilic and hydrophobic drugs either in aqueous and lipoidal vesicular membranes respectively (Kaur et al., 2004; Wadhwa et al., 2009). Alteration in the physical properties of niosomes results in different drug release profiles and and distribution pattern. Niosomal formulations of timolol maleate coated with chitosan or carbopol exhibited significant IOP lowering effect in rabbits compared to pure drug solution (Aggarwal and Kaur, 2005). Apart from having all the advantages of liposomes, low cost, greater stability and easy storage make these non-ionic surfactants a desired alternative for phospholipids.

1.5.7. Nanosuspensions

They are submicron colloidal dispersion consisting of a finely dispersed solid drug particles in an aqueous vehicle. Poorly water-soluble drugs often result in low bioavailability and erratic absorption profile. Nanosuspensions have emerged as an efficient drug delivery system for hydrophobic drugs due to their unique advantages and versatile features (Patravale et al., 2004). Nanosuspension technology reduces the particle size (ranging between 200-600 nm) of drugs and provides increased dissolution rate and enhanced bioavailability. Several drugs such as hydrocortisone, prednisolone and dexamethasone have been incorporated in nanosuspensions and used for ocular delivery. *In vivo* study in rabbits suggested that the nanosuspensions significantly enhanced the ocular bioavailability of glucocorticoids. Nanosuspensions also impart stability and produce sustained drug release. Nanosuspensions of cloricromene (AD6) prepared by using eudragit RS100 and RL100 enhanced the drug stability and bioavailability following ophthalmic application (Pignatello et al., 2006).

1.5.8. Ultrasound

Various physical methods including iontophoresis and sonophoresis have been employed for enhancing the drug concentrations in the eye. Sonophoresis involves the use of ultrasound for increasing the drug absorption and was initially utilized for enhancing systemic bioavailability of transdermally applied drugs. Unlike the conventional passive diffusion process, the ultrasound application enhances drug transport by either thermal effects (due to absorption of sound waves) or non-thermal effects (cavitation, microstreaming and acoustic streaming) (Cherkasov et al., 1974; Fielding, 1996; Filippenko and Tret'iak, 1989;

Gvarishvili and Dushin, 1999; Silverman, 2009). Cavitation is caused by formation of vapor bubbles in the region where liquid pressure falls below its vapor pressure (Miller, 1987). The vapor bubbles collapse forming a high speed jet in a small region which is capable of causing pits on the surface of biologic membranes (Tachibana and Tachibana, 2001; Tang et al., 2001; Zderic et al., 2004). Tsok and his co-workers have studied permeability of 99mTc-pertechnetate, ^{125}I, and $^{45}CaCl_2$ in the rabbit eye tissues including aqueous and vitreous humor, cornea, iris, sclera, crystalline lens, choroid and retina following ultrasound application in varying frequencies (127, 295, 470, 660, 880, 1000, 2750 kHz). Frequency plays a key role in determining drug permeability across various ocular tissues. Sonophoresis at a frequency of 470, 660, 880 kHz and intensities of 0.2 to 0.3 W/cm^2 produced a 10 fold enhancement in corneal permeability (Tsok et al., 1990). Ultrasound has the potential for increasing the ocular bioavailability and can be utilized as a minimally invasive method. But its clinical application is of great concern as the technique may result in structural alteration of the epithelial layer. Feasibility of ultrasound in a clinical setting requires a more complete and detailed safety study.

1.5.9. Iontophoresis

Iontophoresis is a non-invasive technique which involves the application of weak electric current to enhance penetration of ionized molecules across the tissue (Gurny et al., 1997). This technique has been extensively applied in transdermal delivery due to its ability to enhance drug penetration to target tissue thereby minimizing systemic side effects (Ferry, 1995). This technique is based on the principle of electrorepulsion (same charges repel) and

electro-osmosis (opposite charges attract). Iontophoresis requires a very low voltage (≤10 V) necessary to supply a continuous direct current of ≤0.5 mA/cm^2 (Singh and Maibach, 1994). Iontophoretic device consists of a power source, a milliampere meter, a rheostat and two electrodes (a drug delivery electrode and dispersive electrode). In ocular iontophoresis, an electrode containing drug solution is placed on the eye and an opposite electrode is placed on another body surface to complete an electrical circuit (Eljarrat-Binstock and Domb, 2006). The use of iontophoresis in ocular drug delivery was first investigated by a German scientist, Wirtz in the year 1908 (Eljarrat-Binstock and Domb, 2006). Recently, various ocular iontophoresis systems have been investigated like Ocuphor® (Iomed Inc., USA) (Parkinson et al., 2003), Eyegate II Delivery System® (EyeGate Pharma, USA) (Halhal et al., 2004), and Visulex® (Aciont Inc., USA) (Molokhia et al., 2009). All these devices contain either an eye cup filled with drug solution or saturated gel as a drug delivery probe (Eljarrat-Binstock and Domb, 2006). Iontophoresis can be applied for the treatment of anterior and posterior segment diseases either by transcorneal or transscleral application depending on the disease site (Roy, 2007). Transscleral iontophoresis delivers high drug concentrations into the posterior tissues of the eye including the vitreous and retina. In transscleral iontophoresis, the iontophoretic device is placed on the conjunctiva, over the pars-plana area to avoid electrical damage to the retina. It is considered as a potential alternative to multiple intravitreal injections for the treatment of posterior segment diseases including endophthalmitis, uveitis, retinitis, optic nerve atrophy, pediatric retinoblastoma and age-related macular degeneration. Apart from increasing ocular bioavailability,

transscleral iontophoresis eliminates various side effects associated with intravitreal and periocular injections such as retinal detachment, globe perforation, endophthalmitis and cataract (Molokhia et al., 2009). Nicoli and his co-workers have studied *in vitro* permeation of FITC-dextran (FD) of varying molecular weights (4-120 kDa) using transscleral iontophoresis on porcine and human sclera. From these reports it is apparent that iontophoresis can be applied as a potential tool for non-invasive delivery of drugs to the eye. This technique aids in maintaining therapeutic levels both in anterior and posterior segments (Nicoli et al., 2009). Although ocular iontophoresis has been extensively investigated during the last century, it was never accepted as a mainstay procedure for ocular drug delivery due to lack of toxicity data and controlled clinical trials.

CHAPTER 2

RATIONALE FOR INVESTIGATION

2.1. Overview

Drug delivery to the posterior ocular segment poses significant drug delivery challenges due to its unique anatomical and physiological barriers when compared to the anterior segment.The posterior segment of the eye requires site specific drug delivery systems to target RPE, choroid and sclera. Diseases affecting the posterior segment like age-related macular degeneration (AMRD), diabetic macular edema (DME), diabetic retinopathy (DR), cytomegalovirus (CMV), retinoblastoma, proliferative vitreoretinopathy (PVR) and uveitis can cause irreparable vision loss due to inadequate drug levels arising from poor delivery. Transport of molecules between vitreous or retina and systemic circulation is restricted by the blood retinal barrier (BRB) that is made up of retinal pigmented epithelium (RPE) and endothelial cells of the retinal blood vessels.

Corticosteroids are well known as effective anti-inflammatory agents (Nauck et al., 1998). Owing to their potent anti-inflammatory activity, these agents have gained considerable attention as therapeutic candidates for vision threatening retinal diseases AMRD, PVR and DME (Ciulla et al., 2004). Although intravitreal injections deliver molecules directly to the neural retina; adverse effects such as endophthalmitis, retinal detachment and hemorrhage, often result in poor patient compliance (Baum et al., 1982; Velez and Whitcup, 1999). An increase in the understanding of drug absorption mechanisms into the retina from local and systemic administrations has led to the development of various drug delivery systems such as

biodegradable and non-biodegradable implants, microspheres, nanoparticles and liposomes, gels and transporter targeted prodrugs. Such a diversity of approaches is an indication that there is still a need for optimized noninvasive or minimally invasive drug delivery systems for the eye. Though implants overcome many of the disadvantages associated with intravitreal injections, surgical procedure and risk of drug precipitation due to poor solubility may cause side effects (Duvvuri et al., 2003). Subconjunctival drug administration is considered to be a localized noninvasive method and a suitable alternative to intravitreal injections/implants (Geroski and Edelhauser, 2000). Entrapment of steroids in biodegradable nanoparticulate systems may be an alternative strategy for long term drug delivery to posterior segment. Nanoparticles can be further dispersed in PLGA-PEG-PLGA thermosensitive gels which may be conveniently injected subconjunctivally for sustained drug release. Moreover, thermogel systems also help in preventing recirculation back into anterior segment thereby slowing down conjunctival clearance. These systems can form a deposit above the sclera following subconjunctival injection and slowly release the actives for the treatment of posterior segment diseases.

2.2. Statement of Problem

Research into treatment modalities affecting vision is rapidly progressing due to the high incidence of diseases such as diabetic macular edema, proliferative vitreoretinopathy, wet and dry age-related macular degeneration and uveitis. Owing to their potent anti-inflammatory activity these agents have gained considerable attention as therapeutic candidates for vision threatening retinal diseases such as age-related macular degeneration,

proliferative vitreoretinopathy and diabetic macular edema (Ciulla et al., 2004). Steroid administration by conventional routes fail to achieve required therapeutic concentrations in the eye due to the presence of ocular barriers (Bourlais et al., 1998; Kristinsson et al., 1996) Though intravitreal injection directly delivers the compounds to the posterior segment of the eye, their inherent potential side effects like increased intraocular pressure, (Rhee et al., 2006) hemorrhage, (Ozkiris and Erkilic, 2005) retinal detachment, (Chen et al., 2007) cataract, (Thompson, 2006) endophthalmitis, (Jonas, 2006) lead to complications limiting long term therapy (Sanborn et al., 1992). Though implants overcome many of the disadvantages associated with intravitreal injections, surgical procedure and risk of drug precipitation due to poor solubility may cause side effects (Duvvuri et al., 2003). Subconjunctival drug administration is considered to be a localized noninvasive method and a suitable alternative to intravitreal injections/implants (Geroski and Edelhauser, 2000). However, subconjunctival administration may result in the dispersion of drug into anterior chamber. An ideal sustained drug delivery system for the treatment of DME should possess high entrapment efficiency, ability to deliver the drug in zero order fashion, easy to manufacture and a relatively non-invasive delivery route. Entrapment of steroids in biodegradable nanoparticulate systems may be an alternative strategy for long term drug delivery to posterior segment. Polylactide (PLA) and polylactide-co-glycolide (PLGA) are the most widely used biodegradable polymers that are approved by FDA. These polymers are hydrolyzed to form natural metabolites (lactic and glycolic acids) which are eliminated from the body through the Kreb's cycle (Giordano et al., 1995). Nanoparticles can be further

dispersed in PLGA-PEG-PLGA thermosensitive gels which may be conveniently injected subconjunctivally for sustained drug release. Moreover, thermogelling systems also help in preventing recirculation back into anterior segment thereby slowing down conjunctival clearance. These systems can form a depot above the sclera following subconjunctival injection and slowly release actives for the treatment of posterior segment diseases.

2.3. Objectives

I. To examine effect of particle size on the uptake of fluorescent labeled polystyrene nanoparticles (50, 100, 500 and 1000 nm) and delineate the size dependent internalization of these nanoparticles from basolateral side of ARPE-19 cell line.

II. To study the effect of preparation method (dialysis and O/W emulsion solvent evaporation methods) on the entrapment efficiency, surface morphology, particle size and *in vitro* release.

III. To study the effect of lactide/glycolide ratio on the entrapment efficiency, surface morphology, particle size and *in vitro* release rate.

IV. To study the effect of PLGA-PEG-PLGA thermosensitive gel on the *in vitro* release rate of steroids.

V. To develop and validate a fast and sensitive bioanalytical method for the quantitative determination of glucocorticoids in rabbit ocular matrices by liquid chromatography tandem mass spectrometry.

VI. To study the effect of PLGA-PEG-PLGA thermosensitive gel on the permeability of DEX from suspension and nanoparticulate formulations across excised sclera.

VII. To evaluate *in vivo* time dependent ocular bioavailability of DEX (i) alone (ii) nanoparticles suspended in a PLGA-PEG-PLGA thermosensitive gel, following subconjunctival administration, using ocular microdialysis technique in anesthetized rabbit model.

CHAPTER 3

NOVEL NANOPARTICULATE GEL FORMULATIONS OF STEROIDS FOR THE TREATMENT OF MACULAR EDEMA

3.1. Rationale

Macular edema (ME) is caused by central extravascular swelling of the macula resulting in a significant loss of visual activity. The pathology is primarily associated with the leakage of fluids (from retinal blood vessels) and deposition of lipids and proteins beneath the center of the macula resulting in swelling. A more detailed study at the cellular level revealed that hypoxia causes thickening of the basement membrane of vascular endothelium and reduction in pericytes count which support the lining of retinal blood vessels. This thickening gradually spreads and distorts the central vision (Ferris and Patz, 1983; Sigurdsson and Begg, 1980). ME is broadly classified into two types: cystoid macular edema (CME) and diabetic macular edema (DME). Ocular complications resulting from diabetes are the leading cause of adult blindness in the US. Vision loss in diabetic patients is primarily associated with DME. Currently, ME is treated with laser photocoagulation and corticosteroids. Depending on the condition of a patient, laser treatment at different wavelengths may also be indicated in the treatment of ME (Bandello et al., 2003). Laser treatment aids in suppressing further vision loss but may not repair lost vision. Corticosteroids are well known as effective anti-inflammatory agents (Nauck et al., 1998). Owing to their potent anti-inflammatory activity these agents have gained considerable attention as therapeutic candidates for vision threatening retinal diseases such as age-related macular degeneration, proliferative

vitreoretinopathy and diabetic macular edema (Ciulla et al., 2004). Treatment of the posterior segment requires localized drug delivery. In eye clinics corticosteroids are widely applied through local (eye-drops, ointments, implants and intravitreal injections) and systemic routes (oral and parenteral routes) (Kuppermann et al., 2007). Drug administration by conventional routes fails to achieve required therapeutic concentrations in the eye due to the presence of ocular barriers (Bourlais et al., 1998; Kristinsson et al., 1996). Though intravitreal injection directly delivers the compounds to the posterior segment of the eye, their inherent potential side effects like increased intraocular pressure, (Rhee et al., 2006) hemorrhage, (Ozkiris and Erkilic, 2005) retinal detachment, (Chen et al., 2007) cataract, (Thompson, 2006) endophthalmitis, (Jonas, 2006) lead to complications limiting long term therapy (Sanborn et al., 1992). Elimination therapy from the vitreous is governed by molecular weight and polarity. Intravitreal administration is found to be more suitable for high molecular weight (> 500 Da) compounds displaying longer half-lives (Maurice, 2001). Steroid administration to the posterior segment through implants is a promising strategy in the treatment of DME. Two corticosteroid based implants are available in the market which include triamcinolone acetonide (I-vation™ TA, SurModics) and fluocinolone acetonide implant (Retisert®, Bausch & Lomb). Though implants overcome many of the disadvantages associated with intravitreal injections, surgical procedure and risk of drug precipitation due to poor solubility may cause side effects (Duvvuri et al., 2003). Recently, the FDA has approved the intravitreal dexamethasone implant Ozurdex™ (administered via intravitreal injection) for the treatment of macular edema following branch or central retinal vein occlusion. However, it is

associated with many adverse effects such as increased intraocular pressure, conjunctival hemorrhage, conjunctival hyperemia, cataract, ocular hypertension and vitreous detachment (www.ozurdex.com) (Haller et al.). Subconjunctival drug administration is considered to be a localized noninvasive method and a suitable alternative to intravitreal injections/implants (Geroski and Edelhauser, 2000). A recent study demonstrated that subconjunctival injection of dexamethasone disodium phosphate is more effective in delivering dexamethasone into the subretinal fluid of patients compared to peribulbar injection or oral administration in patients suffering from rhegmatogenous retinal detachment (Weijtens et al., 2000). Hence, delivery of corticosteroids subconjunctivally may provide adequate therapeutic drug concentrations in the posterior segment (Geroski and Edelhauser, 2000). However, such treatments require frequent injections which need repeated clinical intervention. The other disadvantage of subconjunctival administration is dispersion of drug into anterior chamber. The effect of instillation volume on the absorption pathways was studied in albino rabbits following subconjunctival administration. The authors concluded that when injection volume was more than 200 μL most of the drug refluxed back into the anterior segment and absorption occurred via the corneal route (Conrad and Robinson, 1980). An ideal sustained drug delivery system for the treatment of DME should possess high entrapment efficiency, ability to deliver the drug in zero order fashion, be easy to manufacture and have a relatively non-invasive delivery route. Entrapment of steroids in biodegradable nanoparticulate systems may be an alternative strategy for long term drug delivery to posterior segment. Polylactide (PLA) and poly lactide-co-glycolide (PLGA) are the most widely used biodegradable

polymers that are approved by FDA. These polymers are hydrolyzed to form natural metabolites (lactic and glycolic acids) which are eliminated from the body through the Kreb's cycle (Giordano et al., 1995). Nanoparticles can be further dispersed in PLGA-PEG-PLGA thermosensitive gels which may be conveniently injected subconjunctivally for sustained drug release (Amrite and Kompella, 2005). Moreover, thermogelling systems also help in preventing recirculation back into anterior segment thereby slowing down conjunctival clearance. These systems can form a depot above the sclera following subconjunctival injection and slowly release actives for the treatment of posterior segment diseases.

As our approach is to deliver the drugs using nanoparticles, it is essential to know the optimum size of particles ideal for sustained release of drugs following subconjunctival administration. So as a part of preliminary studies we have examined effect of particle size on the uptake of fluorescent labeled polystyrene microspheres (0.05, 0.10, 0.5 and 1.0 μm) from basolateral side of ARPE-19 cell line. Further we have delineated the size dependent internalization of these nanoparticles from basolateral side of ARPE-19 cell line. Based on the results obtained we have procceded with the development of steroidal nanoparticles of optimum size using PLGA polymers. PLGA nanoparticles of steroids (DEX, HA and PA) were prepared by dialysis and O/W emulsion/solvent evaporation methods. Nanoparticles were evaluated for entrapment efficiency, surface morphology, particle size and *in vitro* release. Effect of lactide/glycolide ratio on the steroid release rate from the nanoparticles prepared by O/W emulsion/solvent evaporation method was investigated. Mechanism of drug

release from the nanoparticles was delineated. We have also investigated the effect of PLGA-PEG-PLGA thermosensitive gel on the release mechanisms of steroids from PLGA nanoparticles with optimum entrapment efficiency, drug loading, surface morphology, particle size and *in vitro* release characteristics. Finally, permeation studies of DEX from suspension and nanoparticulate formulations were carried out across excised sclera to delineate *ex vivo* drug release pattern.

3.2. Materials and Methods

3.2.1 Materials

Fluoresbrite™ carboxy BB microspheres (2.6% Solids-Latex) of varying sizes (0.05, 0.10, 0.5 and 1.0 μm) were purchased from Polysciences Inc., Warrington, PA. PLGA polymers, i.e. PLGA 50:50 (D,L-lactide : glycolide), molecular weight 45,000-75,000 Da, PLGA 65:35 (D,L-lactide:glycolide), molecular weight 45,000–75,000 Da, dexamethasone (DEX), hydrocortisone acetate (HA), prednisolone acetate (PA), polyvinyl alcohol (PVA, molecular weight 30,000–70,000 Da), tetrabutylammoniumhydrogen sulfate (TBAHS) and polyethylene glycol 1450 were procured from Sigma Chemicals (St Louis, MO). Hydroxyl propyl methyl cellulose (HPMC) - K4M premium grade was obtained from Dow Chemical Company. CellTiter 96® AQ_{ueous} Non-Radioactive Cell Proliferation Assay was obtained from Promega (Madison, WI). Dimethylformamide was obtained from American Scientific Products (Muskegon, MI). [^{3}H]-mannitol (specific activity: 50 mCi/mmol) a paracellular marker was purchased from Amersham Biosciences, Ltd. (Piscataway, NJ). Thermosensitive

gel PLGA-PEG-PLGA (weight average molecular weight [Mwb] - 4759 Da) was synthesized and purified in our lab.

3.2.2. Particle Size Analysis of Polystyrene Nanoparticles

A dynamic light scattering (Brookhaven Zeta Plus instrument, Holtsville, NY) technique was employed to measure the particle size and polydispersity values in triplicates. Size and polydispersity values are shown in Table 4.

3.2.3. Uptake Studies in ARPE-19 Cells Using Polystyrene Nanoparticles

In vitro uptake studies were performed on human RPE cell line ARPE-19 (passage no: 19) obtained from ATCC (American Tissue Cell Culture Collection). These cells were grown in 1:1 mixture of Dulbecco's modified Eagle's and Ham's F12 medium, with 15 mM HEPES buffer, 56 mM final concentration sodium bicarbonate and 2 mM l-glutamine, antibiotic mixtures of 100 U/mL penicillin G and 100 µg/mL streptomycin sulfate, 10% fetal bovine and incubated at 37 ^{o}C in 5% CO_2. Cells were plated on twelve well transwell inserts (diameter 12 mm) for 8-10 days. *In vitro* uptake studies were initiated by the addition of polystyrene nanoparticles of varying sizes in DPBS, pH-7.4 to the basolateral chamber. All experiments were performed at 37 °C. After incubation cells were washed 3 times with 1mL of ice-cold stop solution (210 mM KCl, 2 mM HEPES), to arrest uptake. After each wash cells were centrifuged and separated. Cells were then solubilized in 1mL of 0.1% Triton-X solution in 1% NaOH. Concentration was measured with the help of fluorescence spectrophotometer at 360 nm (excitation wavelength) and 407 nm (emission wavelength).

3.2.4. Development of PLGA Based Nanoparticles

3.2.4.1. Dialysis Method

PLGA based nanoparticles were prepared by dialysis method without the incorporation of any surfactant. Briefly, PLGA 50:50 and steroids (10:1 ratio by weight) were dissolved in 10 mL of dimethylformamide. The solution was introduced into a dialysis bag (MWCO – 3,500 g/mol) and dialyzed against 1L distilled water with continuous stirring at room temperature for 24 h. Water was replaced after every 3 h. The resultant suspension was centrifuged at 22,000 g for 60 min. The nanoparticles were freeze-dried over 48 h (Nah et al., 1998).

3.2.4.2. O/W Emulsion/solvent Evaporation

PLGA nanoparticles containing DEX, HA and PA were prepared by a single oil-in water (O/W) emulsion/solvent evaporation method with a minor modification (Kim and Martin, 2006). In order to maximize drug loading, PLGA (100 mg) was dissolved in dichloromethane (4 mL) and DEX or PA (16 mg) in 1 mL of acetone. DEX or PA in acetone was added to the PLGA in dichloromethane to form the organic phase. In a separate experiment, HA (16 mg) and PLGA (100 mg) were dissolved in 5 mL chloroform. Organic phase was slowly mixed with an aqueous solution containing 2.5%w/v PVA under continuous stirring (Vandervoort and Ludwig, 2002). An O/W type emulsion was formed upon sonication (Fisher 100 Sonic Dismembrator, Fisher Scientific) at a constant power output of 55W for 5 min. The sample was kept in an ice bath during sonication to prevent any overheating of the emulsion. It was stirred gently at room temperature for 12 h. Subsequently, nanoparticle suspension was exposed to vacuum for 1 h to ensure complete removal of organic solvents. Unentrapped

drug and PVA residue were removed by washing nanoparticles three times with distilled water. The resultant suspension was centrifuged at 22,000 g for 60 min. Nanoparticles formed were freeze-dried over 48 h.

3.2.5. Entrapment Efficiency of Drug

For measuring drug entrapment in nanoparticles, 2 mg of freeze-dried sample was dissolved in 2 mL of dichloromethane and mixed thoroughly for 24 h. After that these samples were then dried under inert atmosphere (nitrogen gas) and subsequently dissolved in 200 µL of acetonitrile: water (70:30) and centrifuged at 12,000 *g* for 10 min. The supernatant was aspirated for analysis of drug content by HPLC (Kompella et al., 2003). Entrapment efficiency and drug loading were calculated using Eqs. 1 and 2.

$$\text{Entrapment efficiency (\%)} = \frac{\text{(amount of drug remained in nanoparticles)}}{\text{(initial drug amount)}} \times 100 \qquad \text{Eq. 1}$$

$$\text{Drug loading (\%)} = \frac{\text{(weight of drug in nanoparticles)}}{\text{(weight of nanoparticles)}} \times 100 \qquad \text{Eq. 2}$$

3.2.6. *In vitro* Drug Release

Drug loaded nanoparticles (5 mg) were dispersed in 1mL isotonic phosphate buffer saline (IPBS), pH 7.4 and subsequently introduced into dialysis bags (MWCO - 6275 g/mol). PLGA 65:35 nanoparticles containing DEX, HA or PA were suspended in 1 mL of 23% w/w PLGA-PEG-PLGA aqueous polymer solution and then added to dialysis bags. The polymer solution inside the bags formed gels at 37 °C with exposure times over 30-60 seconds (Duvvuri et al., 2005). The dialysis bags were introduced into vials containing 10 mL IPBS

and 0.025% w/v sodium azide to avoid microbial growth and 0.02% (w/v) and tween 80 to maintain sink condition (Choi and Park, 2000; Duvvuri et al., 2006). The vials were placed in a shaker bath at 37 ± 0.5 °C and 60 oscillations/min. At regular time intervals 200 µL of samples were withdrawn and replaced with equal volumes of fresh buffer. Samples were analyzed by HPLC. Experiments were conducted in triplicate.

3.2.7. HPLC Analysis

High-performance liquid chromatography system (Waters 600 pump; Waters, Milford, MA, USA), equipped with a UV detector (RAININ, Dynamax, Absorbance Detector Model UV-C) and reversed-phase C8 column (5 µm, 100A, Microsrob, Woburn, MA, USA), was employed. All samples were analyzed by isocratic method with a mobile phase containing 10 mM TBAHS (pH 3.0) and 30% acetonitrile pumped at a flow rate of 1mL/min. The detector was set at a wavelength of 254 nm. The retention times of DEX, HA and PA were 16.2, 26.2 and 24.6 min respectively.

3.2.8. Drug Release Mechanism

Depending on the drug release pattern, various kinetic models (zero-order equation or Higuchi equation) were employed in the calculation of release rate constants. In the Higuchi equation (Eq. 3) the cumulative percentage of drug released was plotted against square root of time.

$$Q = K t^{1/2} \qquad \text{Eq. 3}$$

K is the apparent first order release rate constant and t represents time in hours. K values are calculated from data representing less than 60% release (Siepmann and Peppas, 2001). Zero-

order rate equation (Eq. 4) was employed for calculating the release rate constants from gel formulations.

$$Q = K_o t \qquad \text{Eq. 4}$$

K_o is the apparent zero order release rate constant and t represents time in hours.

3.2.9. Surface Morphology

Scanning electron microscopy (FEG ESEM XL 30, FEI, Hillsboro, OR) was employed for studying surface morphology. Freeze dried nanoparticles were attached to a double-sided tape, spray-coated with gold–palladium at 0.6 kV and examined under an electron microscope.

3.2.10. Particle Size

A dynamic light scattering (Brookhaven Zeta Plus instrument, Holtsville, NY) technique was employed to measure the particle size and polydispersity values in triplicate.

3.2.11. Differential Scanning Calorimetry (DSC)

DSC curves were obtained by a Thermal Analysis Instruments-DSC-60, Shimadzu Corporation. Samples (10-15 mg) were loaded in aluminum crucibles and subjected to a heating cycle from 25-350 °C with a heating rate of 10 °C/min. A steady stream of nitrogen gas was used for controlling the heating and cooling rates. Polymer samples, pure drugs and physical mixtures served as controls.

3.2.12. Storage Stability Studies

Lyophilized formulations of FDEX65:35, FHA65:35 and FPA65:35 were sealed in ampoules and stored at 4 °C. At regular time intervals samples were removed and analyzed for gelation behavior and entrapment efficiency.

3.2.13. LCMS/MS Analysis of Steroids

Quantification of steroids following topical/subconjunctival administration in various ocular tissues especially retina requires a rapid, sensitive and robust bioanalytical method. Analysis of glucocorticoid (GC) molecules (DEX, HA, and PA) is somewhat difficult, because of its lipophilic nature. Moreover, these lipophilic compounds are extensively distributed in tissue space resulting in very low biological matrix concentrations. Various analytical methods have been reported in literature to estimate GC concentrations in biological samples. These include high performance liquid chromatography (HPLC) (Glowka et al., 2006; Shibata et al., 1998), and gas chromatography (Rivero-Marabe et al., 2001; Shibasaki et al., 2008), radioimmunoassay (RIA) (Tunn et al., 1990) and capillary separations coupled with various detectors (Lemus Gallego and Perez Arroyo, 2003; Noe et al., 1998). HPLC technique utilizing ultra-violet (UV) detection suffers from disadvantages such as longer retention time, tedious extraction procedure and inadequate limit of quantitation (LOQ) (Frerichs and Tornatore, 2004). Though fluorescence and gas chromatography are highly sensitive they require derivatization steps which are time consuming (Glowka et al., 2006). RIA usually suffers from cross-reactivity and hence resulting in lack of adequate selectivity for GC (Ionita et al., 2009; Tunn et al., 1990). Recently, LC–MS/MS has been applied extensively

for the quantitative estimation of drugs in various biological matrices such as plasma, serum and urine due to its sensitivity, selectivity and reproducibility. To the best of our knowledge, no validated liquid chromatography–tandem mass spectrometry (LC–MS/MS) method has been reported in literature for the quantitative estimation of corticosteroids in ocular matrices and vitreous humor samples. In particular, tandem triple-quadrupole mass spectrometry in the multiple reaction monitoring modes provides uncompromised sensitivity and selectivity (Ismaiel et al., 2007). The aim of the present study is to develop and validate a selective, rapid, rugged and reproducible LC–MS/MS assay for the quantitative determination of corticosteroids in ocular tissue matrices. This method is successfully validated and applied to the quantitative determination of DEX in rabbit ocular tissues following topical administration in a novel mixed micellar eye drop formulation. DEX, PD and HD structures are shown in Fig 11.

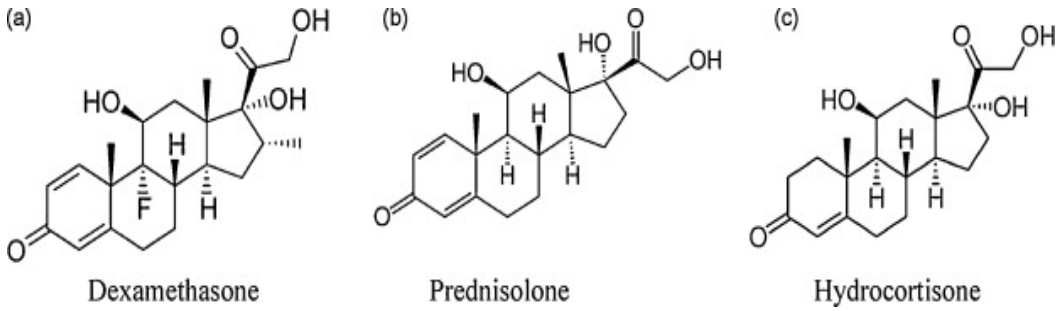

Fig. 11. Corticosteroid chemical structures (A) DEX, (B) PD and (C) HD with parent molecular weights: 392.464, 360.444, and 362.465 Da respectively.

3.2.13.1. Preparation of Stock and Standard Solutions

DEX, PD and HD stock solutions were prepared at 1 mg/mL in methanol. Calibration curve dilutions (30.88, 24.70, 19.79, 14.83, 9.63, 5.30, 1.59, 0.55 and 0.14 µg/mL) and quality control (QC) dilutions (24.70, 14.83, 5.30, 1.59, 0.55 and 0.14 µg/mL) consisting of DEX and PD were prepared in 20% (v/v) methanol. Stock dilution of internal standard (HD) at 10 µg/mL was prepared in 20% (v/v) methanol in water. All the solutions were stored at −80 °C until further use.

3.2.13.2. Liquid-Chromatographic Operating Conditions

Chromatographic analysis was carried out on API 2000 triple quadruple linear ion Qtrap mass spectrometer. High performance liquid chromatographic system consists of Agilent 1100 LC Quaternary pump, Agilent 1100 well plate, autosampler (Agilent technologies, Wilmington, DE) with a reversed phase gemini C18 column (50 mm × 4.6 mm i.d., 5 µm, Phenomenex, Torrance, CA). Isocratic mobile phase composed of 30% of acetonitrile in water containing 0.1% of formic acid, was at a flow rate of 0.2 mL/min.

3.2.13.3. Mass Spectrometer Operating Conditions

MDS Sciex API 2000 Triple Quadrupole linier QTrap mass spectrometry (Applied Biosystems/MDS Sciex, Faster City, CA) system interfaced by turbo ion spray (TIS) with positive ion source in MRM mode was applied for detection. Ultra high pure nitrogen served as collisionally activated dissociation (CAD) at 4 psi and curtain gas at 20 psi. Nebulizer and turbo gas were optimized at 40 and 50 psi respectively. The TIS temperature was maintained at 200 °C, with source voltage and dwell time optimized at 5200 V and 400 ms respectively.

Mass dependent parameters were tuned and optimized for DEX, PD and HD. Parent and daughter ions obtained by direct infusion mode (10µL/min) was injected with built-in Harvard infusion syringe pump and were optimized.

3.2.13.4. Preparation of Reference Standard Solution

Reference standard solution (600 ng/mL) was prepared from stock solutions of DEX and PD by adding 25 µL of 10 µg/mL IS stock dilution. System performance test was conducted by injecting six replicate injections of reference standard solution every day and validation parameters were checked. Percentage of coefficient of variation (%CV) was calculated before each run and found to be less than 4.0%.

3.2.13.5. Preparation of Calibration Curve (CC) and Quality Control (QC) Standards

Validation parameters were carried out according to FDA May 2001 guidelines. LLOQ was considered as 2.70 ng/mL for DEX and 11.00 ng/mL for PD. ULOQ was considered to be 617.60 ng/mL for both DEX and PD. Working calibration curve dilutions were spiked at 0.2% (v/v) in a homogenized rabbit ocular tissue matrix and ocular fluids to obtain various (617.60, 494.00, 395.20, 296.60, 192.60, 106.00, 31.80, 11.00 and 2.70 ng/mL for DEX) spiked CC standards. High QC (494.00 ng/mL), middle QC (296.60 ng/mL), other middle QC (106.00 ng/mL), low QC (11.00 ng/mL) and LLOQ QC (11.00 ng/mL for PD and 2.70 ng/mL for DEX) standards were also prepared in a similar manner.

3.2.13.6. Procedure for Ocular Matrix and Fluid Sample Preparation and Extraction

Homogenized rabbit ocular matrices and fluid samples were thawed at room temperature and vortexed. Using calibrated pipettes, 100 µL of samples were aliquoted into a 1.5 mL

polypropylene microcentrifuge tubes (PPMCT), followed by addition of 25 µL of 10.0 µg/mL freshly prepared IS solution to all samples, except for blank. These solutions were vortexed for 30 s, to which 50 µL of 20% (v/v) perchloric acid was added, and again vortexed for 30 s to precipitate protein. The samples were extracted by the addition of 1000 µL of methyl tertiary butyl ether (MTBE) followed by vortexing for approximately 2 min. After centrifugation at 12,000 rpm at 4 °C for 25 min, 850 µL of organic layer was transferred to a pre-labeled fresh 1.5 mL of polypropylene microcentrifuge tube and evaporated in the Speed Vac® at 35 °C for 60 min. The residue was reconstituted with 100 µL of mobile phase, vortexed for 30 s and transferred into a pre-labeled HPLC autosampler vial with silanized inserts. A 25 µL of the resulting solution was injected into LC–MS/MS.

3.2.13.7. Method Validation Tests

3.2.13.7. 1. Selectivity

Selectivity was performed by analyzing the blank ocular matrix samples from six different rabbit sources. Matrix interference with retention times of DEX, PD and IS (HD) were evaluated with LLOQ concentration. Six samples were injected into LC–MS/MS to determine selectivity for blank. Peak areas of blank interferences should not be more than 20% of mean peak area of LLOQ of DEX and PD and should not be more than 5% of mean peak area of HD samples.

3.2.13.7. 2. Sensitivity and LLOQ Evaluation

Sensitivity was achieved by analyzing spiked and processed LLOQ to samples from selected/screened blank matricies. Six LLOQ samples were injected into LC–MS/MS to determine LLOQ sensitivity for DEX and PD.

3.2.13.7. 3. Precision and Accuracy

Method validation was performed according to most recent recommendation outlined by the FDA in May 2001. Three precision and accuracy batches containing calibration curve standards and six replicates of QC standard samples at four concentration levels were performed in rabbit ocular tissue matrices as well as in normal phosphate buffer samples were extracted and analyzed in three different runs along with one standard zero (blank without IS) and one standard blank (blank with IS) (one used to check the interference contribution at the retention time of analytes).

3.2.13.7. 4. Within-Run and Between-Run Variability

In the case of within-run evaluation a minimum of six QC at each concentration levels were analyzed with one calibration curve standards in one single precision and accuracy batch. For the between-run at least eighteen QC at each concentration level were analyzed in at least three different precision and accuracy batches in three different days.

3.2.13.7. 5. Ruggedness Batch

One set of calibration curve along with six replicates of QC standard samples at four concentration levels were retrieved from −80 °C freezer, processed and analyzed. The batches were processed according to the extraction method described previously by another

analyst or by a different HPLC column (without altering the chemistry and brand of the column).

3.2.13.7. 6. Bench-Top Stability

The spiked calibration curve and QC standards samples were stored at −80 °C. Low and high QC (n = 6) were retrieved from −80 °C freezer and these kept at room temperature on bench top for 6 h. The stability samples were processed and extracted along with the freshly spiked calibration curve standards.

3.2.13.7. 7. Freeze-Thaw Stability

Low and high QC samples (n = 6) were retrieved from −80 °C freezer after three freeze–thaw cycles according to the FDA guide lines. The stability samples were processed and extracted along with the freshly spiked calibration curve standards.

3.2.13.7. 8. Extraction Recovery

Extraction recovery of DEX and PD was determined by analysis of six replicates at low and high QC standards samples concentration for DEX and PD and at one concentration for the IS HD. Absolute extraction recovery was determined by comparing peak areas of the analytes obtained from the extracted QC ocular matrix samples to unextracted standards (postspiked). A relative extraction ratios was determined by comparing peak area ratios of the analytes to internal standard obtained from the extracted QC (ocular matrix samples versus unextracted standards).

3.2.14. Tissue Preparation

Adult New Zealand male rabbits weighing between 2 and 2.5 kg were obtained from Myrtle's Rabbitry (Thompson Station, TN). All procedures were approved by the Institutional Animal Care and Use Committee (IACUC) of University of Missouri- Kansas City (UMKC, Kansas City, MO). Rabbits were anesthetized with intramuscular administration of ketamine HCl (35 mg/kg) and xylazine (5 mg/kg). Animals were euthanized by an overdose of sodium pentobarbital (100 mg/kg) administered through marginal ear vein under deep anesthesia. Eyes were removed carefully; then excised and the posterior segment was separated by cutting along the corneal-scleral limbus junction. Tissue segments were separated and the sclera was placed in a petri dish containing Dulbecco's phosphate buffered saline. The superotemporal region of each globe was retained, avoiding the vortex veins, the anterior ciliary perforating vessels and tissue closer than 2 mm to the optic nerve.

3.2.15. Permeability Studies

The excised tissue was mounted on a Franz-type vertical diffusion cell (PermeGear Inc., Hellertown, PA) for carrying out permeability studies. The episcleral side was placed towards the donor chamber on which the drug depot was placed. The receptor chamber was filled with IPBS containing sodium azide. An aliquot (300 μL) was withdrawn at regular time intervals and replaced with equal amounts of fresh buffer. All the experiments were carried under sink conditions. Histological examination and [^{3}H]-mannitol permeability studies across sclera were carried out to observe the basic changes in the anatomy of the

sclera tissues. [^{3}H]-mannitol permeability samples were transferred in to scintillation vials, mixed with 5 mL scintillation cocktail and analyzed for radioactivity. All the permeability studies were carried out in triplicate.

Permeability (P_{app}) of the drug from suspension and formulations was calculated using Eq. 5.

$$\text{Permeability } (P_{app}) = \text{Flux}/C_d \qquad \text{Eq. 5}$$

Flux (J) is calculated by dividing the slope obtained by plotting cumulative amount of drug permeated (M) through the sclera vs time (t) with cross sectional area of the membrane (A) exposed to the drug. C_d is the initial drug concentration in the donor chamber.

3.2.16. *In vitro* Recoveryof Probes for DEX

The recovery rate of DEX was measured from individual probes by immersing the probes in 1 mL (50 µg/mL of DEX in IPBS) in ependorff tubes. The probes were continuously perfused at constant flow rate of 2 µL/min. The recovery of DEX was calculated by Eq. 6.

$$\hat{C}_{in} = \hat{C}_{out}/\text{Recovery}_{\text{ in vitro}} \qquad \text{Eq. 6}$$

$\hat{C}_{out}$ is the drug concentration in the sample collected and $\hat{C}_{in}$ is the concentration in aqueous or vitreous humor. The recovery of DEX was found to be 4.05 ± 0.37%.

3.2.16. Anesthetized Animal Model

Briefly, rabbits were anesthetized with ketamine hydrochloride (35 mg/kg) and xylazine (3.5 mg/kg) administered intramuscularly. To the right eye of anesthetized rabbits a drop of tetracaine (0.5 %) was administered, which was followed by topical instillation of 25% povidone iodine. After five minutes, the eye was proptosed and a 25G needle is inserted diametrically across the posterior chamber ~3–4 mm below the limbus on the nasal side.

Upon exiting, the outlet end of the linear probe was carefully placed into the needle at bevel edge. It was then slowly pulled back leaving the dialysis membrane of the probe (center part) within the sphere of mid vitreous. The probe was carefully placed so that the entire membrane area lies at the center of vitreous chamber, slightly angled, before suturing. This prevents the contact between the probe and the lens. After probe implantation, the animals are allowed to stabilize for 2 h. Intermittently, the probes are perfused with IPBS, pH-7.4 at a flow rate of 2µL/min using CMA/100 microinjection pump. This duration has been shown to be sufficient for the restoration of intraocular pressure and replenishment of the vitreous humor originally lost during probe implantation. Rabbits were briefly anesthetized before subconjunctival administration and then microdialysis samples were collected at 2 mL/min every 60 min for 10 h. The dialysis samples were analysed for drug content using LCMS/MS technique.

3.3. Results

The particle size of fluorescent labeled polystyrene microspheres (0.05, 0.10, 0.5 and 1.0 µm) was determined by using dynamic light scattering technique. The values were summarized in Table 4. From the concentration dependent uptake studies it was clearly evident that the concentration of 0.050 µm particles increased linearly with increasing concentration, while 0.10, 0.50, 1.0 µm particles exhibited saturation at 500 µg/mL (Fig. 12). So, further time, temperature and pH dependent uptake studies were carried out at 250 µg/mL. Time-dependent uptake of different size polystyrene microparticles was carried out at 250 µg/mL. Uptake of nanoparticles increased with time (Fig. 13). However, after 60 min no significant

increase was observed with 0.10, 0.50, and 1.0 μm particles. Thus, further temperature and pH dependent uptake studies were carried out at 250 μg/mL for 30 min. The effect of pH on the uptake of polystyrene microparticles was carried at pH's 3.4, 5.4 and 7.4 for 30 min. Uptake of 0.05, 0.10, and 0.50 μm particles increased with increase in pH, while uptake of 1.0 μm particles was found to be highest at pH 5.4 (Fig. 14). The uptake of polystyrene microspheres was carried at three different temperatures (4, 25, and 37^{o}C). Uptake of microspheres increased with temperature (Fig. 15). Particle uptake mechanisms were studied using various inhibitors such as 10 mM sodium azide or 0.2 mM 2,4- dinitrophenol (metabolic inhibitors) in a glucose-free DPBS at 37 °C, 10 μM cytochalasin D (actin inhibitor) and 10 μM colchicine (depolymerizes microtubules) and nystatin 5 μg/mL (caveolin pathway inhibitor). Sodium azide, 2,4-dinitrophenol and cytochalasin D inhibited the uptake of microspheres (Figs. 16 and 17). However, uptake of 1 μm particles was inhibited nystatin which is a caveolin pathway inhibitor (Fig. 17). This indicates that particles of size ~1 μM enter the cells via caveolin mediated pathway while the lower size particles enter the cells via endocytotic process. The diameter of collagen fibers in the sclera is variable and ranges between 30-300 nm (Komai and Ushiki, 1991). Moreover the center-to-center spacing varies between 250-280 nm and the lamellae run parallel roughly from anterior to posterior (Fig. 18). Based on these studies we have concluded that the particles of size ~200 nm may be optimum for sustained delivery of drugs to RPE following subconjunctival injection. Further, steroidal nanoparticles of optimum size (~200 nm) were

synthesized and their, entrapment efficiency and *in vitro* release properties were characterized.

Emulsion/solvent (O/W) evaporation method resulted in higher steroid entrapment efficiencies compared to the dialysis method. Nanoparticle entrapment efficiencies for DEX, HA and PA by dialysis method with PLGA 50:50 were found to be low (5-15 %). Table 5 represents the experimental values of entrapment efficiencies and drug loading. Although, steroids are fairly lipophilic (LogP values between 1.6-1.8) entrapment efficiency and drug loading values by dialysis method were unexpectedly low (Table 5). Nanoparticles prepared by the dialysis method exhibited a biphasic release pattern and could not sustain the release of DEX, HA and PA over extended time periods. DEX was completely released from nanoparticles within 48 h. In case of HA and PA the release was observed over 96 h.

Table 4. Particle size values of fluorescent labeled polystyrene microspheres

Size (nm) as per manufacturer	Experimental Size (nm)	Polydispersity
50	51.7	0.099
100	85.3	0.040
500	473.5	0.008
1000	965.4	0.022

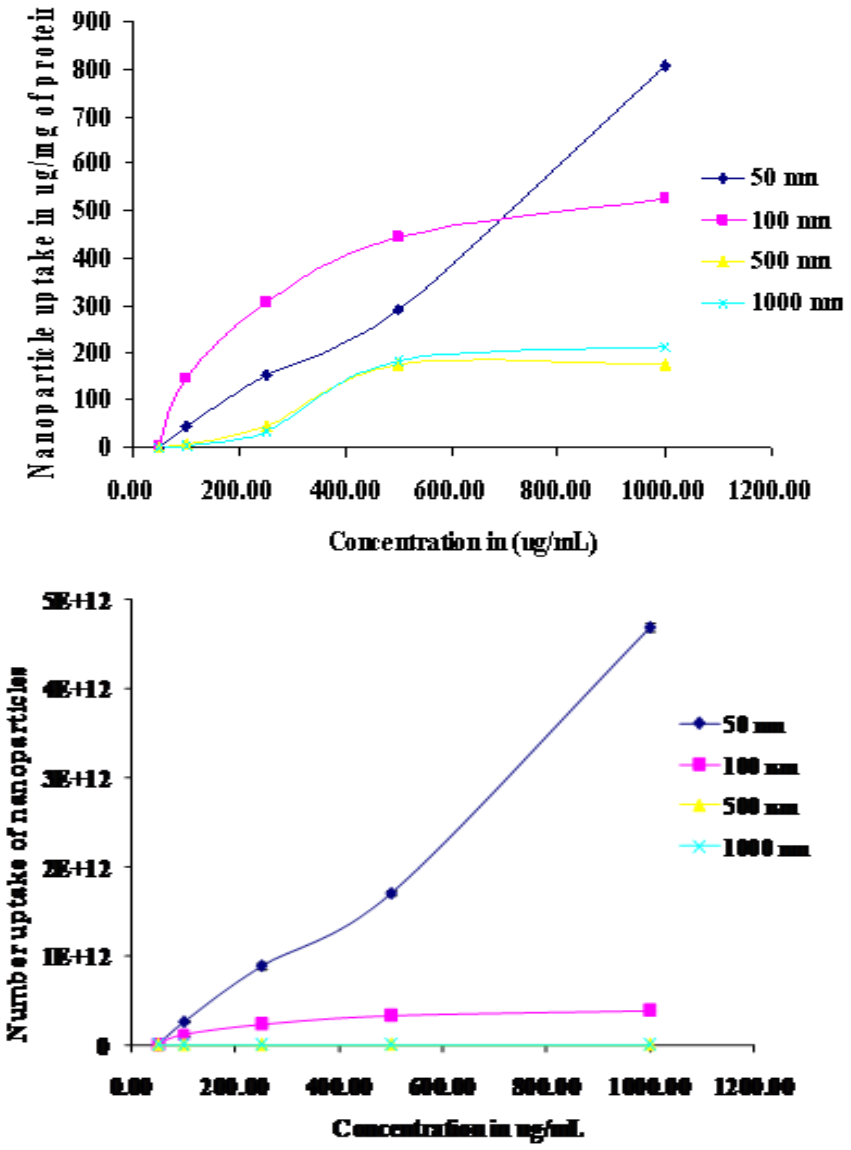

Fig. 12. Concentration dependent uptake of different size (0.05, 0.10, 0.50 and 1.00 µm) polystyrene microparticles from basolateral side of ARPE-19 cell line

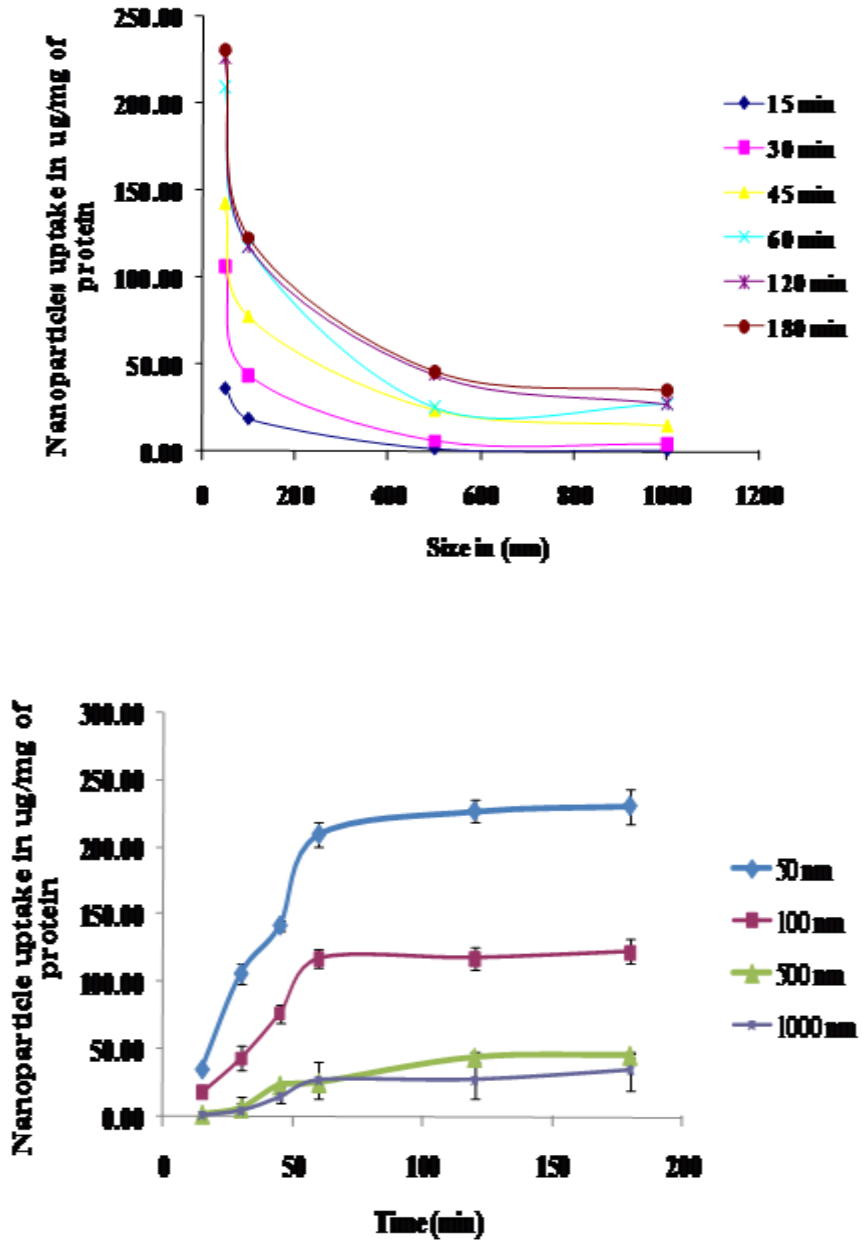

Fig. 13. Time-dependent uptake of different size (0.05, 0.10, 0.50 and 1.00 µm) polystyrene microparticles from basolateral side of ARPE-19 cell line

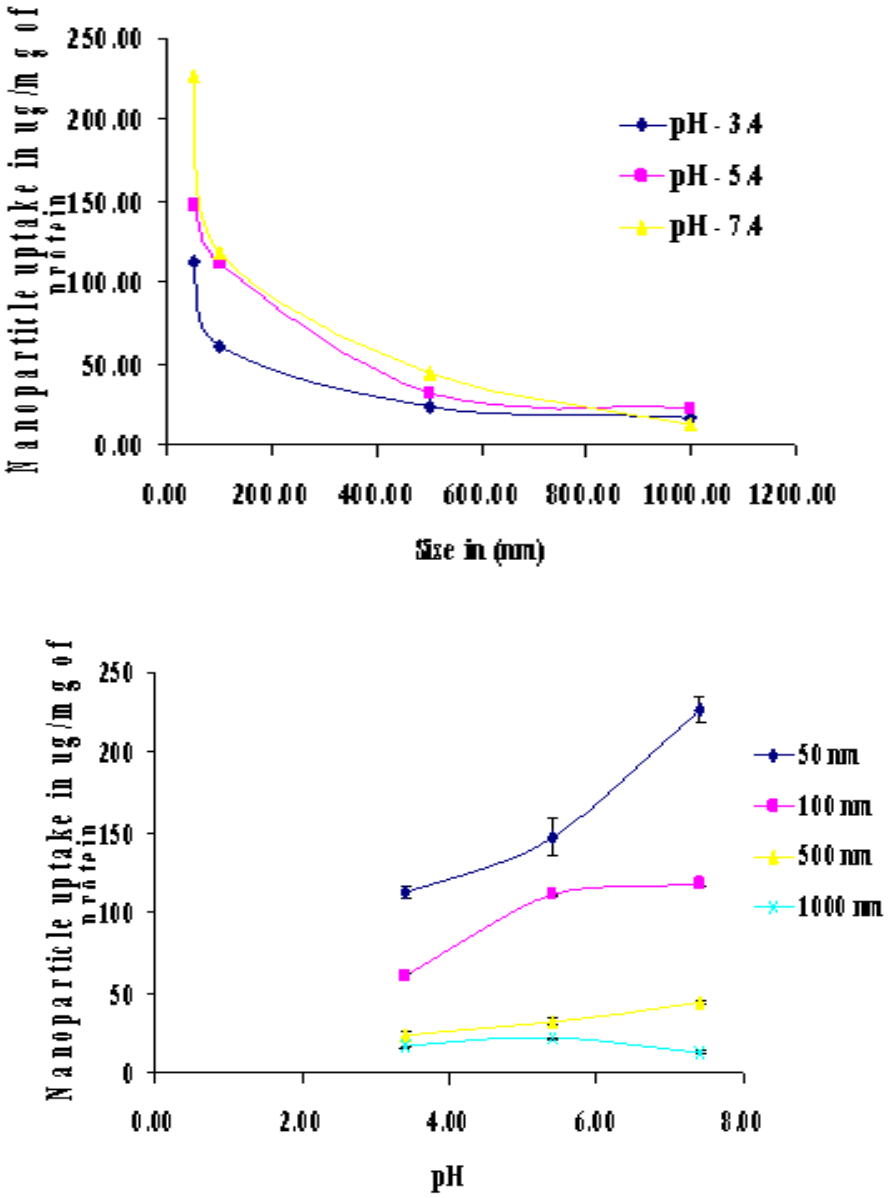

Fig. 14. pH dependent uptake of different size (0.05, 0.10, 0.50 and 1.00 µm) polystyrene microparticles from basolateral side of ARPE-19 cell line

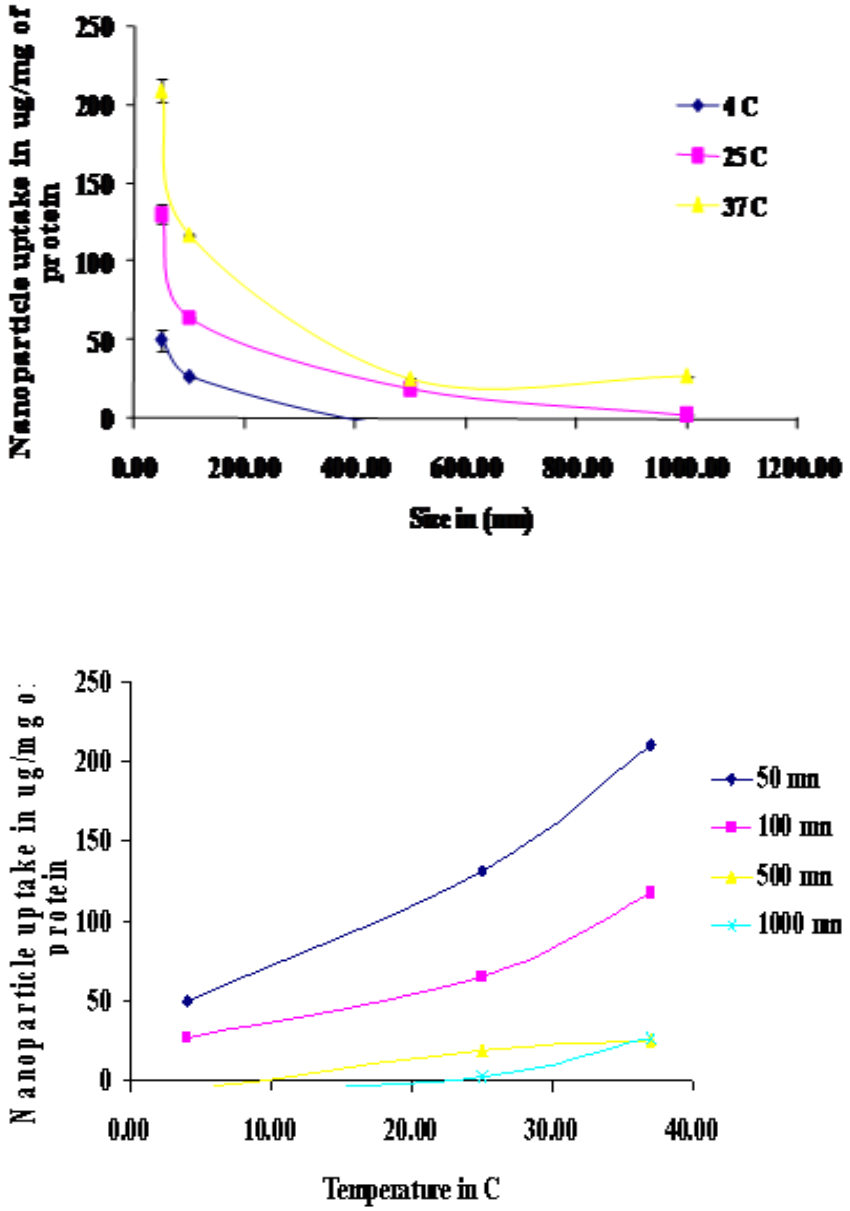

Fig. 15. Temperature dependent uptake of different size (0.05, 0.10, 0.50 and 1.00 µm) polystyrene microparticles from basolateral side of ARPE-19 cell line

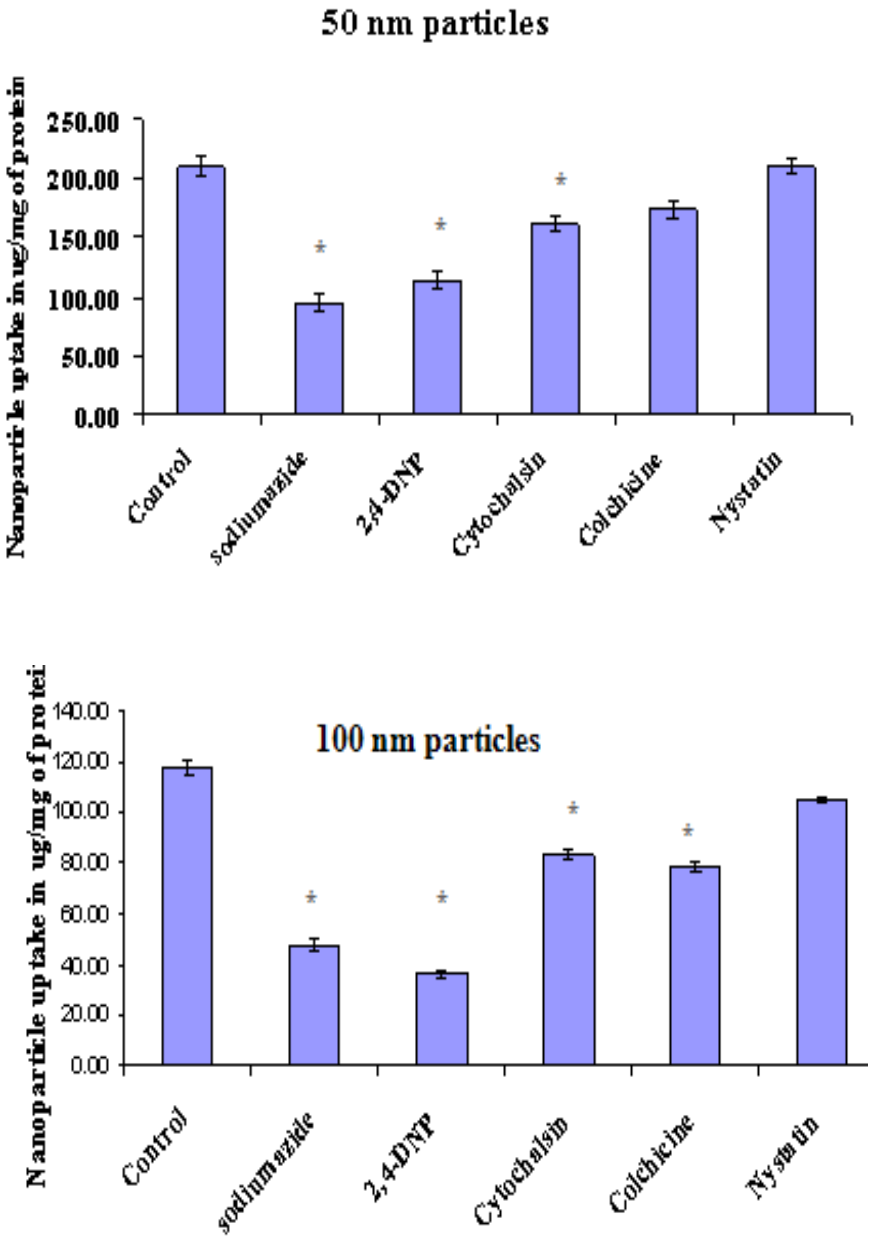

Fig. 16. Uptake of different size (0.05 and 0.10 µm) polystyrene microparticles from basolateral side of ARPE-19 cell line in presence of inhibitors

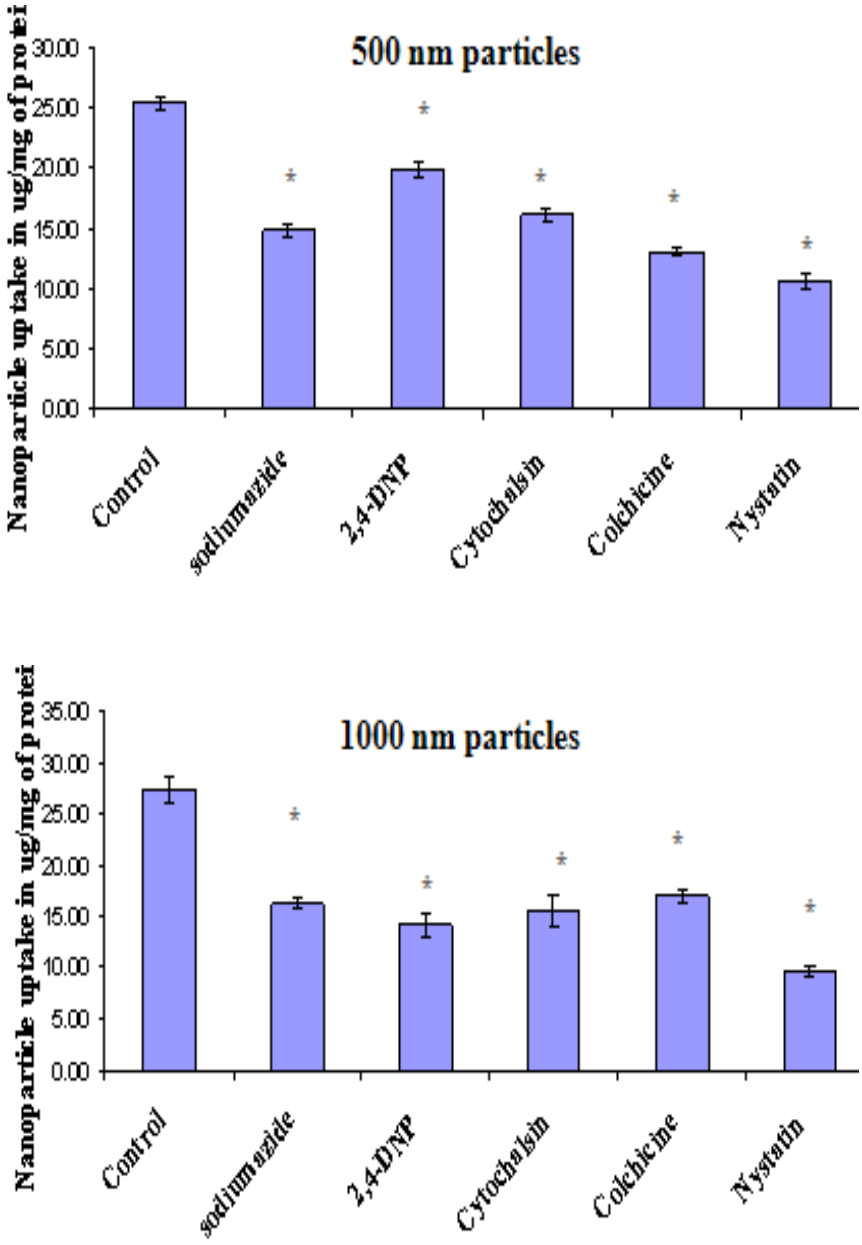

Fig. 17. Uptake of different size (0.50 and 1.00 µm) polystyrene microparticles from basolateral side of ARPE-19 cell line in presence of inhibitors

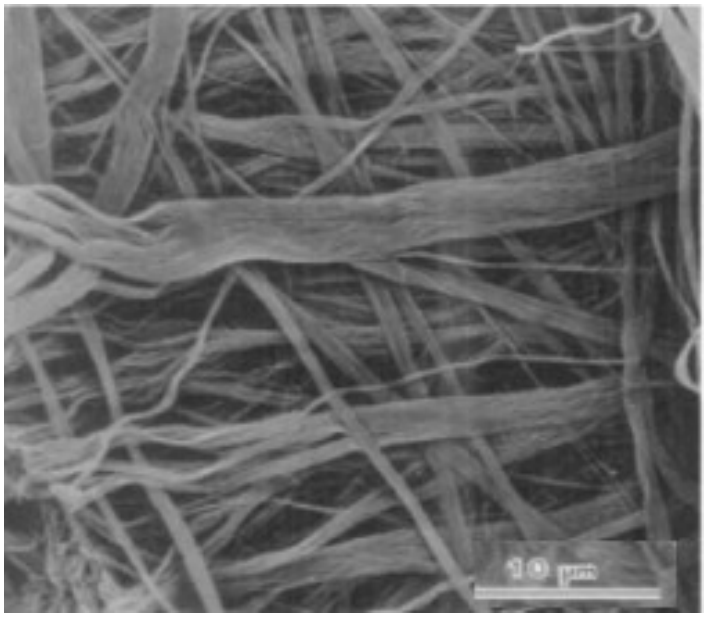

Fig. 18. TEM image of sclera, Courtesy*:* This figure has been modified from (Komai and Ushiki, 1991)

Table 5. Entrapment efficiency of nanoparticles prepared by dialysis method and O/W emulsion/solvent evaporation method

Drug	**Dialysis method**		**O/W emulsion/solvent evaporation method**			
	PLGA 50:50 (mean±S.E.M)%	**DL (%)**	**PLGA 50:50** (mean±S.E.M)%	**DL (%)**	**PLGA 65:35** (mean±S.E.M)%	**DL (%)**
DEX	7.2±3.5	0.71±0.11	77.3±4.4	10.1±1.1	76.6±3.1	9.9±2.2
HA	12.1±2.7	1.19±0.39	91.3±3.5	11.2±1.5	92.3±2.9	12.1±1.4
PA	14.3±1.3	1.40±0.24	92.3±5.1	10.9±1.2	94.3±3.3	11.1±0.9

DL: drug loading, S.E.M: Standard error of Mean

Table 6. Particle size and polydispersity values of nanoparticles prepared by dialysis method and O/W emulsion/solvent evaporation method

Drug	Dialysis method		O/W emulsion/solvent evaporation method			
	PLGA 50:50		PLGA 50:50		PLGA 65:35	
	Particle size (nm) mean±S.E.M	Polydispersity	Particle size (nm) mean±S.E.M	Polydispersity	Particle size (nm) mean±S.E.M	Polydispersity
DEX	216±4	0.10	204±4	0.057	203±3	0.033
HA	251±3	0.09	226±3	0.040	214±2	0.019
PA	237±6	0.12	183±1	0.047	193±2	0.005

S.E.M: Standard error of Mean

Dialysis method resulted in various sizes ranging between 200-250 nm with unimodal size distribution and fairly high polydispersity values (Table 6). Release data of DEX, HA and PA was plotted according to Higuchi equation for estimating the release rate constants which were found to be 16.0, 5.4 and 7.10 $h^{-1/2}$ for DEX, HA and PA respectively (Table 7). Release profiles of DEX, HA and PA are illustrated in Fig 19. Drug release data was fitted into Koresmeyer-Peppas equation (data not shown). A better linear regression coefficient was obtained by plotting the release data according to Higuchi model (Eq. 3) relative to Koresmeyer-Peppas model. O/W emulsion/solvent evaporation method resulted in higher entrapment efficiency ranging between 70-95% for DEX, HA and PA. PVA was added as a stabilizing agent in the preparation of nanoparticles as it is known to considerably reduce the size of nanoparticles (Vandervoort and Ludwig, 2002). O/W emulsion/solvent evaporation method resulted in nanoparticles with unimodal size distribution (Fig. 20). The mean particle size of steroid nanoparticles (~ 200 nm) and polydispersity values are shown in Table 6. Entrapment efficiency and particle size did not change appreciably with lactide/glycolide ratio (PLGA 50:50 and PLGA 65:35) in the polymers. The polydispersity values were found to be close to zero. Emulsion/solvent (O/W) evaporation method resulted in uniform size particles with significant increase in entrapment efficiency and drug loading as compared to the nanoparticles prepared by dialysis method. Further characterization studies were carried out for the nanoparticles prepared by O/W emulsion/solvent evaporation method. SEM pictures (Fig. 21) confirm the size uniformity and spherical shape of the particles with a smooth surface texture.

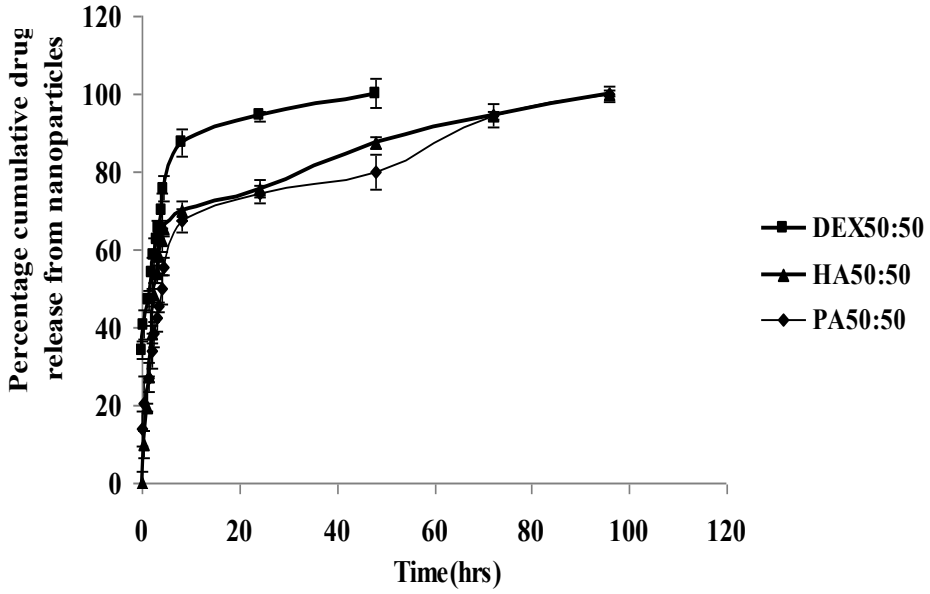

Fig. 19. Release profiles of DEX, HA and PA from nanoparticles prepared by dialysis method

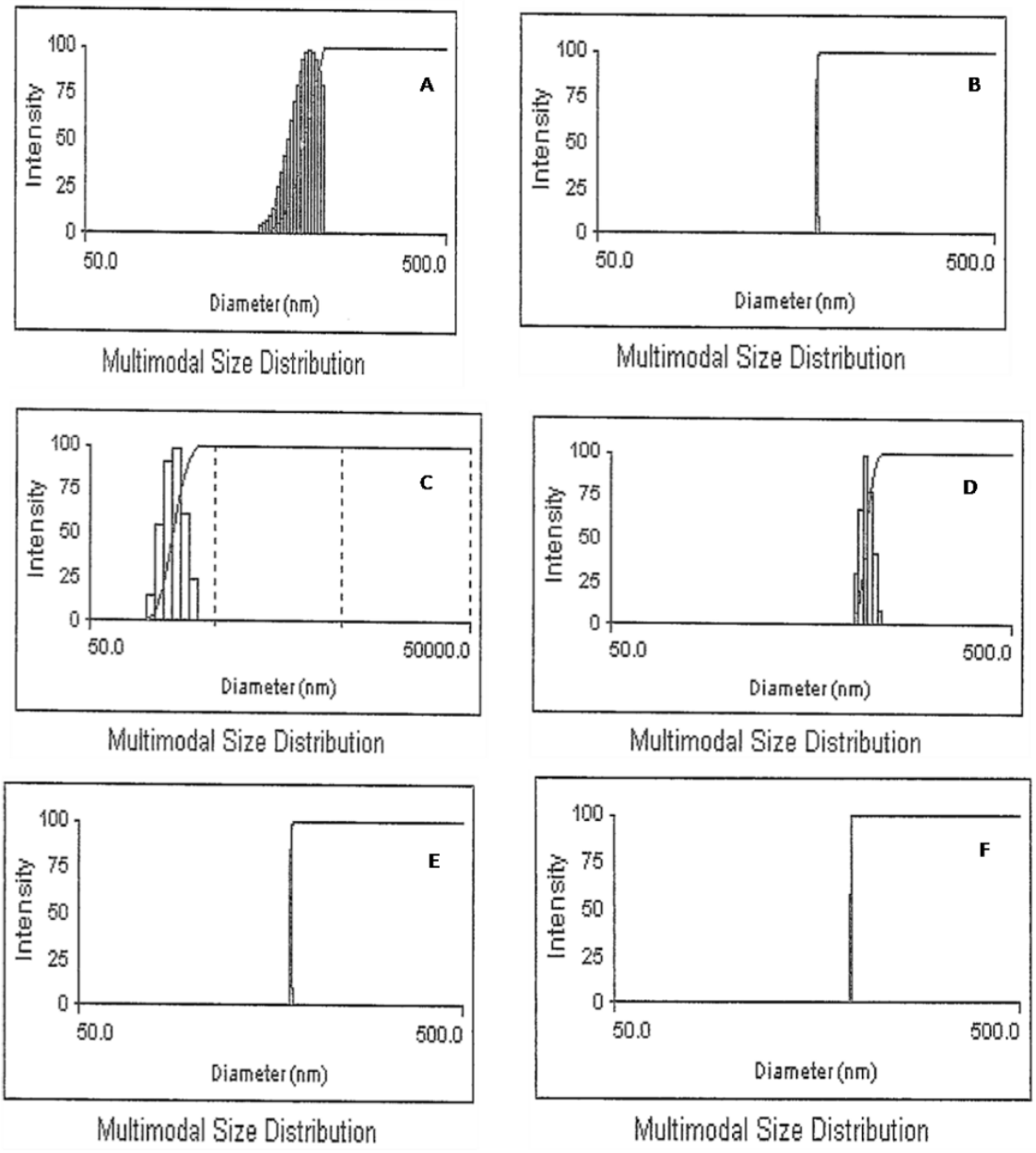

Fig. 20. Particle size distribution curves of nanoparticles prepared by O/W emulsion/solvent evaporation method. (A) DEX 50:50, (B) DEX 65:35, (C) HA 50:50, (D) HA 65:35, (E) PA 50:50, (F) PA 65:35

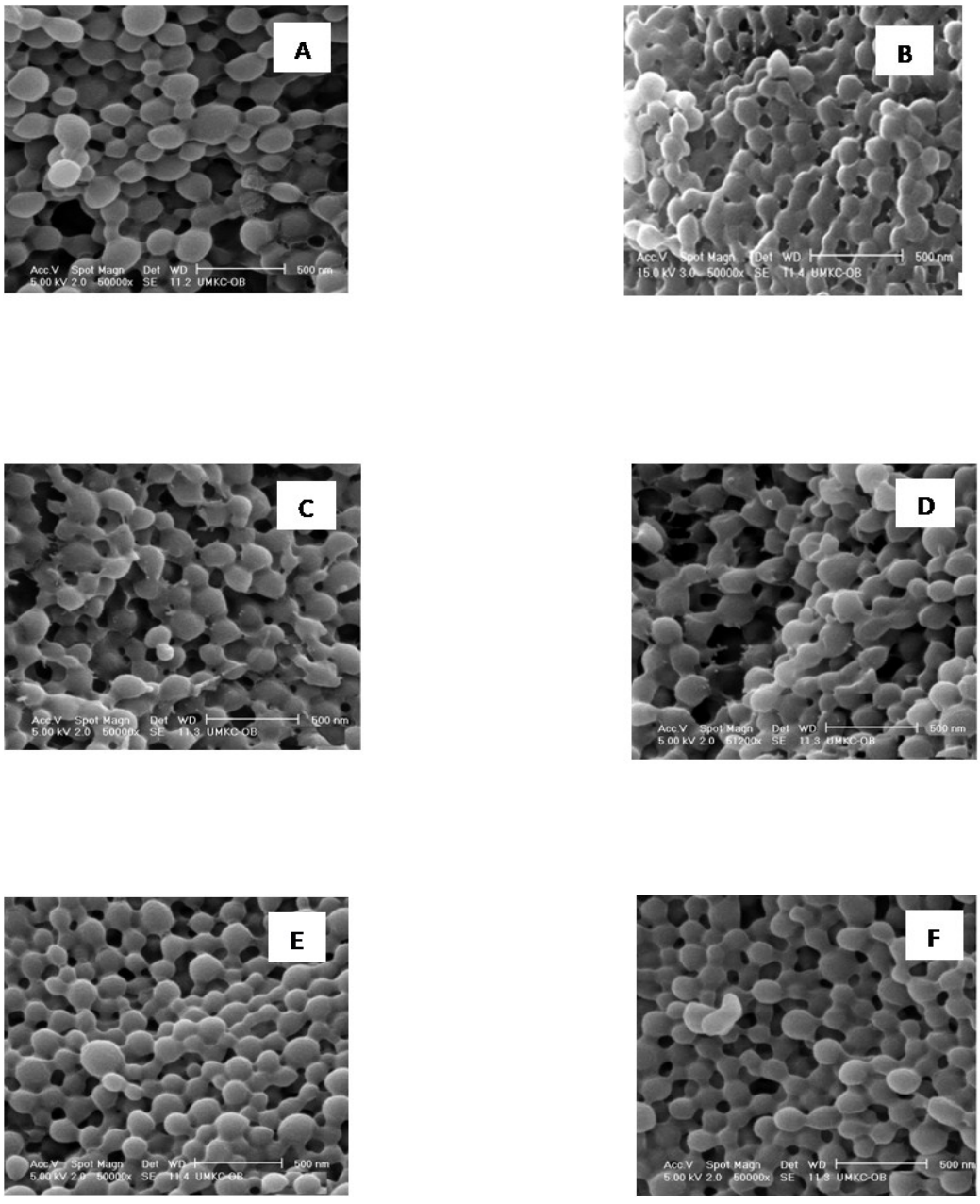

Fig. 21. SEM pictures of nanoparticles prepared by O/W emulsion/solvent evaporation method. (A) DEX 50:50, (B) DEX 65:35, (C) HA 50:50, (D) HA 65:35, (E) PA 50:50, (F) PA 65:35.

Irrespective of the lactide/glycolide ratio, a biphasic release pattern was observed with the nanoparticles. An initial rapid phase (burst) followed by sustained release of the steroids was observed in all cases. Release data of DEX, HA and PA was plotted according to Higuchi equation. The release rate constants of DEX, HA and PA were found to be 6.73, 2.24 and 3.40 $h^{-1/2}$ respectively. Higher lactide to glycolide ratio in PLGA altered the release pattern of steroids. Initial burst release of DEX, HA and PA was found to be less in nanoparticles prepared from PLGA 65:35. Release rate constants were found to be 5.11, 1.31 and 3.16 $h^{-1/2}$ for DEX, HA and PA respectively from PLGA 65:35 nanoparticles (Table 7). Release profiles of DEX, HA and PA are illustrated in Fig. 22. Raising the lactide/glycolide ratio further prolonged the release of steroids from nanoparticles (Duvvuri et al., 2006). This effect may be due to the increase in polymer hydrophobicity which in turn retards the rate of water penetration into polymer matrices. The release rate constants along with regression values are shown in Table 7. Based on the *in vitro* release data, PLGA 65:35 is superior to PLGA 50:50 for the preparation of steroid nanoparticles. Hence we proceeded further with the characterization of PLGA 65:35 nanoparticles. DSC studies were conducted to determine crystalline/amorphous nature of the entrapped drug inside the PLGA 65:35 nanoparticles (Musumeci et al., 2006). PLGA 65:35 exhibited a glass transition temperature at 49.78 °C (Fig. 23A). DEX, HA and PA (Figs. 23B, C and D) exhibited a sharp endothermic peak corresponding to the melting points (263.14 °C, 224.36 °C and 241.9 °C) possibly indicating their crystalline nature.

Table 7. Release rate constants of drugs from nanoparticles prepared by dialysis method, O/W emulsion/solvent evaporation method and formulations

Drug	Dialysis method		O/W emulsion/solvent evaporation method				Formulations (PLGA 65:35 nanoparticles in thermosensitive gels)	
	PLGA 50:50		PLGA 50:50		PLGA 65:35			
	$Q = K t^{1/2}$						$Q = K_o t$	
	K ($h^{-1/2}$) mean±S.E.M	**R^2**	**K ($h^{-1/2}$)** mean±S.E.M	**R^2**	**K ($h^{-1/2}$)** mean±S.E.M	**R^2**	**K (µg/h)** mean±S.E.M	**R^2**
DEX	16.0±0.40	0.93	6.73±0.30	0.95	5.11±0.12	0.97	0.24±0.01	0.92
HA	5.40±0.30	0.93	2.24±0.18	0.98	1.31±0.20	0.96	0.21±0.04	0.95
PA	7.10±0.60	0.92	3.40±0.20	0.95	3.16±0.14	0.97	0.23±0.02	0.97

S.E.M: Standard Error of Mean

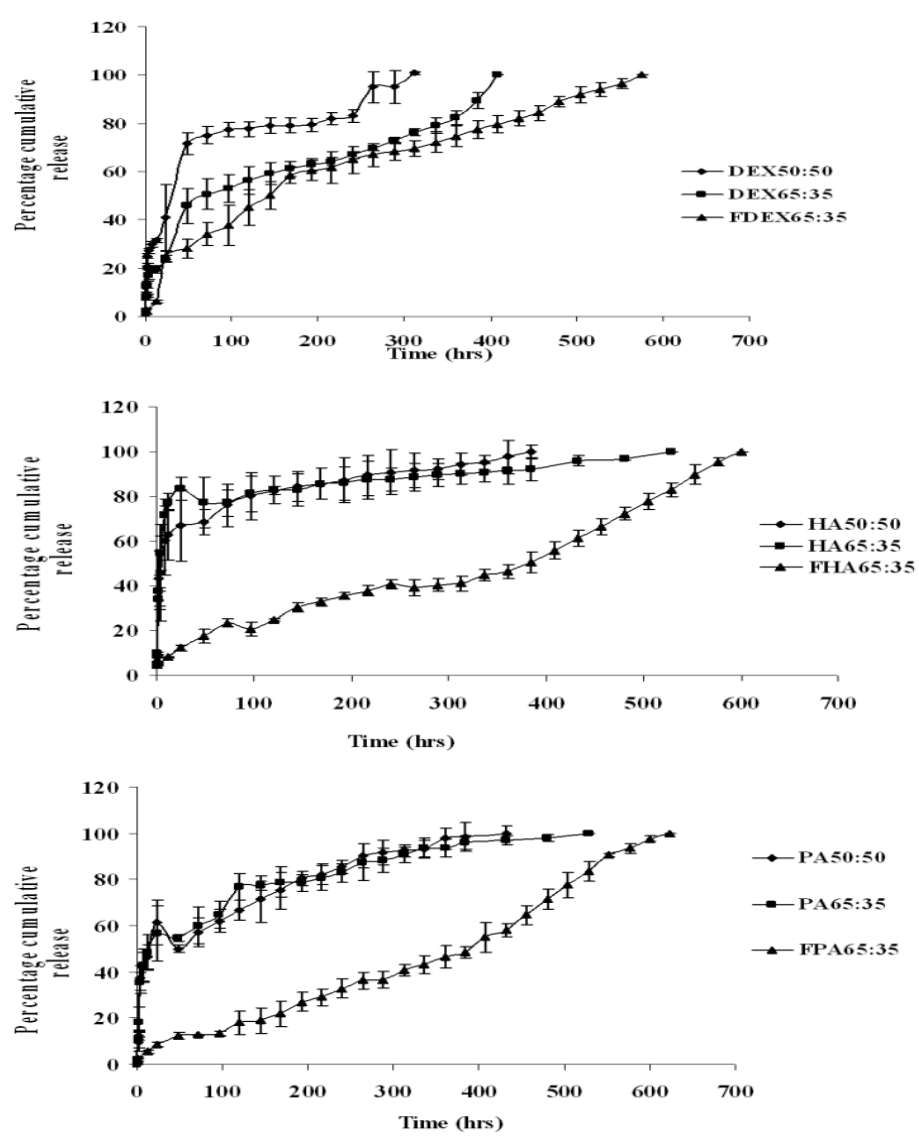

Fig. 22. Percent cumulative release profiles of steroids from nanoparticles prepared by O/W emulsion/solvent evaporation method (n=3) and nanoparticles suspended in thermosensitive gels. (A) DEX from PLGA 50:50, PLGA 65:35 nanoparticles and formulation (DEX-PLGA65:35 suspended in PLGA-PEG-PLGA gels), (B) HA from PLGA 50:50, PLGA 65:35 nanoparticles and formulation (HA-PLGA65:35 suspended in PLGA-PEG-PLGA gels), (C) PA from PLGA 50:50, PLGA 65:35 nanoparticles and formulation (PA-PLGA65:35 suspended in PLGA-PEG-PLGA gels). Error bars represent the standard error of mean (S.E.M).

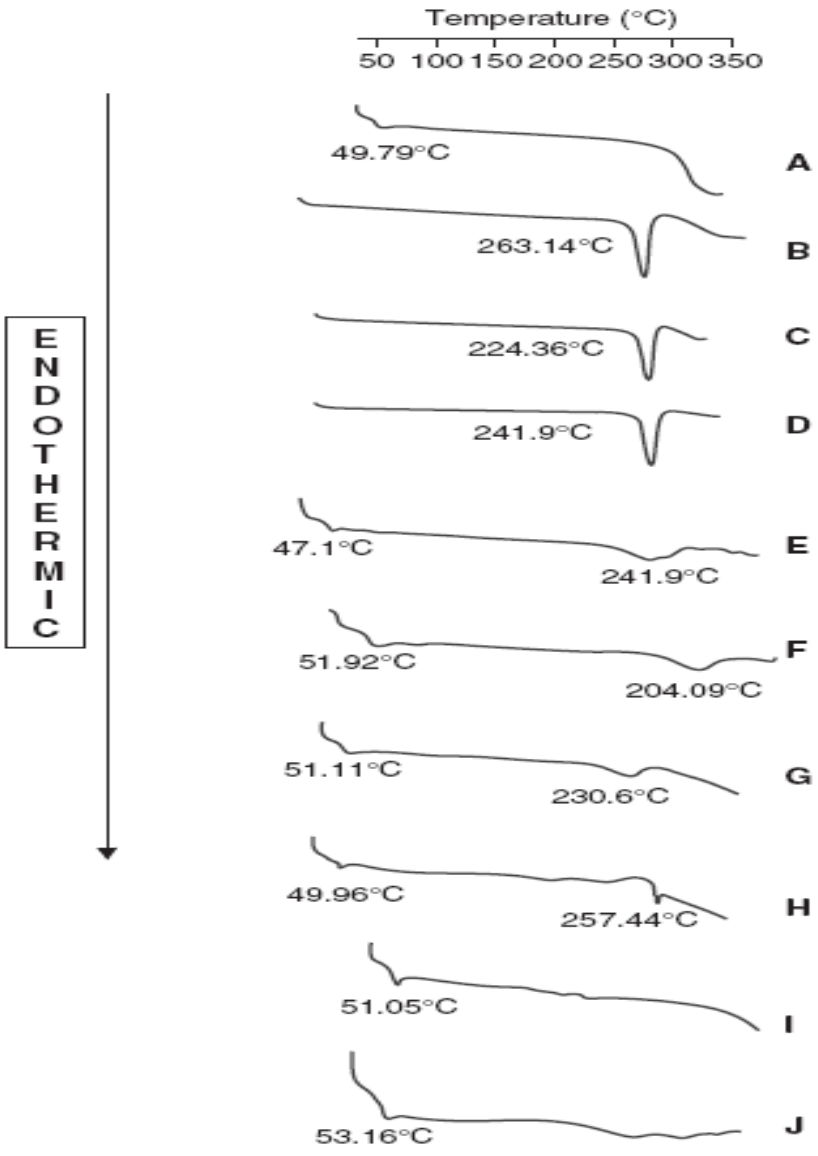

Fig. 23. DSC thermograms of (A) PLGA65:35, (B) DEX, (C) HA, (D) PA, (E) physical mixture of DEX+PLGA65:35, (F) physical mixture of HA+PLGA65:35, (G) physical mixture of PA+PLGA65:35, (H) DEX 65:35 nanoparticles, (I) HA 65:35 nanoparticles, (J) PA 65:35 nanoparticles.

Endothermic peaks of both polymer and drug in the physical mixtures (Figs. 23 E, F and G) are clearly evident. Melting peak of drugs completely disappeared in nanoparticles of HA and PA (Figs. 23 I and J). While nanoparticles of DEX exhibited slight melting point peak (Fig. 23 H) evident at 257.44 °C. Profiles of DEX, HA and PA release from the formulations prepared by dispersing PLGA 65:35 nanoparticles in PLGA-PEG-PLGA thermosensitive gel are also obtained. Synthesis and characterization of triblock copolymer PLGA-PEG-PLGA (weight average molecular weight [M_{wb}] determined by gel permeation chromatography – 4759 Da) has already been published from our laboratory (Duvvuri et al., 2005). Phase transition studies revealed the polymer concentrations ranging between 20-25% w/v forms gel at 32-60 °C (Duvvuri et al., 2005). As the temperature inside the eye ranges from 34.0-37.0 °C such polymeric gels may be appropriate for delivery (Watson and Young, 2004). Burst release of active ingredients has been considerably retarded when nanoparticles are dispersed in thermosensitive gels. Moreover, a clear zero order release pattern of steroids was observed from these formulations (Fig. 22). Storage stability studies were carried out for FDEX 65:35, FHA 65:35 and FPA 65:35 at 4 °C. No significant change in the physical appearance and entrapment efficiency was observed after 3 months storage. Gelation property of the formulations was tested by tube inversion method at 34-37 ^{o}C. All the formulations exhibited gelation in less than 60 seconds (Table 8, Fig. 24).

Table 8. Storage stability data of FDEX 65:35, FHA 65:35 and FPA 65:35 at 4 °C

Samples	**Time**			
	0 month		**3 months**	
	Encapsulation efficiency (%)	**Gelation time (sec)**	**Encapsulation efficiency (%)**	**Gelation time (sec)**
FDEX 65:35	75.3±1.9	30-60	76.1±2.1	30-60
FHA 65:35	93.1±2.1	30-60	92.3±1.9	30-60
FPA 65:35	93.4±2.3	30-60	94.5±1.9	30-60

S.E.M: Standard Error of Mean

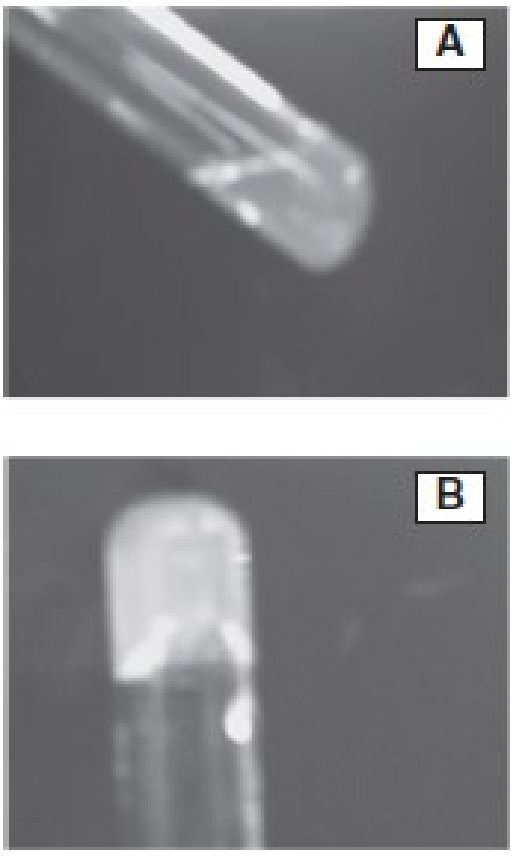

Fig. 24. Gelation and uniform particle dispersion of FDEX 65:35 after 3 months storage at 4 °C. A) FDEX 65:35 in solution at 25 °C; B) FDEX 65:35 in gel form at 34-37 °C

Chromatographic conditions, especially the composition and acidic nature of the mobile phase, were optimized to achieve best resolution. This also increased the signal to mix ratio and was used to minimize run times. Total run time of the method was 7.0 min at 200 μL/min flow rate and injection volume was 25 μL. Under these conditions the retention times of the chromatographic peaks were 4.27, 3.99 and 4.07 min for DEX, PD and HD respectively.

In order to optimize electrospray ionization condition for DEX, PD and HD, full scan mass spectra were acquired in the positive ion mode. During a direct infusion experiment, the mass spectra for DEX, PD and the internal standard HD revealed peaks at mass to charge ratio (m/z) 393.20, 361.30 and 363.20, respectively as the protonated molecular ions $[M+H]^+$. The most stable abundant fragment ion observed in each product MS/MS spectrum were at m/z 355.30 for DEX, 147.20 for PD and 121.0 for IS. These spectra were achieved by optimizing the collision energies at 18.0, 30.0 and 18.0V respectively, as shown in Fig. 25. Quantitative determination was performed in MRM scan positive ion mode with the following mass transitions: 393.20→355.30 for DEX, 361.30→147.20 for PD and 363.20→121.0 for HD as illustrated in Fig. 25. A typical chromatogram from blank (free of analytes and IS) and ocular matrix spiked with DEX and PD at LLOQ and ULOQ concentration levels along with IS are shown in Fig. 26. No interfering peaks from blank samples were observed. Sensitivity and lower limit of quantitation (LLOQ) for DEX and PD were optimized at 2.70 and 11.00 ng/mL respectively.

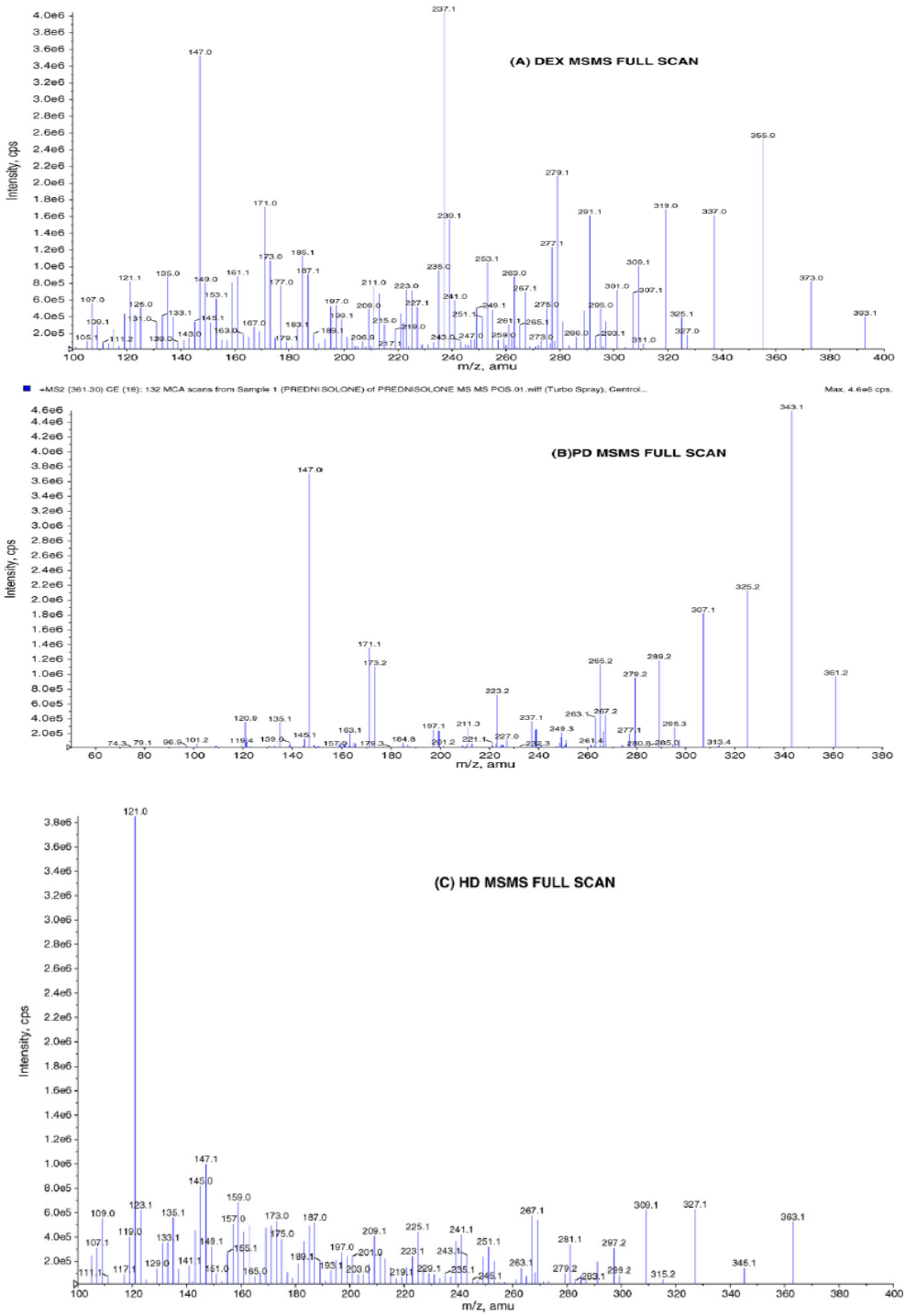

Fig. 25. MS/MS mass spectrum (A) for DEX m/z 393.3→355.3, (B) for PD m/z 361.3→147.2 and (C) for HD 363.1→121.0.

The mean within and between day precision and accuracy for DEX at 2.70 ng/mL and for PD at 11.00 ng/mL are summarized in Table 9A. Precision and accuracy batches were determined by analysis of QC samples. Within the batch assay, precision and accuracy are evaluated by multiple analyses (n = 6) of the five QC samples (2.70, 11.00, 106.00, 296.60 and 494.00 ng/mL) during a validation run and presented in Table 9A and B. Percent CV for DEX (10.2–13.3%) and PD (3.2–10.6%) was observed at LLOQ of 2.70 ng/mL and 11.00 ng/mL respectively. Linearity of DEX and PD was obtained over the concentration range of 2.70–617.60 and 11.00–617.60 ng/mL respectively in a rabbit ocular tissue matrix, serum and isotonic phosphate buffer solution (pH 7.4). Linear regression, "no weighting" mean linear correlation coefficient (r) were calculated to be 0.9990 and 0.9989 for PD and DEX respectively. Regression equation (y) = 0.000543x + 0.0019 for DEX where as slope (m) is 0.000543, intercept (c) is 0.0019 and regression equation (y) = 0.000251x + 0.0000706 for PD where as slope (m) is 0.000251, intercept (c) is 0.0000706. Regression equation (y) =mx+ c, where y-axis is the area ratio of analyte area and IS area, x-axis is the concentration ratio of analyte concentration and IS concentration, m is the slope of the linear regression line and c is the intercept point of the linear regression line and the y-axis. Between day assay precision and accuracy evaluated by multiple analyses of the QCsamples during each validation run are presented in Table 9A–C. The precision was within 11.3% for DEX and 11.1% for PD at LLOQ.

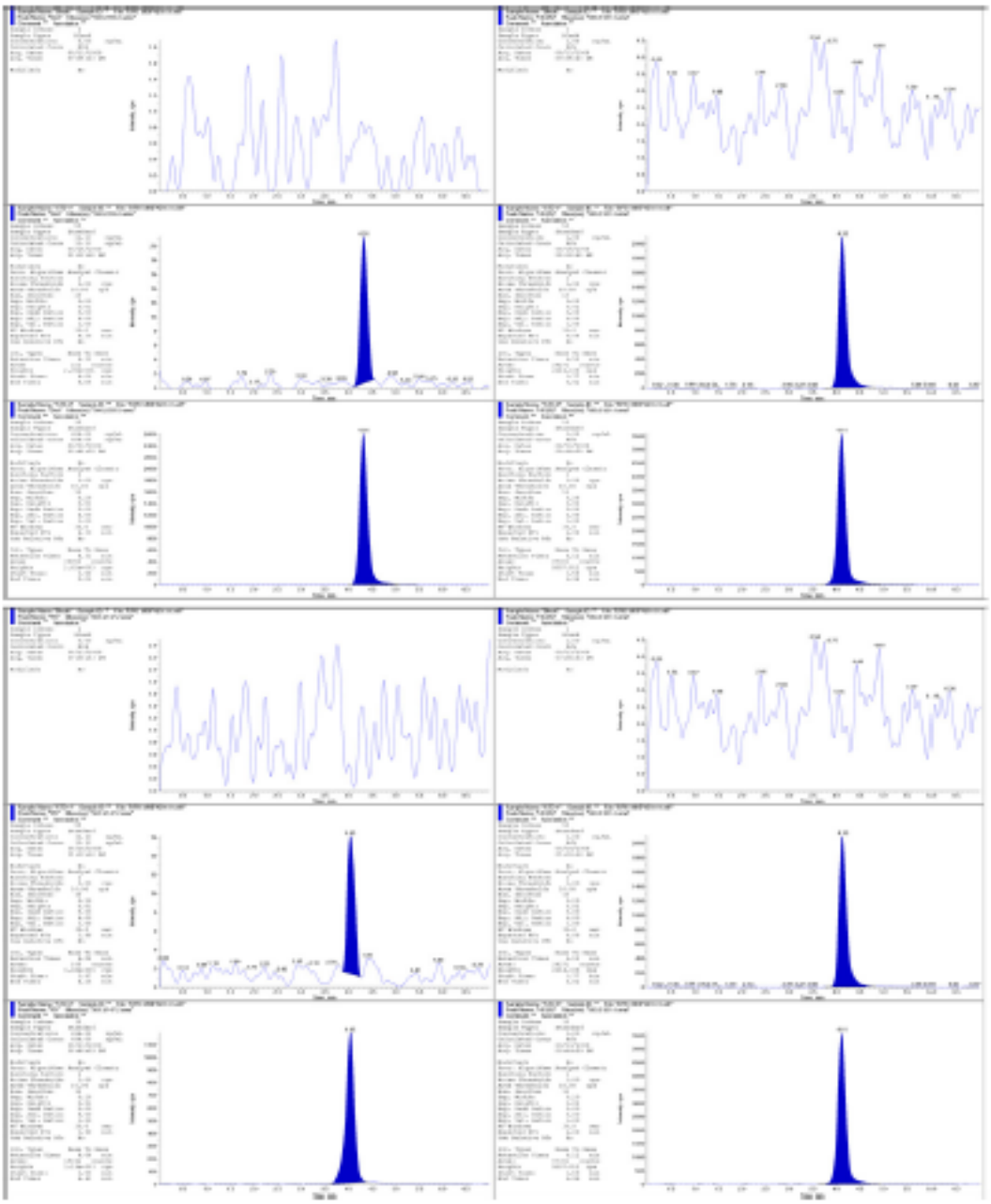

Fig. 26. Chromatograms in MRM mode [A] for DEX (upper three rows) blank (without IS) and with IS (HD right side column) at LLOQ and ULOQ, [B] for PD (lower three rows) blank (without IS) and with IS (HD right side column) at LLOQ and ULOQ concentrations from top-down of the figure.

The stability of stored QC ocular matrix samples was determined with freshly spiked calibration curve standards. Freeze–thaw stability studies were carried out with low and high QC in six replicates for both DEX and PD. In each freeze–thaw cycle samples were frozen for at least 24 h before thawing at room temperature. For bench top stability studies the QC samples (n = 6) were retrieved from −80 ^{o}C storage and kept at room temperature for 6 h before processing. Stability assessments of DEX and PD under various anticipated conditions were revealed. Preclinical samples are received, stored and processed as presented in Table 9E with low (31.80 ng/mL) and high QC (494.00 ng/mL) concentrations for both analytes. Both DEX and PD appears to be stable through multiple freezing and thawing cycles. DEX appears to be less degradation than PD through multiple freezing and thawing cycles. Bench top stability studies are stable for 6 h at room temperature. Results from these studies are summarized in Table 9D. No significant degradation of DEX and PD were observed in any of the sample preparation. Recovery of corticosteroids from ocular matrix by protein precipitation followed by liquid–liquid extraction procedure resulted in clean samples with high extraction efficiency. We have investigated various sample extraction methods including protein precipitation and liquid–liquid extraction with different organic solvents (acetonitrile, methanol, isopropyl alcohol, perchloric acid, ethyl acetate, methyl (t)-butyl ether, dichloromethane, hexane and diethyl ether). Perchloric acid and isopropyl alcohol efficiently precipitated proteins from the serum and vitreous fluid. Addition of saturated potassium chloride solution further improved accuracy but reduces recovery of analytes. The

above sample preparation and extraction method produced no significance endogenous chromatographic peak interference from rabbit vitreous and plasma. The extraction recoveries of the two analytes were: DEX 86.9% at LQC and 91.6% at HQC, PD 86.4% at LQC and 79.1 at HQC. Extraction recovery (%) expressed as the ratio of the mean peak area of the analytes spiked into ocular matrix before extraction to the mean peak area of the analytes spiked into ocular matrix after extraction multiplied by 100. Postspiked samples were treated as 100% recovery samples. *Ex-vivo* permeability studies of DEX were carried out across excised rabbit sclera. Suspension of DEX (containing 0.5% w/v HPMC), DEX 65:35 nanoparticles and FDEX 65:35 (nanoparticles of dexamethasone prepared by PLGA 65:35 dispersed in PLGA-PEG-PLGA thermosensitive gels) were employed for permeation studies. Histological sections of sclera were examined by hematoxylin-eosin stain. No change in integrity, density and interlacing of fibers was observed after 1, 2 and 4 days. The nuclei of fibroblasts were clearly visible even after 4 days of experimentation (Fig. 27). The membrane integrity of sclera was further confirmed by carrying out [^{3}H]-mannitol permeability studies. Permeability values (mean±S.E.M) of [^{3}H]-mannitol on days 1 and 4 were found to be 1.47(±0.25) X 10^{-05} and 2.01(±0.06) X 10^{-05} cm/sec respectively. No significant difference in the permeability of [^{3}H]-mannitol was evident. Permeabilities values ($P*10^6$) of DEX from suspension, DEX 65:35 nanoparticles and FDEX 65:35 were found to be 2.23, 0.40 and 0.11 cm/sec respectively (Fig. 28, Table 10). Cumulative amount of DEX permeated across the sclera from suspension, DEX 65:35 nanoparticles and FDEX 65:35 were found to be 5.94, 0.85 and 0.28 µg/h respectively (Table 10).

Table. 9. Precision and accuracy, plasma stabilities of DEX and PD in rabbit ocular matrix.

Precision and accuracy, plasma stabilities of DEX and PD in rabbit ocular matrix.

Name	DEX					PD			
	Nominal conc. (ng/mL)	Mean conc. (ng/mL)	SD (±)	% CV	% Mean accuracy	Mean conc. (ng/mL)	SD (±)	% CV	% Mean accuracy
(A and B) Within batch assay precision and accuracy for DEX and PD CCS ($n=2$), QC ($n=6$)									
CCS-1	617.60	624.20	115.27	18.5	101.1	610.29	10.34	1.7	98.8
CCS-2	494.08	499.55	29.63	5.9	101.1	490.01	5.76	1.2	99.2
CCS-3	395.26	428.24	7.95	1.9	108.3	404.84	13.55	3.3	102.4
CCS-4	296.45	303.74	28.16	9.3	102.5	295.88	0.81	0.3	99.8
CCS-5	192.69	176.82	6.11	3.5	91.8	185.94	9.55	5.1	96.5
CCS-6	105.98	99.59	2.06	2.1	94.0	103.91	2.93	2.8	98.0
CCS-7	31.79	35.78	0.76	2.1	112.5	34.17	3.36	9.8	107.5
CCS-8	11.13	11.38	1.04	9.1	102.2	10.88	0.35	3.2	97.8
CCS-9	2.70	3.14	0.32	10.2	116.3				
High QC	494.08	530.12	10.28	1.9	107.3	515.11	15.66	3.0	104.3
Middle QC	296.45	301.20	6.79	2.3	101.6	273.99	5.26	1.9	92.4
Middle1 QC	105.98	109.06	3.34	3.1	102.9	98.91	0.86	0.9	93.3
LOQ	11.13	10.59	0.54	5.1	95.1	11.01	1.17	10.6	101.1
LLOQ	2.70	3.20	0.42	13.3	118.5				
(C) Between batch assay precision and accuracy for DEX and PD CCS ($n=2$), QC ($n=18$)									
CCS-1	617.60	596.65	45.70	7.7	96.6	572.67	11.79	2.1	92.7
CCS-2	494.08	450.59	30.75	6.8	91.2	432.29	4.86	1.1	87.5
CCS-3	395.26	422.25	11.05	2.6	106.8	427.34	3.85	0.9	108.1
CCS-4	296.45	313.61	33.98	10.8	105.8	281.96	10.78	3.8	95.1
CCS-5	192.69	206.98	8.45	4.1	107.4	210.01	4.16	2.0	109.0
CCS-6	105.98	103.38	14.35	13.9	97.5	115.21	2.39	2.1	108.7
CCS-7	31.79	31.58	5.85	18.5	99.3	35.76	0.06	0.2	112.5
CCS-8	11.13	11.15	0.79	7.1	100.2	11.50	1.28	11.1	103.3
CCS-9	2.70	3.06	0.35	11.3	113.2				
High QC	494.08	530.12	10.27	1.9	107.3	441.82	32.41	7.3	98.3
Middle QC	296.45	301.19	6.79	2.3	101.5	284.82	25.76	9.0	96.1
Middle1 QC	105.98	109.06	3.15	3.1	102.9	103.98	5.79	5.6	98.1
LOQ	11.13	10.59	0.54	5.1	96.3	11.63	1.24	10.7	104.5
LLOQ	2.70	3.22	0.11	3.5	119.3				
(D and E) Matrix stability assay precision and accuracy for DEX and PD CCS ($n=2$), bench top QC ($n=6$), freeze and thaw QC ($n=6$)									
CCS-1	617.60	616.77	6.55	1.1	99.9	596.87	46.02	7.7	96.6
CCS-2	494.08	560.58	132.81	23.7	113.5	439.72	15.37	3.5	89.0
CCS-3	395.26	441.82	51.09	11.6	111.8	419.24	15.30	3.6	106.1
CCS-4	296.45	334.28	23.21	6.9	112.8	298.85	13.10	4.4	100.8
CCS-5	192.69	174.53	24.59	14.1	90.6	201.63	16.02	7.9	104.6
CCS-6	105.98	108.21	1.29	1.2	102.1	114.79	1.80	1.6	108.3
CCS-7	31.79	33.94	5.78	17.0	106.7	32.44	4.63	14.3	102.0
CCS-8	11.13	11.52	0.27	2.3	103.5	10.44	0.93	8.9	93.8
CCS-9	2.70	3.15	0.64	20.2	116.7				
(D) Bench top stability samples precision and accuracy for DEX and PD QC ($n=6$)									
High QC	494.08	457.63	32.96	7.2	92.6	462.17	25.15	5.4	93.5
Middle QC	31.79	29.14	1.62	5.5	91.7	33.46	2.91	8.7	105.3
(E) Freeze and thaw stability samples precision and accuracy for DEX and PD QC ($n=6$)									
High QC	494.08	499.33	44.59	8.9	101.1	433.61	36.36	8.4	87.8
Middle QC	31.79	32.19	2.67	8.1	101.2	32.19	3.53	11.0	101.3

CCS: Calibration curve standard, QC: Quality control standard, % CV: Coefficient of variation, SD: Standard deviation

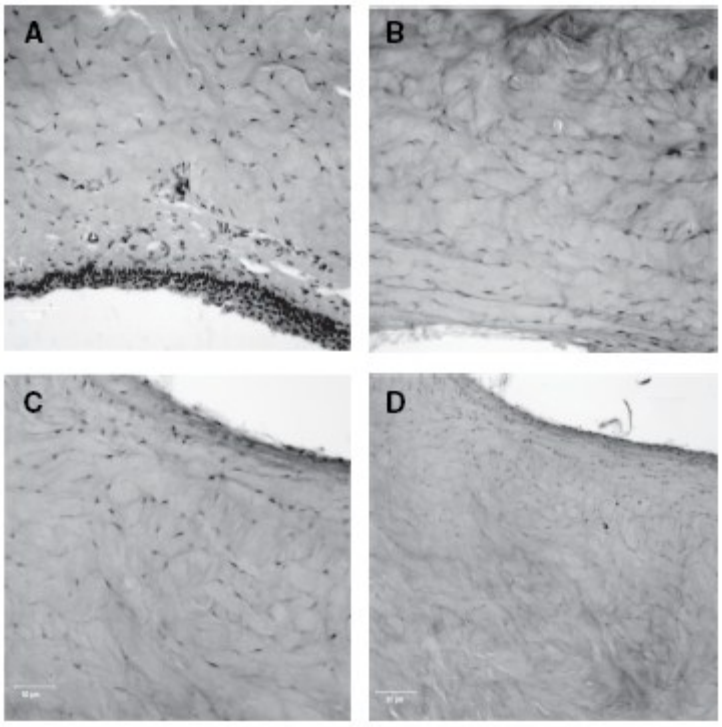

Fig. 27. Histological sections of scleral samples stained by hematoxylin-eosin dye; A) Control; B) After 1 day; C) After 2 days; D) After 4 days. Bar represents 50 µM. The black color dots represent the nuclei of the scleral fibroblast cells.

Table 10. *Ex vivo* permeability of DEX from suspension, DEX 65:35 nanoparticles, and FDEX 65:35 (DEX 65:35 nanoparticles suspended in thermosensitive gels)

S. No	Samples	Cumulative amount (µg) of DEX permeated per hour (mean ±SEM)	Permeability (cm/sec)* 10^6 (mean ±SEM)	R^2
1	DEX suspension	5.94± 0.50	2.23±0.12	0.97
2	DEX 65:35 nanoparticles	0.85±0.05	0.40±0.08	0.97
3	FDEX 65:35	0.28± 0.03	0.11±0.02	0.96

S.E.M: Standard Error of Mean

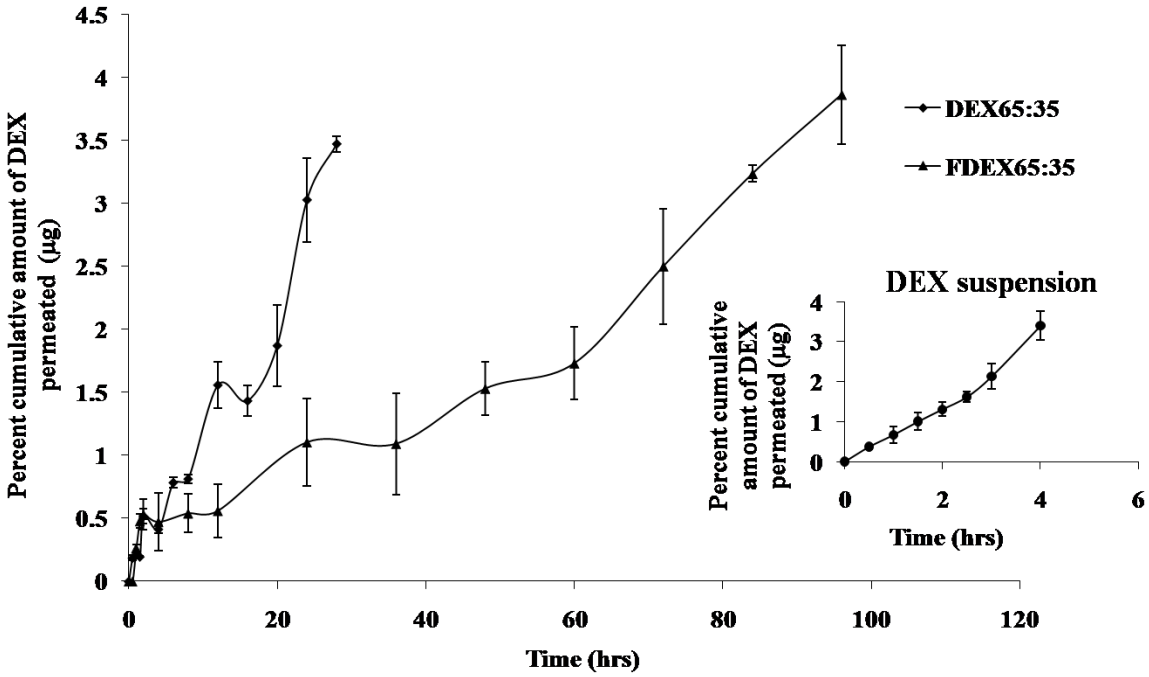

Fig. 28. Permeability of DEX from suspension, DEX 65:35 nanoparticles and FDEX 63:35 (DEX 65:35 nanoparticles suspended in thermosensitive gels). Inset: Permeability of DEX from suspension containing 0.5% w/v HPMC. Error bars represent the standard error of mean (S.E.M).

Vitreal concentrations of DEX were compared after subconjunctival administration of either DEX suspension (containing 50 µg of DEX) or FDEX 65:35 (containing 50 µg of DEX) after regular time intervals (Kompella et al., 2003). Vitreous humor samples (100 µL) obtained from the microdialysis probe were aliquoted into a 1.5 mL polypropylene microcentrifuge tubes (PPMCT), followed by addition of 25 µL of 10.0 µg/mL freshly prepared IS (HA) solution to all samples, except for blank. These solutions were vortexed for 30 s, to which 50 µL of 20% (v/v) perchloric acid was added, and again vortexed for 30 s to precipitate proteins. The samples were extracted by the addition of 1000 µL of methyl tertiary butyl ether (MTBE) followed by vortexing for approximately 2 min. After centrifugation at 12,000 rpm at 4 °C for 25 min, 850 µL of the organic layer was transferred to a pre-labeled fresh 1.5 mL of poly propylene microcentrifuge tube and evaporated in the Speed Vac® at 35 °C for 60 min. The residue was reconstituted with 100 µL of mobile phase, vortexed for 30 s and transferred into a pre-labeled HPLC autosampler vial with silanized inserts. A 25 µL of the resulting solution was injected into LC–MS/MS. Surprisingly; no concentrations of DEX were obsereved in the dialyzed samples even up to 10 h.

3.4. Discussion

Treatment of severe DME infections require sustained delivery of steroids to the posterior segment of the eye. Delivery of high corticosteroid doses intravitreally has limitations due to side effects such as endophthalmitis, retinal detachment and other undesirable events related to repeated injections. Subconjunctival deposition is a promising approach for the drug delivery to retina/choroid. Incorporation in nanoparticles will protect these anti-inflammatory

agents from enzymatic degradation and will provide sustained release which may in turn reduce the dosing frequency. DEX tissue concentrations in ocular tissues were compared after frequent topical dosing and subconjunctival injection. DEX concentrations were found significantly higher following subconjunctival injection (Weijtens et al., 2002). Sustained drug delivery to the posterior segment can be achieved by subconjunctival administration of steroid nanoparticles in ME patients (Geroski and Edelhauser, 2000). Moreover drugs administered subconjunctivally easily reach retinal pigment epithelium because sclera and choroid offer very limited resistance to drug transport (Ranta and Urtti, 2006). In the present study PLGA nanoparticles of DEX, HA and PA were prepared, characterized and tested for the *ex vivo* drug release profiles in excised rabbit sclera. Such delivery systems may generate therapeutic levels from low doses of DEX, HA and PA at the retina/choroid reducing inflammation and toxicity. Moreover, drug encapsulation in polymer matrices may enhance drug stability and reduce toxicity.

PLGA nanoparticles belong to colloidal drug delivery systems with size ranging from 10-1000 nm. Size of particles plays an important role in the delivery of drugs. As a part of preliminary studies we have examined effect of particle size on the uptake of fluorescent labeled polystyrene microspheres (0.05, 0.10, 0.5 and 1.0 μm) from basolateral side of ARPE-19 cell line. Following subconjunctival injection nanoparticles are exposed to basolateral side of RPE, hence the uptake studies were carried out from basolateral side of ARPE-19 cells. Particles of size ~50 nm did not exhibit any saturation in concentration and time dependent uptake studies. However, higher size particles (0.10, 0.5 and 1.0 μm)

exhibited saturation at higher concentrations (>500 μg/mL) and time (> 60 min). Based on the TEM studies, the center-to-center spacing of collagen fibrils vary between 250-280 nm and the lamellae run parallel roughly from anterior to posterior. Based on these studies we have concluded that the particles of size ~200 nm may be optimum for sustained delivery of drugs to RPE following subconjunctival injection. Smaller size (< 50 nm) particles may permeate across the firbrous structure of scleara and get drained into the systemic circulation by the choroidal blood vessels. On the other hand, higher size (> 200-300 nm) may retain in the subconjunctial space for a longer duration and release the actives in a sustained fashion. Moreover, higher size particles (> 200-300 nm) may result in occlusion of 30G needle used for subconjunctival injection. Polystyrene (carboxylate modified, negatively charged) particles of size ≥ 200 nm retain for a longer duration following subconjunctival administration (Amrite and Kompella, 2005). Unlike the nonbiodegradable polystyrene particles, PLGA polymer used in our study is biodegradable in nature and known to exhibit burst release of drugs. Our main intension is to prevent the burst release of steroids by dispersing the PLGA nanoparticles in thermosensitive gels. These formulations may provide sustained retina/choroid delivery of steroids following episcleral administration. As steroids are fairly lipophilic (Table 11) dialysis method was employed in the preparation of PLGA nanoparticles. However, this method resulted in nanoparticles with poor encapsulation efficiency and could not sustain the drug release over longer durations. In dialysis method nanoparticles are formed by continuous precipitation of polymer and drug inside the dialysis bag with the removal of organic solvent. The rate of precipitation depends on the relative

Table 11. Physical properties of drugs

Properties	**Dexamethasone**	**Hydrocortisone acetate**	**Prednisonole acetate**
Log P	1.9	2.2	2.4
Molecular weight (Da)	392.5	404.5	402.5
Solubility	0.1 mg/ml in water. soluble in ethanol, methanol, acetone, dioxane and slightly soluble in chloroform	Partially soluble in diethyl ether, acetone. Very slightly soluble in methanol. Insoluble in cold water	Soluble in methanol, acetone. Insoluble in cold water
Melting point (^{o}C)	263.14	224.36	241.9

lipophilicities of polymer and drug. Since PLGA polymer is highly lipophilic and practically insoluble in water, it precipitates at a faster rate relative to drug. As a result drug molecules are adsorbed on to the surface of the polymer rather than being entrapped inside the core of the particles. Moreover, dialysis is carried out for 24 h, which may result in release of the adsorbed/entrapped drug into the aqueous phase. In contrast O/W emulsion/solvent evaporation method proved to be superior to the dialysis method in terms of entrapment efficiency and uniformity. O/W emulsion/solvent evaporation method resulted in consistently low entrapment values of DEX as compared to HA and PA. This may be attributed to the higher affinity of DEX to external aqueous phase as compared to HA and PA resulting in lower drug content inside the matrix of nanoparticles. Uniform particle sizes were obtained with mean effective diameters of 180-230 nm and polydispersities of 0.005-0.057. Size of nanoparticles depends on the various formulation parameters such as volume of the aqueous phase, drug and polymer concentration in the organic phase and concentration of the surfactant in the aqueous phase (Budhian et al., 2007). Dexamethasone nanoparticles of 400-600 nm were obtained following the use of dichloromethane: acetone (1:1 ratio) and a polymer concentration of 27 mg/mL (Kim and Martin, 2006). In the present study we have added dichloromethane: acetone in a ratio of 4:1 and maintained a polymer concentration of 20 mg/mL in organic phase. This solvent composition significantly reduced the particle size to 180-230 nm with more uniform distribution. This result can be attributed to the decrease in organic phase viscosity which in turn leads to a net increase in shear stress experienced by the organic phase. Moreover, the slow and steady diffusion of acetone in to external aqueous

phase leads to the formation of smaller and more uniform size particles. Use of chloroform in the preparation of HA nanoparticles slightly increased the particles size irrespective of the polymer used. Except for the duration, the release patterns of HA and PA was similar from PLGA 50:50 and PLGA 65:35 matrices. DEX nanoparticles prepared with PLGA 65:35 released the cargo in a sustained and controlled fashion (Fig. 22A). This may be due to the crystalline arrangement of DEX inside the nanoparticles which is also evident from the DSC results (Fig. 23H). DSC studies of PLGA 65:35 nanoparticles indicate the presence of drug particles (HA and PA) either in amorphous or disordered crystalline state(Venkateswarlu and Manjunath, 2004).

DSC thermograms depict the phase transition temperatures (Tg or Tm) of polymer and drugs either in pure form or in combination with polymer. Drug and polymer matrix may exist in four different forms: a) amorphous drug in crystalline polymer b) amorphous drug in amorphous polymer c) crystalline drug in amorphous polymer and d) crystalline drug in crystalline polymer. DSC thermogram also aids in delineation of abrupt changes in the drug/polymer matrix due to specific drug polymer interactions. DEX, HA and PA exhibited a sharp endothermic peak corresponding to the melting points indicating their crystalline nature. Melting peak of drugs completely disappeared in nanoparticles of HA and PA suggesting that the drug particles may be in amorphous or disordered crystalline form. While nanoparticles of DEX exhibited some crystallinity which was indicated by the slight melting point peak (Fig. 23 H) evident at 257.44 °C (Panyam et al., 2004). Burst release phase from PLGA nanoparticles may be attributed to the presence of the active ingredients in amorphous

state. Water can penetrate more easily through the amorphous/disordered crystalline matrices as compared to crystalline matrices initiating burst release (Gupta et al., 2004). The release duration of HA and PA from the nanoparticles was slightly higher compared to DEX. This may be attributed to the higher lipophilicity of HA and PA better interaction of the drug with the polymer (Table 11). Such effect is completely eliminated when nanoparticles are dispersed in thermosensitive gels. This may be due to the polymer adhesion to nanoparticle suspended in thermosensitive gels. Such nanoparticulate formulations may provide sustained release of steroids following subconjunctival administration. Previous studies from our laboratory indicated that the rate of drug release from microparticles *in vivo* is significantly slower than *in vitro* conditions. This effect may be due to more rapid and continuous agitation as well as faster penetration of the solvent (Duvvuri et al., 2007). Moreover nanoparticles can be suitably formulated into the thermosensitive gels which are liquid at room temperature and can be administered subconjunctivally. The gel aids in controlling the burst release of drugs from the nanoparticles and also prevents dispersion of nanoparticles into anterior chamber after subconjunctival injection. The formulations can also help in the formation of a depot at the site of administration providing a robust concentration gradient for rapid and efficient permeation of drugs across the sclera in a sustained manner (Amrite and Kompella, 2005). No significant change in the entrapment efficiency of steroids was observed after 3 months storage at 4 °C. All formulations exhibited spontaneous gelation with no visible clumping of nanoparticles. This indicates the uniform nanoparticle dispersion inside thermosensitive gel. Posurdex™ (Allergan) is a biodegradable implant of DEX which

contains either 350 or 700 µg dose in poly-lactide-co-glycolide copolymer. This system has undergone phase II clinical trial in patients suffering from DME, post cataract surgery and uveitis. Promising results were obtained from the implants containing 700 µg DEX. Significant improvement in the vision was obtained from the implants as compared to the control group. Moreover, the drug from these implants is released over the duration of 5 weeks (Fialho et al., 2008). In the present study nanoparticles containing DEX equivalent to 700 µg were used for carrying out transcleral studies. Samples were collected from the receptor chamber at regular time intervals and sink conditions were maintained throughout the experiment. Permeability studies were carried out until 5% of the donor drug concentration appeared in the receptor chamber. This approach avoids the preconceived notion of back diffusion of drug and also helps to maintain constant steady state concentration gradient. Permeation of DEX from suspension containing 0.5% HPMC occurred for nearly 4 h (i.e. 25-35 µg of DEX permeated the sclera in 4 h). DEX 65:35 nanoparticles on the other hand sustained drug release for 40 h. Further prolongation in the duration of release was observed when nanoparticles were suspended in thermosensitive gels. Permeability values of DEX significantly decreased when drug was entrapped in the nanoparticles and suspended in thermosensitive gels. The release of DEX from these formulations may act as the major rate limiting step for the transcleral permeation. Significant difference in the duration of release was observed from FDEX 65:35 under *in vitro* and *ex vivo* conditions. This result may be attributed to the surface area of suspended particles (suspended in dialysis) which is exposed to the release medium, continuous motion

of shaker bath and nature of dialysis bag membrane. However, *in vitro* release conditions may not be applicable in the actual *in vivo* environment (following subconjunctival injection). Transcleral permeability studies simulate the *in vivo* conditions to a large extent provided proper sink conditions are maintained. Histological examination of sclera samples did not exhibit any noticeable changes after the completion of permeability studies. This observation was further confirmed by transport of [^{3}H]-mannitol across the sclera. As more than 60% of the sclera is made of water channels [3H]-mannitol can be used as a good marker for membrane integrity (Watson and Young, 2004). No significant difference in [^{3}H]-mannitol transport was observed which confirms tissue integrity of sclera.

In target tissues such as retina/choroid/vitreous, DEX concentrations ranging from 10-4000 ng/mL are required for effective treatment of various inflammatory conditions. From the *in vitro* release studies we could observe a clear zero order release pattern of steroids from the formulations. Further, from the *ex vivo* permeability data the cumulative amount of DEX permeated across the sclera from nanoparticles suspended in thermosensitive gels was found to be 0.28 μg/h. This data clearly indicates the combined role of PLGA 65:35 and PLGA-PEG-PLGA in controlling the permeability of DEX across the sclera. Using the formulations described in this article DEX concentrations can be maintained well above the minimum effective concentrations for duration of several months following single episcleral administration. Depending on the severity of inflammation various combinations of nanoparticles and thermosensitive gels (with varying molecular weights) loaded with steroids can be tailor made so as to match the particular dosing requirements of a particular patient.

Moreover, these nanoparticulate formulations may sustain the duration of drug release for a longer time period than Posurdex™ (duration of drug release only 5 weeks). Hence, these formulations have an edge as compared to the implantable systems both in terms of duration of drug release and mode of administration.

Vitreal concentrations of DEX were compared after subconjunctival administration of either DEX suspension (containing 50 µg of DEX) or FDEX 65:35 (containing 50 µg of DEX) after regular time intervals (Kompella et al., 2003). Surprisingly, no concentrations of DEX were obsereved in the dialysate samples even upto 10 h. LC-MS/MS is a sensitive and powerful technique for analyzing the drug concentrations in various biological matrices. However, the vitreal concentration of DEX was below the lower limit of quantification. This may be due to the lipophilic nature of DEX and relatively low recovery of dialysis probes. Conventional pharmacokinetic technique may be more suitable for analyzing the drug concentrations of lipohilic molecules in the vitreous humor.

3.5. Conclusion

In summary, we have provided proof for a novel injectable and controlled-release formulations of DEX, HA and PA which can be used in the treatment of macular edema. Based on these studies we have concluded that the particles of size ~200 nm may be optimum for sustained delivery of drugs to RPE following subconjunctival injection. PLGA 65:35 nanoparticles are found to be superior in terms of polydispersity and drug release profile. Burst release of drug from nanoparticles may be successfully controlled and/or eliminated by suspending in PLGA-PEG-PLGA thermosensitive gels. Moreover entrapment

inside the gel structure allows nanoparticle retention at the site of administration and thereby releasing the drug in a continuous manner. Histological studies and [^{3}H]-mannitol data confirmed the integrity of sclera was not compromised with these thermosensitive gel formulations. Following complete drug release from formulations, the remaining nanoparticulate shells degrade inside the body obviating the need for surgical removal as required for implants. *In vivo* pharmacokinetic studies should be carried out to determine the choroidal/retinal/vitreal concentrations following subconjunctival administration. Novel formulation strategies of nanoparticles suspended in thermosensitive gels can serve as an alternative to the current therapies like implants and intravitreal injections.

CHAPTER 4

RATIONALE FOR INVESTIGATION

4.1. Overview

Retinoblastoma is a major vision threatening intraocular malignancy affecting 1 in 18,000 to 30,000 live births worldwide (Aerts et al., 2006; Albert, 1987; Bishop and Madson, 1975). It is common in children between the age of 3 to 7 (Pesin and Shields, 1989). Marginal tumor regression is usually evident following a combination therapy with cyclophosphamide, vincristine, doxorubicin, melphalan, thiotepa, nimustine and cisplatin (Chan et al., 2005; Ragab et al., 1975; White, 1991). The nucleus is the site of DNA intercalation or binding for anticancer agents including carboplatin, etoposide and topotecan. However, cellular uptake of these agents is significantly reduced due to the presence of efflux pumps on plasma membrane. Upon exposure to anticancer agents, expression levels of efflux pumps appear to be elevated causing lower drug accumulation inside cell cytoplasm as well as nucleus. Polymeric micelles may evade efflux pumps and can deliver therapeutic concentrations inside cytoplasm. However, the release duration of drugs from polymeric micelles is very short (~24-48 h). This may require frequent intravitreal administration of drug loaded polymeric micelles which is associated with patient non-compliance. Thermosensitve gels have been widely used for sustained release of drugs. Polymeric micelles can be dispersed in PLGA-PEG-PLGA thermosensitive gels which may be conveniently injected intravitreally for increasing the overall duration of drug release. Moreover, thermogel systems also prevent the rapid elimination of polymeric

micelles following intravitreal administration. These systems can form a depot above the vitreous fluid following intravitreal injection and slowly release the polymeric micelles for the treatment of retinoblastoma.

4.2. Statement of Problem

The main purpose of a treatment strategy in retinoblastoma should be to cure the disease as well as globe salvation to retain vision. Several treatment strategies are available and the choice depends on the disease progression. Groups IV and V (according to Reese-Ellsworth classification system) are considered as very advanced and difficult stage and do not respond well to chemotherapy (De Potter, 2002). In such cases, external beam radiotherapy (EBR) and enucleation are employed as the last recourse. Both treatments leave the survivors with complete or nearly complete vision loss. EBR is an option for children who develop bilateral disease and show recurrance after chemotherapeutic treatment (Chintagumpala et al., 2007). In EBR, radiation is applied to the entire retina, lens, lacrimal gland and optic nerve; whereas exposure to normal tissue is avoided. Currently, EBR is no longer a viable option due to long term side effects like optic neuropathy, cataract, retinopathy and chronic dry eye (Eng et al., 1993). Development of secondary tumors in the area exposed to the radiation after a long time period is the major reason that discourages the application of EBR (Eng et al., 1993). Enucleation is the only treatment option for group V tumors. These tumors also display one or more of side effects i.e., neovascular glucoma, retinal detachment, involvement of optic nerve, sclera, orbit, anterior chamber or choroid, pars plana tumor seeding apart from tumor. Enucleation is surgical removal of the eye ball sparing the eye lids and extraocular muscles.

In the last decade, chemotherapy has played a vital role in treating the disease and sparing the eye globe. Several reports suggest that chemotherapy is successful in treating the group I to III tumors but not very effective in group IV and V (De Potter, 2002). This is due to the presence of vitreal seeds responsible for disease recurrence (Chintagumpala et al., 2007). Chemotherapy helps in the reduction of tumor size so that focal therapy can be applied to a relatively small area and the tumor can be shrunk without loss of vision. Tumor regression is usually evident following a combination therapy with cyclophosphamide, vincristine, doxorubicin, melphalan, thiotepa, nimustine and cisplatin (Chan et al., 2005; Ragab et al., 1975; White, 1991). Generally, chemotherapeutic agents are administered by intravenous route which in the absence of any targeting strategy exposes normal cells to high levels of anticancer agents resulting in cytotoxicity (Rizzuti et al., 2008). Though intravitreal injections achieve therapeutic drug concentrations in the retinoblastoma cells, adverse effects such as retinal detachment from repeated injections, hemorrhage, endophthalmitis and toxicity to healthy retinal cells often results in patient noncompliance (Janoria et al., 2007). Direct IVT administration of chemotherapeutic agents lead to drug induced cataract in the lens and clouding of the cornea (Phylactos and Unger, 1998). An ideal drug delivery system for the treatment of RB should possess high encapsulation efficiency and selectively deliver drugs to tumor cells in a sustained manner.

4.3. Objectives

1. To synthesize and characterize PLGA-PEG-folate polymer.
2. To study the effect of solvents on the entrapment efficiency, surface morphology, particle size and polydispersity of polymeric micelles.
3. To study the effect of PLGA-PEG-PLGA thermosensitive gel on the *in vitro* release rate of DOX from polymeric micelles
4. To study the qualitative and quantitative uptake of DOX from PLGA-PEG-folate micelles in retinoblastoma cells.
5. To study the cytotoxicity of DOX loaded polymeric micelles in retinoblastoma cells.

CHAPTER 5

IN VITRO EVALUATION OF A TARGETED AND SUSTAINED RELEASE SYSTEM FOR RETINOBLASTOMA CELLS USING DOXORUBICIN AS A MODEL DRUG

5.1. Rationale

Retinoblastoma (RB) represents a common form of intraocular malignancy affecting the retina (Albert, 1987; Bishop and Madson, 1975). Eighty-seven percent of children who are diagnosed with RB do not survive very long due to invasion, metastasis and hematogenous spread (Honavar and Singh, 2005; Sanchez de Toledo, 2008). It is common in children between the age of 3 and 7 (Pesin and Shields, 1989). The Reese-Ellsworth (RE) classification system is applied most widely for describing intraocular tumors (Aerts et al., 2006; Henkes et al., 1977). As per the classification, RB tumor is divided into five groups as shown in Table 12. Though it is not a real staging system it has served as an excellent tool for determining and comparing different treatment strategies. RE groups IV and V are considered very advanced and do not respond well to chemotherapy (De Potter, 2002). In such cases, external beam radiotherapy (EBR) and enucleation are employed as the last recourse. Both treatments leave the survivors with complete or nearly complete vision loss (Chintagumpala et al., 2007). Currently, EBR is no longer a viable option due to long term side effects like optic neuropathy, cataract, retinopathy and chronic dry eye (Eng et al., 1993). Development of secondary tumors in the area exposed to the radiation after a long time period is the major reason that discourages the application of EBR (Eng et al., 1993). Enucleation is the only treatment option for RE group V tumors.

Table 12. Reese-Ellsworth system for intraocular retinoblastoma (Aerts et al., 2006; Henkes et al., 1977)

Group I Very favorable	a) Solitary tumor, < 4 disc diameters in size, at or behind the equator b) Multiple tumors, none > 4 disc diameters in size, all at or behind the equator
Group II Favorable	a) Solitary tumor, 4 to 10 disc diameters in size, at or behind the equator b) Multiple tumors, 4 to 10 disc diameters in size, behind the equator
Group III Doubtful	a) Any lesion anterior to the equator b) Solitary tumors > 10 disc diameters behind the equator
Group IV Unfavorable	a) Multiple tumors, some > 10 disc diameters b) Any lesion extending anteriorly to the ora seratta
Group V Very unfavorable	a) Massive tumors involving over half the retina b) Vitreous seeding

In the last decade, several reports suggest that chemotherapy is successful in treating the RE group I to III tumors (De Potter, 2002). This is due to the presence of vitreal seeds that are responsible for disease recurrence (Chintagumpala et al., 2007). However, exposing the eye to another external beam radiation may result in complications caused by a high radiation dose. Chemotherapy helps in the reduction of vitreal seeds and tumor size; so that focal therapy (photocoagulation, hyperthermia, cryotherapy or radioactive plaque) can be applied to a relatively small area and the tumor can be shrunk without loss of vision (Beck et al., 2000; De Potter, 2002; Murphree et al., 1996). Systemic chemotherapy for RB was introduced in the 1960's. Recent work has reported the use of topotecan, etoposide, carboplatin and vincristine for the treatment of RB (De Potter, 2002; Rizzuti et al., 2008). Some investigators have added cyclosporin in the regimen as a P-glycoprotein (P-gp) inhibitor assuming that anticancer agents will show better efficacy, but this therapeutic regime remains controversial (Gallie et al., 1996). One of the major impediments to drug development in RB has been the lack of knowledge regarding intraocular disposition, elimination, blood ocular transport and retinal uptake of chemotherapeutic agents. For effective therapy, chemotherapeutic agents should enter tumor cells in required therapeutic concentrations. Generally, chemotherapeutic agents are administered by intravenous route which in the absence of any targeting strategy exposes normal cells to high levels of anticancer agents resulting in cytotoxicity (Rizzuti et al., 2008). In addition, initial drug exposure causes up regulation of multidrug resistant (MDR) genes resulting in increased expression of efflux pumps (P-gp, MRP and BCRP) leading to increased drug efflux (Chin and Liu, 1994). RB cells are known to express efflux proteins

such as P-gp and MRP (Chan et al., 1989; Kuo, 2007). A majority of anticancer agents are good substrates for these efflux pumps and reduces drug concentrations in retinal tissues (Kartner et al., 1985; Li et al., 2009).

In the past few years, research in drug delivery to the posterior segment by intravitreal (IVT) injections has grown significantly. Though IVT injections can achieve therapeutic drug concentrations in the neural retina, adverse effects such as retinal detachment from repeated injections, hemorrhage, endophthalmitis and other retinal toxicities due to high drug concentrations achieved from IVT bolus dose administration may result in patient noncompliance (Janoria et al., 2007). Direct IVT administration of chemotherapeutic agents leads to drug induced cataract in the lens and clouding of the cornea (Phylactos and Unger, 1998). An ideal drug delivery system for the treatment of RB should possess high encapsulation efficiency and selectively deliver drugs to tumor cells in a sustained manner. Drug targeting via receptors is an effective way to cell-selective drug delivery, since this process allows a satisfactory transport rate and ligand-dependent cell specificity. Folic acid, an essential vitamin enters into cells through a membrane associated folate binding protein in addition to classical high affinity/low capacity carrier system (Shiokawa et al., 2005; Weitman et al., 1992). Targetability of various delivery systems such as liposomes, polymer conjugates, polymeric micelles and nanoparticulates has been achieved with a covalently attached folate on the surface (Yoo and Park, 2004). For chemotherapeutics agents such as doxorubicin (DOX), biodegradable polymeric micelles have been utilized for passive and active targeting to various solid tumors (Yoo and Park, 2004; Zhao and Yung, 2008).

Selective targeting and higher cytotoxicity in folate receptor-positive cancer cells has been achieved with folate conjugated polymeric micelles (Park et al., 2005; Yoo and Park, 2004). However, no studies have been reported regarding the effectiveness of polymeric micelles in the treatment of intraocular tumors. Drugs entrapped inside polymeric micelles are released rapidly within a short span of 24-48 h. Yoo et al. conjugated DOX to PLGA-PEG block copolymer and utilized this construct for the preparation of polymeric micelles. DOX-PLGA-PEG micelles exhibited sustained drug release over 2-3 weeks (Yoo and Park, 2001). However, this strategy is tedious and expensive as the chemistry involved in the conjugation of a polymer to a ligand needs to be optimized for each drug.

In this study, we made an attempt to develop and evaluate a novel folate receptor targeted drug delivery system for RB cells. Doxorubicin (DOX), a fluorescent molecule was used as a model drug for the studies. Previous studies from our laboratory have confirmed the presence of folate receptors on RB (Y-79) cell line (Kansara et al., 2008). We have synthesized poly (D,L-lactide-*co*-glycolide)-poly(ethylene glycol)-folate (PLGA-PEG-FOL) for selective delivery to RB cells. Biodegradable DOX-loaded poly(D,L-lactide-*co*-glycolide)-poly(ethylene glycol)-folate (PLGA-PEG-FOL) micelles (DOXM) were prepared from various solvents (DMSO, acetone and DMF). Effects of solvents on entrapment efficiency, size and polydispersity were examined. Further, the effect of thermosensitive gel (PLGA-PEG-PLGA) on the release of DOX from DOXM is also described.

5.2. Materials and Methods

5.2. Materials

Polyoxyethylene bis(amine) M_w 3,000, folic acid, doxorubicin HCl, dimethylsulfoxide (DMSO), dicyclohexylcarbodiimide (DCC), triethylamine (TEA), acetone and polyethylene glycol 1450, and dialysis tubing made of cellulose membrane were procured from Sigma Chemicals (St Louis, MO). Resazurin dye was obtained from Biotium, Inc. (Hayward, CA). Dimethylformamide (DMF) was obtained from American Scientific Products (Muskegon, MI). PLGA (RG502H) (weight average MW: 8000) was obtained from Boehringer Ingelheim (Germany). Thermosensitive gel PLGA-PEG-PLGA (weight average molecular weight [M_{wb}] - 4759 Da) was synthesized and purified.

5.2.1. Synthesis of PLGA-PEG-FOL

PLGA-PEG-FOL was synthesized according to a previously published procedure with minor modifications: step 1- activation of PLGA; step 2- synthesis of PLGA-PEG-NH_2; step 3- synthesis of PLGA-PEG-FOL (Yoo and Park, 2004).

5.2.1.1. Step 1- Activation of PLGA

PLGA was activated with DCC and *N*-hydroxysuccinimide (NHS) in dichloromethane (molar ratio of DCC: NHS: PLGA= 1.2:1.2:1) under inert atmosphere for 24 h. Activated PLGA was precipitated with ice-cold diethyl ether followed by filtration and vacuum drying for 24 h.

5.2.1.2. Step 2- Synthesis of PLGA-PEG-NH_2

One gram of activated PLGA was dissolved in dichloromethane (5 mL). In a separate flask 2.1 g of PEG-bis-amine was dissolved in 2 mL of dichloromethane and added to PLGA solution in a drop-wise manner (PLGA:PEG-bis-amine::1:5). The reaction mixture was stirred under an inert atmosphere. PLGA-PEG-NH_2 was dialysed (MWCO:10 kDa) against deionized water for 48 h to remove unreacted PEG-bisamine and freeze dried (VirTis Wizard 2.0 Freeze Dryer Control System).

5.2.1.3. Step 3- Synthesis of PLGA-PEG-FOL

Folic acid was activated with N-hydroxysuccimide (NHS) and dicyclohexylcarbodiimide (DCC) at a molar ratio of folic acid/NHS/DCC=1:2:2. Folate-conjugated di-block copolymer was synthesized by coupling PLGA-PEG-NH_2 (500 mg) in DMSO to activated folic acid. The reaction was performed under inert atmosphere at room temperature over 12 h. The reaction mixture was mixed with 50 mL of distilled water and centrifuged at 5000 g and pellet of dicyclourea was discarded. The supernatant was dialyzed (MWCO: 10 kDa) extensively against deionized water for 48 h and then freeze dried.

5.2.2. Characterization of PLGA-PEG-FOL

The structure of PLGA-PEG-FOL was confirmed by ^{1}H NMR spectroscopy (Varian-400 MHz NMR spectrometer) in d_6-DMSO. Chemical shifts (δ) were expressed in parts per million (ppm) relative to the NMR solvent signal (d_6-DMSO) using tetramethylsilane as an internal standard. The amount of folic acid conjugated to PLGA-PEG-FOL was determined by a UV-visible calibration curve of folic acid in DMSO at 340 nm.

5.2.3. Preparation of DOX-loaded PLGA-PEG-FOL Micelles (DOXM)

DOX was neutralized with 2 mol excess of TEA in 2 mL of DMSO or acetone or DMF. Dialysis tubing used in the study was resistant to the solvents DMSO and acetone and DMF. Briefly, 5 mg of DOX (after TEA treatment) and 20mg of PLGA-PEG-FOL were dissolved in 5 mL of DMSO or acetone or DMF and vortexed for 10 min. This solution was dialyzed (MWCO: 10 kDa) for a period of 48 h against distilled deionized water to remove solvent and unentrapped DOX. Micelles thus formed were freeze dried and characterized for entrapment efficiency, particle size, polydispersity, morphology and *in vitro* release characteristics (Zhao and Yung, 2008). PLGA-PEG micelles of DOX (DOXMC) were also prepared in the similar manner and used as control in the uptake studies.

5.2.4. Entrapment efficiency studies

Two mg of freeze dried DOXM was dissolved in DMSO and DOX content was analyzed using microplate reader (DTX 880 Series Multimode Detector, Multimode Detection Software, Beckman Coulter, Inc, CA) at 485 nm (excitation wavelength) and 595 nm (emission wavelength). Entrapment efficiency was calculated using Eq. 1. All experiments were conducted in triplicate.

5.2.5. Particle size analysis

Dynamic light scattering (Brookhaven Zeta Plus instrument, Holtsville, NY) technique was employed to measure particle size of DOXM. Polydispersity values were also measured.

5.2.6. Morphology of polymeric micelles

Transmission electron microscopy (Philips CM12 STEM, Hillsboro, OR) was utilized for examining the morphology of the polymeric micelles. A drop of micellar solution was placed on a carbon-coated copper grid and the excess fluid was removed by a piece of filter paper. The sample was then stained with 2% phosphotungstic acid solution and excess solution was removed using a filter paper. TEM images were taken after the sample was completely dried.

5.2.7. *In vitro* drug release

Five milligrams of DOXM were dispersed in 1mL isotonic phosphate buffer saline (IPBS), pH 7.4 or 1 mL of 23% w/w PLGA-PEG-PLGA polymer solution and subsequently introduced into a dialysis bags (MWCO-6275 Da). The polymer solution inside the bags was allowed to form a gel at 37 ^{o}C for 30-60 seconds. The dialysis bags were introduced into vials containing 10 mL IPBS and 0.025% w/v sodium azide to avoid microbial growth and 0.02% (w/v) and Tween 80 to maintain sink conditions. The vials were placed in a shaker bath with temperature maintained at 37 ± 0.5 °C and constant agitation of 60 oscillations/min. At regular time intervals 200 µL samples were withdrawn and replaced with equal volumes of fresh buffer. Samples were analyzed with microplate reader at 485 nm (excitation wavelength) and 595 nm (emission wavelength). All experiments were conducted in triplicate.

5.2.8. Morphology of polymeric micelles suspended in thermosensitive gels

Scanning electron microscopy (FEG ESEM XL 30, FEI, Hillsboro, OR) was employed for studying the surface morphology. Freeze dried powder of polymeric micelles suspended in

thermosensitive gels were attached to a double-sided tape, spray-coated with gold–palladium at 0.6 kV and then examined under the electron microscope.

5.2.9. Cell culture

Human retinoblastoma cell line (Y-79) was obtained from American Type Culture Collections (ATCC). Y-79 cells were used for estimating the qualitative and quantitative uptake of DOX from micelles. Further cytotoxicity studies were also performed on these cells. Y-79 cells were incubated in 75 cm^2 tissue culture flasks as a suspension in RPMI 1640 medium supplemented with 15% non-heat inactivated fetal bovine serum, 1 mM glutamine, penicillin (100 units/mL) and streptomycin (100 µg/mL) cells were maintained at 37 ^oC, in a humidified atmosphere of 5% CO_2 and 90% relative humidity.

5.2.10. Uptake Studies

Y-79 cells were centrifuged and washed three times with a Dulbecco's phosphate-buffered saline (DPBS), pH 7.4, containing 0.03 mM KCl, 130 mM NaCl, 1 mM $CaCl_2$, 7.5 mM Na_2HPO_4, 1.5 mM KH_2PO_4, 0.5 mM $MgSO_4$, and 5 mM glucose to remove endogenous folates bound to folate receptors on the cell surface. Uptake studies were carried out in DPBS, pH-7.4. Uptake was initiated by the addition of 200 µg/mL of DOX, DOXMC, DOXM and DOXM solutions in presence of excess folic acid (~1 mM) for 1 h. After incubation cells were centrifuged and rinsed 3 times with 1mL of ice-cold stop solution (210 mM KCl, 2 mM HEPES) to arrest uptake. After each wash, cells were centrifuged and separated. Cells were then solubilized in 1mL of 0.1% Triton-X solution in 1% NaOH. DOX

concentration was measured using a fluorescence spectrophotometer at 485 nm (excitation wavelength) and 595 nm (emission wavelength) (Kansara et al., 2008).

5.2.10. Confocal Studies

Y-79 cells were incubated with DOX solution, DOXM and DOXM in presence of excess folic acid (~1 mM) for 30 min in DPBS. DOX concentration equivalent to 10 µg/mL was maintained in solutions. Following incubation the cells were washed 3 times to remove un-internalized DOX and then exposed to 4% buffered paraformaldehyde for 20 min at 4 ^{o}C, rinsed thrice with DPBS and then mounted on glass slides using mounting gel. Slides were observed under confocal laser fluorescence microscope. Series of images were acquired in the z-axis (0.5 µm apart) with Olympus FV300 confocal laser scanning unit coupled to an Olympus BX61 upright microscope (Center Valley, PA). Pictures were processed by Fluoview™ software and edited using Adobe Photoshop CS3 (Adobe Systems Inc., San Jose, CA, USA).

5.2.11. Cell Viability Studies in Y-79 cells

As Y-79 cells do not attach to the substratum, the 96 well plates were initially coated with coated 50 µg/mL poly-d-lysine solution. Approximately 5000 cells/well were plated and incubated with RPMI-1640 medium containing laminin (12.5 µg/mL, added to the medium), at 37 ^{o}C for 24 h. The cells were then exposed to various concentrations (0-10 µM) of DOX solution and DOXM. Cells with medium alone were used as negative control. Cells were incubated for 48 h and drug solutions were aspirated and then 100 µL of resazurin dye solution was added to each well. The plate was incubated for 1 h at 37 ^{o}C and the amount of

absorbance in each well was measured at 600 nm. Resazurin is a blue colored compound and turns pink upon oxidation in presence of live cells. Amount of absorbance reflects the number of viable cells.

5.3. Results

The biodegradable copolymer PLGA-PEG-FOL was successfully synthesized according to a previously published procedure with minor modifications (Yoo and Park, 2004). Figure 29 demonstrates various proton peaks associated with PLGA-PEG-FOL polymer. Small peaks at 6.6, 7.6 and 8.7 ppm indicate protons associated with folate. Peak at 3.6 ppm is due to $-CH_2-$ protons of PEG block of the polymer. The peaks at 1.6 and 5.2 ppm are due to $-CH_3$ and -CH- protons of PLA block. The peak at 4.8 ppm belongs to the $-CH_2-$ protons of PGA block of the polymer. On molar ratio basis the conjugation percentage of folate to PLGA-PEG was found to be 53%. Micelles containing DOX (DOXM) were successfully prepared by the dialysis method. Table 13 shows the effect of particle size, polydispersity and entrapment of DOX in various solvents. Based on size, polydispersity and entrapment efficiency DMF was found to be suitable for the preparation of DOXM. Particle size of DOXM in DMSO, acetone and DMF were observed to be 85, 101 and 75 nm with a polydispersity of 0.31, 0.23 and 0.08 respectively.

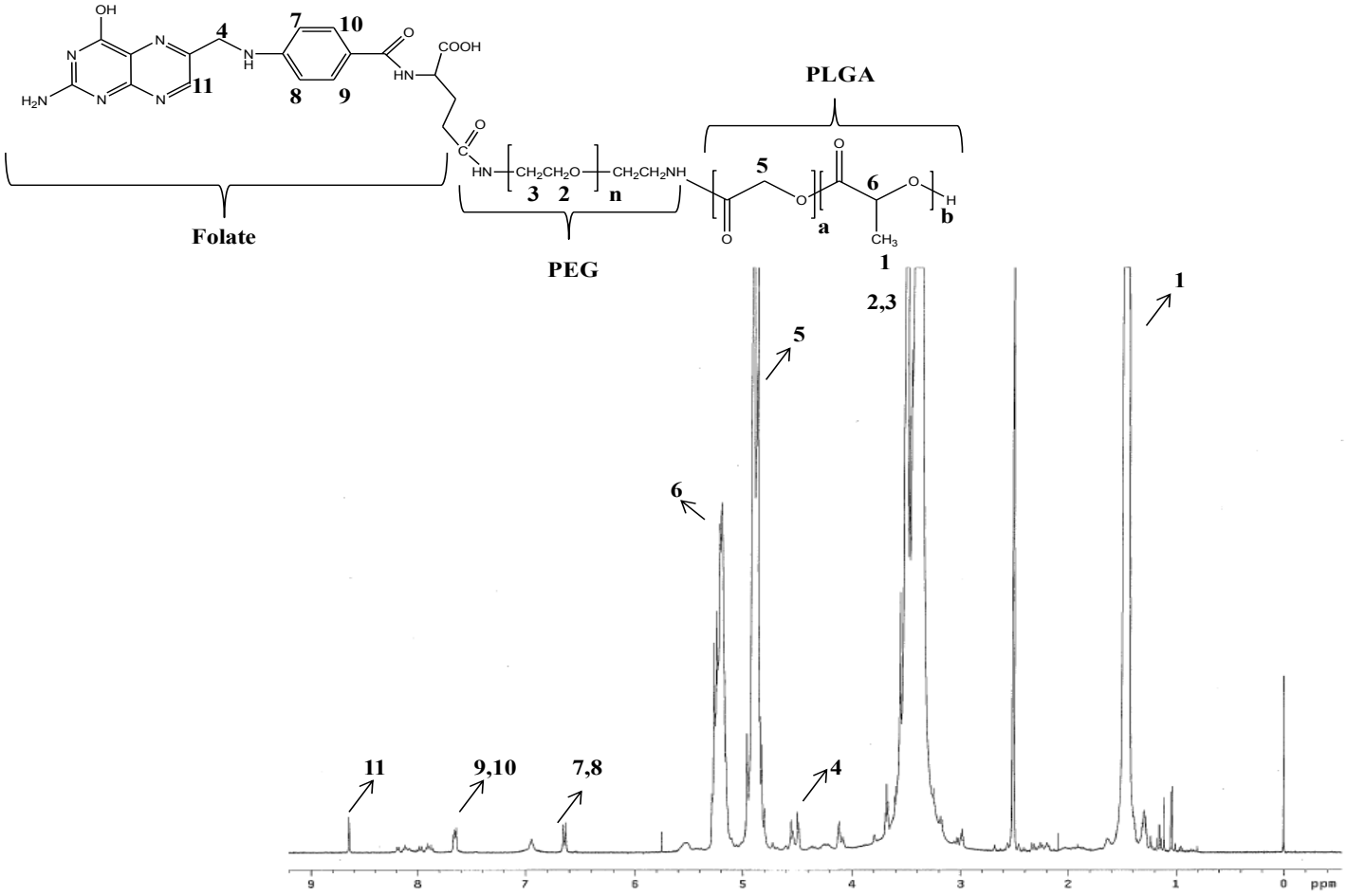

Fig. 29. ^{1}H NMR spectrum of PLGA-PEG-FOL conjugate

Entrapment efficiencies of DOX in DMSO, acetone and DMF were found to be 58, 52 and 60% respectively. DOXM micelles were further characterized for morphology and *in vitro* release. Spherical morphology of DOXM was confirmed by TEM (Fig. 30). The *in vitro* drug release study revealed a biphasic release pattern with an initial rapid release (burst release) followed by sustained release over a period of 48 h (Fig. 31). Release of DOX from DOXM was retarded in presence of PLGA-PEG-PLGA gel. Synthesis and characterization of triblock copolymer PLGA-PEG-PLGA (weight average molecular weight [M_{wb}] determined by gel permeation chromatography - 4759 Da) has already been published by our laboratory (Duvvuri et al., 2005). Phase transition studies revealed that the polymer at concentrations ranging between 20-25% w/v forms a gel at 32-60 ^{o}C. Since the temperature inside the eye ranges from 34-37 ^{o}C such polymeric gels may be appropriate for drug delivery (Figs. 32A and B) (Duvvuri et al., 2007).

Table 13. Effect of solvents on particle size, polydispersity and encapsulation efficacy of doxorubicin

Solvent	**Particle size (nm)**	**Polydispersity**	**Encapsulation Efficiency (%)**
DMSO	85.30±4.53	0.31	58.20±2.01
Acetone	101.20±5.63	0.23	52.45±3.74
DMF	75.20±2.40	0.08	60.32±2.56

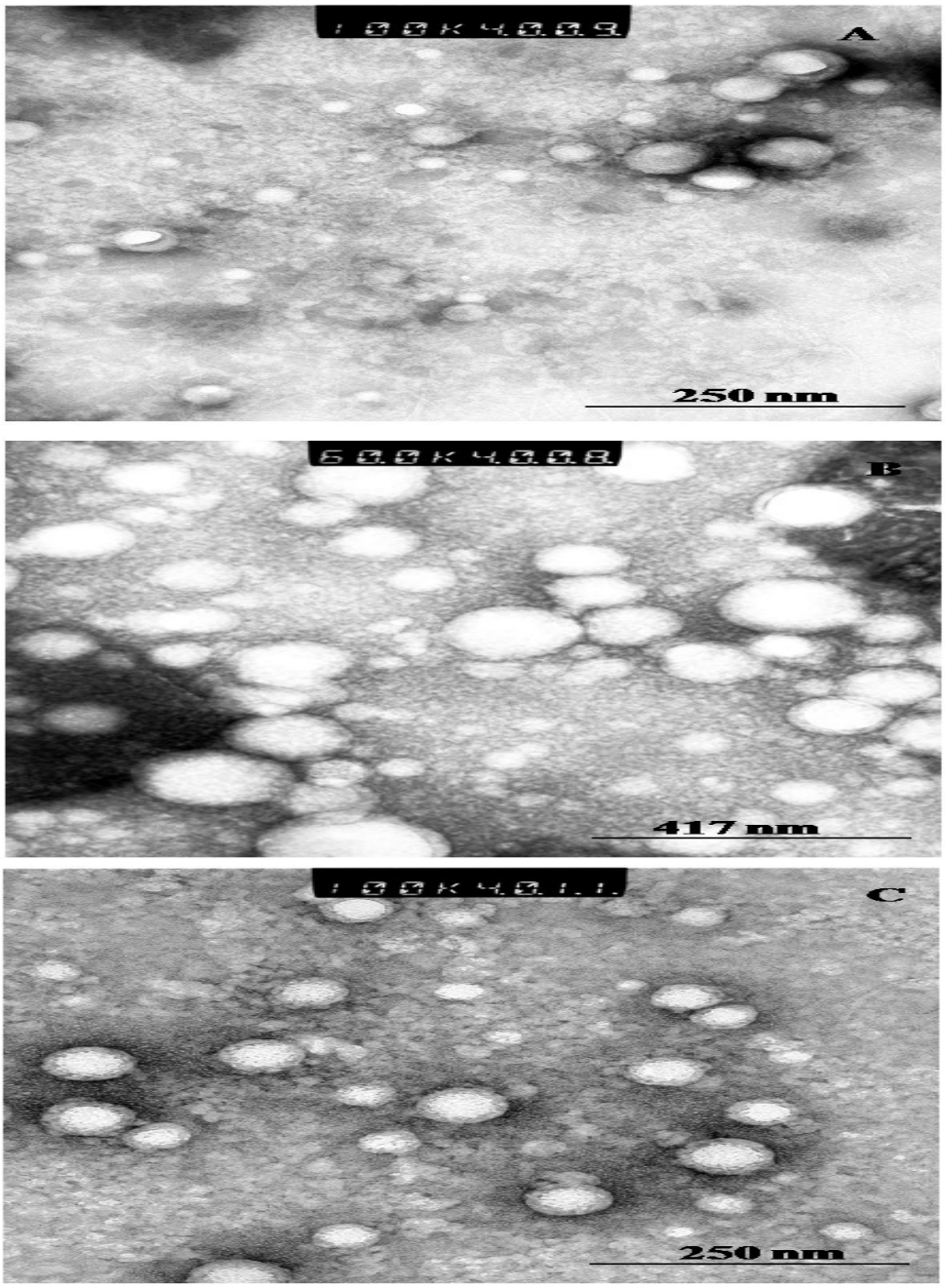

Fig. 30. Transmission electron microscopy image of DOX-loaded PLGA-PEG-FOL micelles (DOXM). (A) DOXM prepared by DMSO, (B) DOXM prepared by acetone, (C) DOXM prepared by DMF

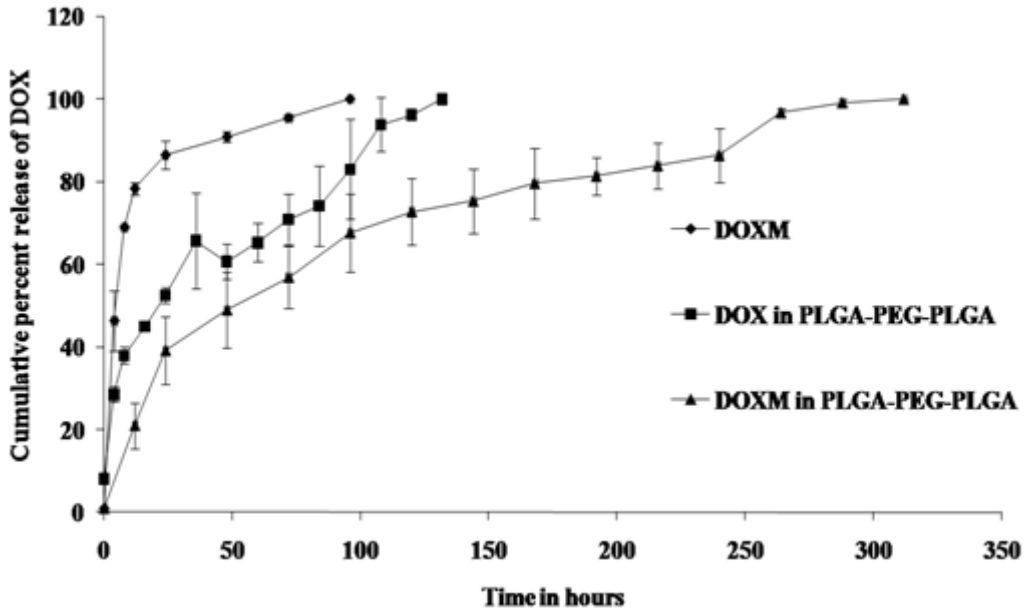

Fig. 31. *In vitro* release profile of doxorubicin from (◆) DOX-loaded PLGA-PEG-FOL micelles (DOXM); ■) DOX suspended in PLGA-PEG-PLGA thermosensitive gel and (▲) DOX-loaded PLGA-PEG-FOL micelles (DOXM) suspended in PLGA-PEG-PLGA thermosensitive gel. Each data point is the average of three samples. Error bars represent the standard error of mean (S.E.M)

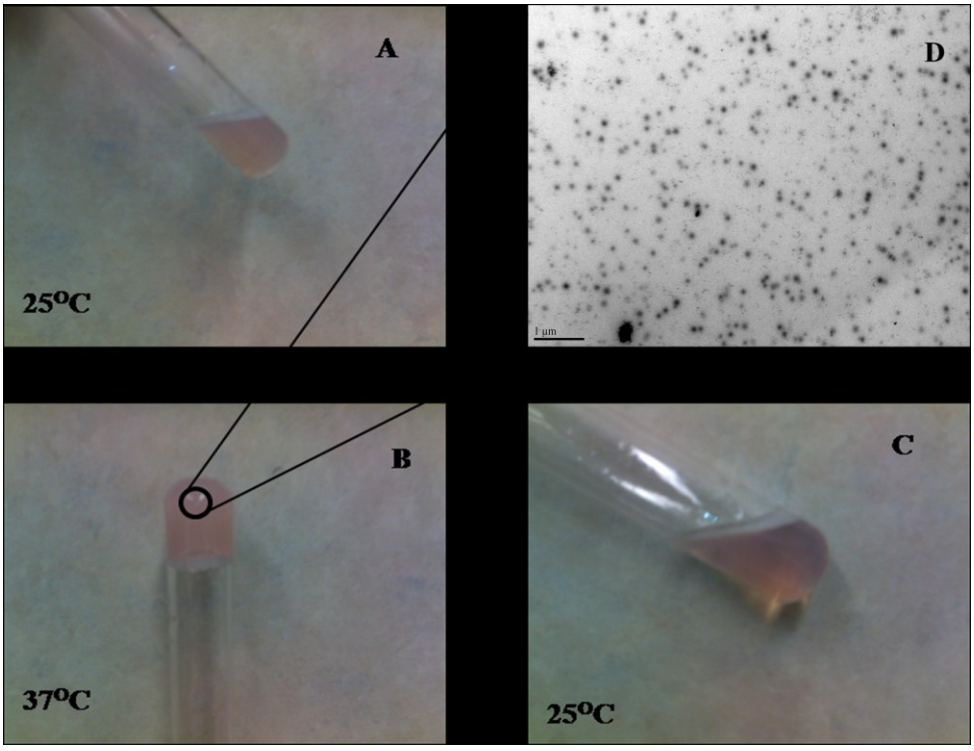

Fig. 32. Gelation and uniform dispersion of polymeric micelles in PLGA-PEG-PLGA thermosensitive gel A) DOXM suspended in PLGA-PEG-PLGA thermosensitive gel at 25 °C; B) DOXM suspended in PLGA-PEG-PLGA thermosensitive gel at 34-37 °C; C) SEM images of DOXM suspended in PLGA-PEG-PLGA thermosensitive gel; D) Reverse transition of gel to solution at 25°C

PLGA-PEG-PLGA gel sustained the release of DOX over a period of 132 h. Surprisingly, dispersion of folate conjugated polymer micelles in the PLGA-PEG-PLGA gel structure sustained the drug release over a period of 2 weeks (Fig. 31). An SEM image of DOXM dispersed in thermosensitive gels revealed a dense network structure (Fig. 32C). The reversibility of the PLGA-PEG-PLGA gel was tested by slowly reducing the temperature from 37-25 ^{o}C, in order to achieve a clear solution (Fig. 32D). Uptake of DOX from pure drug solution, DOXM and DOXM in presence of folic acid was carried out with confocal microscopy in Y-79 cells. DOXM exhibited higher fluorescence relative to free DOX (Figs. 33A and 33B). Fluorescence intensity was reduced in the presence of excess folic acid suggesting uptake of micelles via folate receptor (Fig. 33C). Z-stack images were taken to confirm the presence of DOXM inside Y-79 cells (Fig. 33D-33K). Uptake of both DOX and DOXM was quantitatively estimated in Y-79 cells. Uptake of DOX was approximately four times higher in the presence of DOXM (Fig. 34).

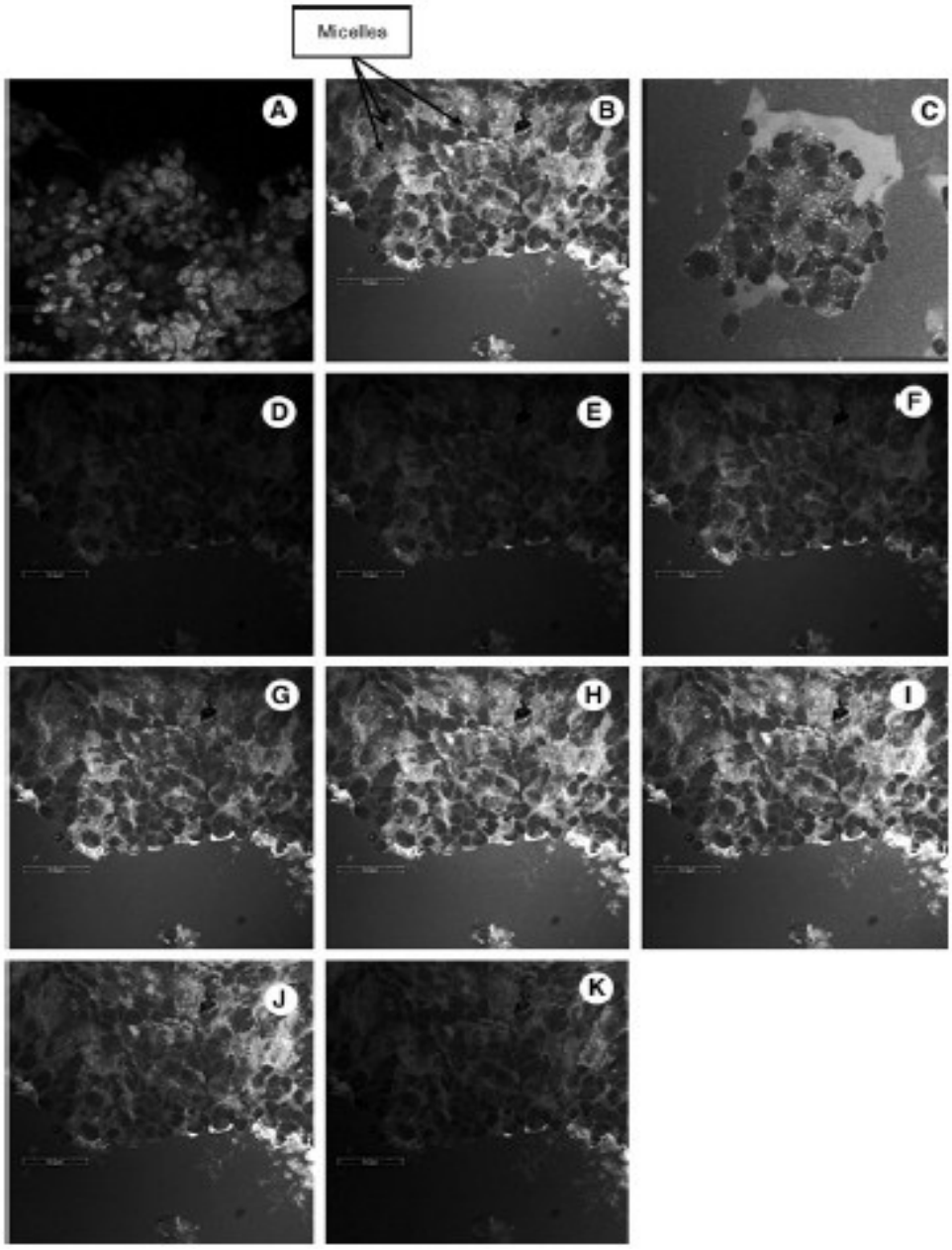

Fig. 33. Confocal images of Y-79 cells following treatment with DOX and DOX-loaded PLGA-PEG-FOL micelles (DOXM). (A) pure DOX, (B) DOXM, (C) DOXM in presence of folic acid, (D-K) Z-stack images of DOXM to show that micelles are inside Y-79 cells. Bar represents 50 μm.

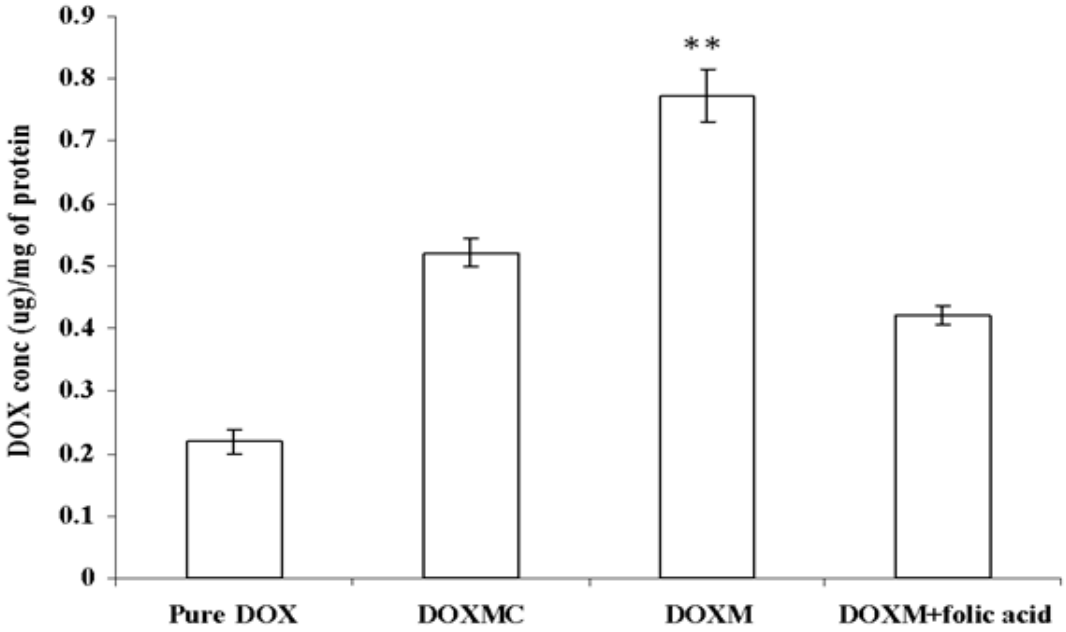

Fig.34. Quantitative uptake of DOX in Y-79 cells using pure DOX, DOX-loaded in PLGA-PEG micelles/non-targeted micelles (DOXMC), DOX-loaded PLGA-PEG-FOL micelles (DOXM) and DOXM in presence of folic acid. ** $P < 0.05$

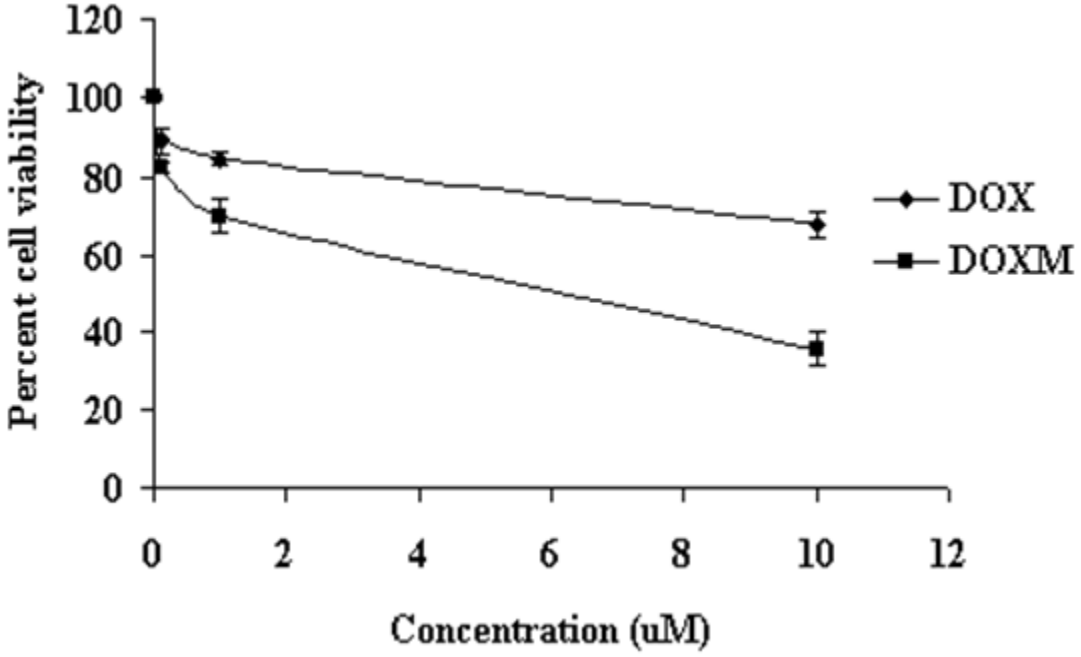

Fig. 35. Cell viability studies of DOX in Y-79 cells following treatment with DOX and DOX-loaded PLGA-PEG-FOL micelles (DOXM).

Cytotoxicity studies of DOX formulations (free DOX and DOXM) were carried out in retinoblastoma cell line (Y-79 cells). At concentrations ranging from 0-10 μM, DOXM exhibited higher cytotoxicity in Y-79 cells expressing folate receptors (Fig. 35) (Aukunuru et al., 2001; Treupel et al., 1991).

5.4. Discussion

Systematically administered antineoplastic agents exhibit limited permeability into the retina and vitreous mainly due to blood retinal barrier (Janoria et al., 2007). Moreover, the presence of efflux pumps such as P-gp and MRP further restrict the permeation of various chemotherapeutic agents (Gaudana et al., 2009). Though intravitreal injections deliver drugs to the retina directly, potential side effects like increased intraocular pressure, hemorrhage, retinal detachment, cataract and endophthalmitis lead to complications limiting long term therapy (Janoria et al., 2007). Recent advances in drug delivery system design led to the development of intravitreal implants that can be placed inside the vitreous to deliver constant drug levels over prolonged periods. However such a system requires repeated surgery for the implantation and removal of implants (Janoria et al., 2007). Keeping these facts in mind we have developed an alternative strategy which employs *in situ* gelling polymers for sustaining drug release from surface modified polymeric micelles to target the drug to RB cells. Polymeric micelles have been successfully utilized as targeted drug delivery systems (Jones and Leroux, 1999). However, polymeric micelles tend to dissociate upon dilution in biological fluids after injection which results in burst release (Bae and Yin, 2008). The exact mechanism involved in the destabilization of polymeric micelles is not clear. Recent studies

by Chen and his colleagues revealed that potential interactions of polymeric micelles with various biological components may affect the release pattern of entrapped drugs (Chen et al., 2008). We hypothesized that thermogel system (eg. PLGA-PEG-PLGA) as delivery vehicles, might prevent the dilution and interaction of polymeric micelles with biological components. Previous studies reported a 44.8% (molar ratio basis) conjugation of folate to PLGA-PEG (Yoo and Park, 2004). In the present study the conjugation of folate was found to be 52.7%. At fixed ratio of drug to polymer::1:4, the effect of solvents on entrapment efficiency, size and polydispersity was studied. DMF resulted in low polydispersity values indicating uniform micellar size as compared to DMSO and acetone. Particle size of DOXM was found to be higher in case of acetone. Slight variations in entrapment efficiency and size may be attributed to the differences in miscibility/solubility of organic solvents in water (Jeon et al., 2000). Further characterization was carried out for DOXM prepared from DMF as the initial solvent. DOX release rate was faster from DOXM in the first 8 h and then became progressively lower and sustained for 48 h thereafter. Release from polymeric micelles mainly involves two mechanisms: diffusion and copolymer degradation. However several studies suggest that when rate of drug release is greater than the rate of copolymer degradation the diffusion mechanism predominates (Liu et al., 2005). Burst release is mainly due to DOX molecules adsorbed within the corona or at the interface of core/corona (Zhao and Yung, 2008). When dispersed in PLGA-PEG-PLGA thermosensitive gels the *in vitro* release of DOX from DOXM was sustained for 2 weeks. The exact mechanism involved in the sustained release of DOX from DOXM suspended in PLGA-PEG-PLGA is not presently

clear. Temperature sensitive polymeric gels such as PLGA–PEG–PLGA, remains in solution form at room temperature and gels at body temperature. At room temperature the hydrogen bonding between water molecules and the PEG chains dominate and forces the copolymer molecules to stay in solution. At body temperature the hydrophobic forces among the PLGA segments dominate and hydrogen bonding becomes weaker thus leading to sol–gel transition. The release of drugs from the hydrogels mainly occurs by two mechanisms: (i) an initial phase consists of drug diffusion from the hydrogel and (ii) a later phase consisting of erosion of the hydrogel matrix (Qiao et al., 2005). The external surface of polymeric micelles is hydrophilic in nature and tends to partition in the PEG domains (Fig. 36).

We anticipate that during the initial phase, polymeric micelles (~70-100 nm) tend to slowly diffuse through the hydrophilic porous channels, while in the later stage the release may be due to combination of diffusion and erosion of the polymeric gel matrix. Moreover, it is likely that thermosensitive polymers upon gelation at body temperature (34-37 ^{o}C) prevent the dilution of DOXM from the external fluids. Hence these polymeric micelles may remain intact inside the thermosensitive gels and gradually release its cargo as the gel degrades. Release of DOXM from PLGA-PEG-PLGA gels acts as the major rate limiting step in the release rate of DOX.

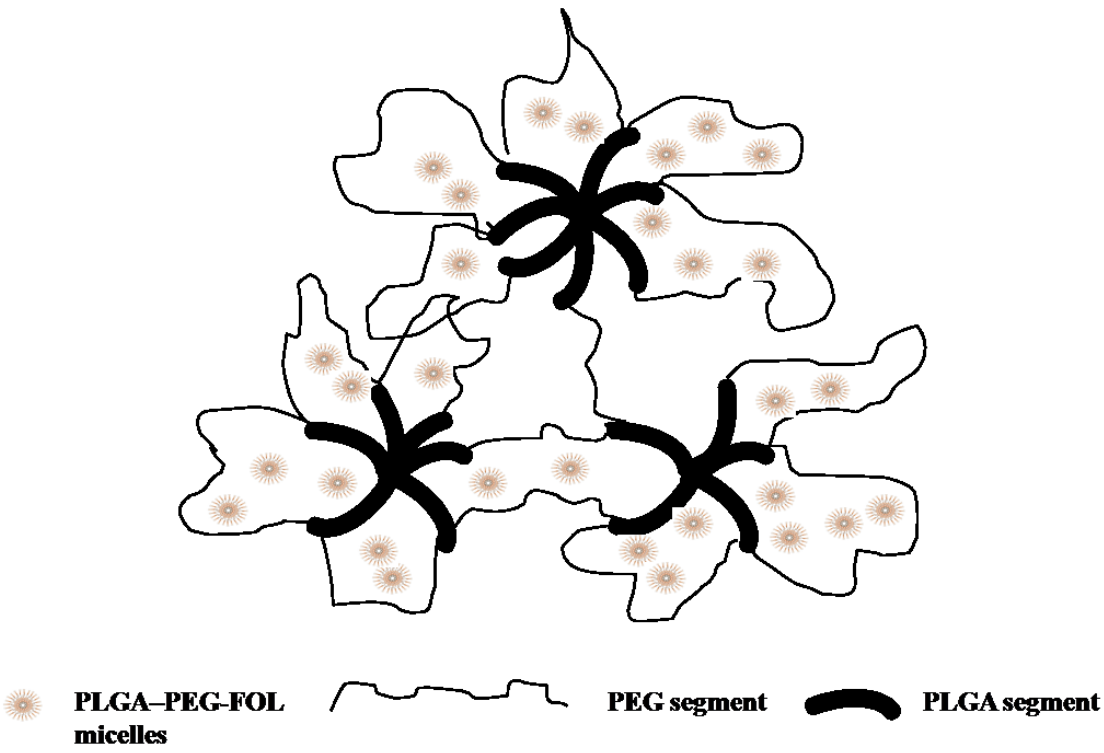

Fig. 36. Release mechanism of DOX-loaded PLGA-PEG-FOL micelles from PLGA-PEG-PLGA thermosensitive gel

Qualitative uptake analysis with confocal imaging of Y-79 cells over-expressing folate receptor revealed that DOXM exhibits a much larger extent of cellular uptake than pure DOX. This was further confirmed by quantitative uptake studies. Z-stack images clearly depict internalization of DOXM in Y-79 cells. DOX is a well known substrate for multidrug resistant (MDR1) efflux pumps which are highly expressed on Y-79 cells. These efflux pumps lower entry of DOX into Y-79 cells (Kartner et al., 1985). However, DOXM enters the cells via folate receptors on the surface of Y-79 cells. PEG acts as a linker between PLGA and folate moiety to form nanomicelles such that folate can easily bind to the folate receptor on Y-79 cells. With equivalent drug loading in the culture medium, DOXM showed much higher cell cytotoxicity than DOX, in Y-79 cells. Folate receptor expression was found to higher on the basolateral side of ARPE-19 cells as compared to the apical side (Huang et al., 1997). This shows that DOX when administered as polymeric micelles conjugated to folic acid can specifically target the retinoblastoma cells sparing the healthy retinal cells, which do not express folate receptor.

Previous studies from our laboratory concluded that intravitreal delivery of ganciclovir (GCV)-loaded poly(d,l-lactide-co-glycolide) microspheres in thermogelling PLGA-PEG-PLGA gel resulted therapeutic vitreal concentrations over 14 days (Duvvuri et al., 2007). Moreover, this formulation did not produce any major breakdown in the retinal cell structure. We anticipate that our current formulation will be safe for the healthy retinal cells and toxic for the RB cells.

5.5. Conclusion

In summary, we have provided proof for a novel injectable drug carrier system for the local and targeted delivery of drugs to RB cells using DOX as a model. Release of DOX from DOXM was successfully retarded by PLGA-PEG-PLGA gel system. Qualitative uptake studies revealed that DOXM exhibited higher cellular uptake than pure DOX in Y-79 cells over-expressing folate receptors. This result was further confirmed from the quantitative uptake studies. Polymeric micellar systems suspended in thermosensitive gels may provide sustained and targeted delivery of anticancer agents (topotecan, etoposide, carboplatin and vincristine) to RB cells.

CHAPTER 6

RATIONALE FOR INVESTIGATION

6.1. Overview

During the last decade, polymeric nanoparticles have gained lot of attention due to their versatile properties including: long shelf stability, high drug loading capacity, and ability to deliver both hydrophilic and hydrophobic drug molecules via peroral, transmucosal and inhalation routes (Langer, 2000; Pandey and Khuller, 2005). They have been sucessfully used for passive and active targeting of drugs. Active targeting helps in delivering the drug molecules to the site of action and minimizes drug exposure to non-target regions. Active targeting of nanoparticles can potentially increase the efficacy and reduce the toxicity of therapeutic agents (Zhao et al., 2008). Folic acid (FA) has been widely used in the delivery of anticancer agents due to its small size, low cost, high tumor tissue specificity and non-immunogenic nature (Lu and Low, 2002). In this study, we propose an alternative and relatively easy strategy for the preparation of surface modified nanoparticles for both hydrophilic and hydrophobic drug molecules. This study involves the use of poly(lactide-co-glycolide)-poly(ethylene glycol)-folate (PLGA-PEG-FOL) conjugate in the preparation of nanoparticles. PLGA-PEG-FOL polymer was synthesized and characterized using ^{1}H NMR, GPC and FTIR. Further, the ability of PLGA-PEG-FOL polymer to form folate conjugated nanoparticles was investigated using three different techniques. Doxorubicin (DOX), a chemotherapeutic agent widely used in the treatment of non-Hodgkin's lymphoma, Ewing sarcoma, multiple myeloma, acute

leukemias, Wilm tumor, Kaposi sarcoma, and cancers of the lung, breast, adrenal cortex, ovary, and endometrium was utilized in the preparation of nanoparticles (Abraham et al., 2005; Carvalho et al., 2009). The polarity of DOX was sufficiently varied and then entrapped in the nanoparticles using double emulsion (W/O/W) solvent evaporation (DESE), single emulsion (O/W) solvent evaporation (SESE) or dialysis methods. Nanoparticles were evaluated for entrapment efficiency, morphology, particle size and *in vitro* release. The presence of folate on the nanoparticle surface was confirmed by using ^{1}H NMR and transmission electron microscopy (TEM) studies. Quantitative uptake and cell viability studies were carried out in FOL receptor-positive ovarian cancer (SKOV3) cells.

6.2. Statement of Problem

Various approaches have been utilized in the preparation of folate conjugated nanoparticles. Labhasetwar and his co-workers have reported the chemical conjugation of ligands after the nanoparticle preparation (Labhasetwar et al., 1998; Sahoo et al., 2004). This approach is associated with significant loss of drug during the conjugation process. Moreover introduction of multiple ligands on the surface becomes tedious. Alternative methods have been reported in the literature to overcome these disadvantages. Kim and his colleagues have developed cancer cell targeted nanoparticulate delivery system using poly(l-lysine)-poly(ethylene glycol)-folate (PLL-PEG-FOL) conjugate. In this strategy the positively charged PLL binds to the surface of negatively charged PLGA nanoparticles (Kim et al., 2005). PLL−PEG−FOL coated PLGA nanoparticles exhibited

higher uptake in KB cells as compared to unmodified nanoparticles. Patil and his co-workers have reported the interfacial activity assisted surface functionalization (IAASF) technique for the preparation of surface modified polymeric nanoparticles (Patil et al., 2009). This method involves the addition of copolymer ligand to primary emulsion containing polymer and drug which then localizes and orients at the interface upon solvent evaporation. However, this technique may not be applicable for the delivery of hydrophilic molecules including proteins and peptides.

6.3. Objectives

I. To synthesize and characterize PLGA-PEG-folate polymer.

II. To formulate and characterize DOX loaded folate conjugated nanoparticles by using double emulsion (W/O/W) solvent evaporation , single emulsion (O/W) solvent evaporation and dialysis methods

III. To study the qualitative presence of folate on the PLGA-PEG-folate nanoparticles.

IV. To study the quatitative presence of folate on the PLGA-PEG-folate nanoparticles.

V. To study the uptake and cytotoxicity of DOX loaded folate conjugated nanoparticles polymeric micelles in SKOV3 cells.

CHAPTER 7

PART II*: IN VITRO* EVALUATION OF A TARGETED AND SUSTAINED RELEASE SYSTEM FOR RETINOBLASTOMA CELLS USING DOXORUBICIN AS A MODEL DRUG

7.1.Rationale

Nanoparticles are colloidal particulate systems with particle sizes ranging between 10-1000 nm. During the last decade, polymeric nanoparticles have gained lot of attention due to their versatile properties including: long shelf stability, high drug loading capacity, and their ability to deliver both hydrophilic and hydrophobic drug molecules via peroral, transmucosal and inhalation routes (Langer, 2000; Pandey and Khuller, 2005). Generally they are made up of biocompatible and biodegradable polymers obtained from either natural (chitosan, albumin, sodium alginate and gelatin) or synthetic (poly (lactic acid), poly (d,l-glycolide), poly (lactide-co-glycolide), poly (caprolactones) and poly (cyanoacrylates)) sources (Soppimath et al., 2001). The polymer selection depends on the physicochemical properties of drug molecules to be included and duration of drug release desired (Malaekeh-Nikouei et al., 2006). Over the past two decades nanoparticulate systems have been successfully utilized for passive and active targeting of drugs. Passive targeting is achieved by modification of nanoparticulate surface using various hydrophilic linkers such as polyethylene glycol (PEG), poloxamer, polyethylene oxide (PEO), polysorbate and lauryl ethers (Soppimath et al., 2001). These linkers prevent the uptake of

nanoparticles by reticuloendothelial system (RES) and thereby increase the circulation time in blood (Shakesheff et al., 1997). These longer circulating nanoparticles accumulate in tumor cells due to their high microvascular permeability and defective lymphatic drainage. Active targeting helps in delivering the drug to the site of action and minimizes its exposure to non-target regions. Active targeting of nanoparticles can potentially increase the efficacy and reduce the toxicity of therapeutic agents (Zhao et al., 2008). This is achieved by decorating the surface of nanoparticles using cell specific ligands. Cell targeting ligands can be classified into 3 types: small molecules (folate, biotin, galactose, glucose and mannose), small peptides (RGD), and proteins (transferrin and antibodies) (Gao et al., 2004; Jain, 2005; Park et al., 1997). Folic acid (FA) has been widely used in the delivery of anticancer agents due to its small size, low cost, high tumor tissue specificity and non-immunogenic nature (Lu and Low, 2002). FA linked nanocarriers have fairly high binding affinity to folate receptors (FR) expressed on tumor cells (Reddy et al., 2005).

Various drug carriers such as liposomes (Goren et al., 2000), polymer conjugates, lipid nanoparticles (Sudimack and Lee, 2000), polymeric micelles (Yoo and Park, 2004) and nanoparticles (Sonvico et al., 2005) have been successfully linked to FA for targeted delivery of drugs to cancer cells. Folate linked liposomes and polymeric micelles are prepared from polymers which are covalently linked to targeting moiety. However, in case of nanoparticles these ligands are chemically conjugated after the nanoparticle preparation (Labhasetwar et al., 1998; Sahoo et al., 2004). This approach is associated

with significant loss of drug during the conjugation process. Moreover, introduction of multiple ligands on the surface becomes tedious. Alternative methods have been reported in the literature to overcome these disadvantages. Kim and his colleagues have developed cancer cell targeted nanoparticulate delivery system using poly(l-lysine)-poly(ethylene glycol)-folate (PLL-PEG-FOL) conjugate. In this strategy the positively charged PLL anchors on the surface of negatively charged PLGA nanoparticles (Kim et al., 2005). PLL−PEG−FOL coated PLGA nanoparticles exhibited higher uptake in KB cells as compared to unmodified nanoparticles. Patil and his co-workers have reported interfacial activity assisted surface functionalization (IAASF) technique for the preparation of surface modified polymeric nanoparticles (Patil et al., 2009). This method involves the addition of copolymer ligand to primary emulsion containing polymer and drug which then localizes and orients at the interface upon solvent evaporation. However, this technique may not be applicable for the delivery of hydrophilic molecules including proteins and peptides.

In this study we have proposed an alternative and relatively easy strategy for the preparation of surface modified nanoparticles for both hydrophilic and hydrophobic drug molecules. This study involves the use of poly(lactide-co-glycolide)-poly(ethylene glycol)-folate (PLGA-PEG-FOL) conjugate in the preparation of nanoparticles. PLGA-PEG-FOL polymer was synthesized and characterized using ^{1}H NMR, GPC and FTIR. Further the ability of PLGA-PEG-FOL polymer to form folate surface modified nanoparticles was investigated using three different techniques. Doxorubicin (DOX), a

chemotherapeutic agent widely used in the treatment of non-Hodgkin's lymphoma, Ewing sarcoma, multiple myeloma, acute leukemias, Wilm tumor, Kaposi sarcoma, and cancers of the lung, breast, adrenal cortex, ovary, and endometrium was utilized in the preparation of nanoparticles (Abraham et al., 2005; Carvalho et al., 2009). The polarity of DOX was sufficiently varied and then entrapped in the nanoparticles using double emulsion (W/O/W) solvent evaporation (DESE), single emulsion (O/W) solvent evaporation (SESE) and dialysis methods. Nanoparticles were evaluated for entrapment efficiency, morphology, particle size and *in vitro* release. Presence of folate on the nanoparticle surface was confirmed by using ^{1}H NMR and transmission electron microscopy (TEM) studies. Quantitative uptake and cell viability studies were carried out in FOL receptor-positive ovarian cancer (SKOV3) cells.

7.2.Materials and Methods

7.2.1 Materials

PLGA polymers, i.e. PLGA 65:35 (d,l-lactide : glycolide), molecular weight 40,000-75,000 Da, polyvinyl alcohol (PVA, molecular weight 30,000–70,000 Da), folic acid and dialysis tubing made of cellulose membrane were procured from Sigma Chemicals (St Louis, MO). Resazurin dye was obtained from Biotium, Inc. (Hayward, CA). Dimethyl sulfoxide (DMSO) and dichloromethane were obtained from Fisher Scientific (Pittsburgh, PA). PEG-bis-amine, molecular weight 3400 Da, was obtained from Fluka Analytical, Germany.

7.2.2. Synthesis of PLGA-PEG-FOL

PLGA–PEG–FOL was synthesized as follows: 1) activation of PLGA, 2) conjugation of activated PLGA with PEG-bis-amine, and 3) conjugation of FA to PLGA–PEG.

7.2.3. Step 1: Activation of PLGA

PLGA was activated with DCC and *N*-hydroxysuccinimide (NHS) in dichloromethane (molar ratio of DCC: NHS: PLGA = 2:2:1) under inert atmosphere for 24 h. Activated PLGA was precipitated with ice-cold diethyl ether followed by filtration and freeze drying for 24 h.

7.2.4. Step 2: Conjugation of activated PLGA with PEG-bis-amine

Activated PLGA was dissolved in methylene chloride. In a separate flask, PEG-bis-amine was dissolved in methylene chloride and added to PLGA solution in a drop-wise manner (PLGA:PEG-bis-amine::1:3). The reaction mixture was stirred under inert nitrogen atmosphere for 6 h. The resulting solution was precipitated by the addition of ice-cold diethyl ether. The precipitated product, amine-terminated di-block copolymer, PLGA-PEG-NH_2 was filtered and dissolved in DMSO. The solution was dialyzed (MWCO: 7 kDa) against distilled water for 48 h to remove the unreacted PEG-bis amine and then freeze dried.

7.2.5. Step 3: Conjugation of FA to PLGA–PEG

FA was activated with dicyclohexylcarbodiimide (DCC). In a separate flask, PLGA-PEG-NH_2 was dissolved in DMSO and added to activated FA in a drop-wise manner (PLGA-PEG-NH_2:FA:DCC::1:2:2.5). The reaction was performed under inert nitrogen atmosphere at room temperature over 12 h. The solution was dialyzed (MWCO: 10 kDa)

against distilled water for 48 h to remove the unreacted FA and freeze dried. The structure of PLGA-PEG-FOL was confirmed by ^{1}H NMR spectroscopy (Varian INOVA-400 MHz NMR spectrometer) in d_6-DMSO. Chemical shifts (δ) were expressed in parts per million (ppm) relative to the NMR solvent signal (d_6-DMSO) using tetramethylsilane as an internal standard. Amount of FA conjugated to PLGA-PEG-FOL was determined using a calibration curve of FA generated in DMSO at 340 nm.

7.2.6. Characterization of PLGA-PEG-FOL by gel permeation chromatography (GPC)

The weight average molecular weight of PLGA-PEG-FOL was determined by GPC. A Waters® 410 Diffraction Refractometer and Waters® Styragel HR4E column (7.8 × 300 mm) were used in the analysis. The mobile phase (dimethylformamide) was delivered by a Waters® 515 HPLC pump. A standard curve was obtained by using PEG standards in the size range of 100–15000 Da (Polysciences, PA).

7.2.7. Characterization of PLGA-PEG-FOL by FTIR

The presence of amide linkages in PLGA-PEG-FOL was confirmed with a Perkin-Elmer Spectrum One Fourier transform infrared spectrophotometer (FTIR) with a resolution of 4 cm^{-1} in the ATR sampling mode. Approximately 10 mg of control (a mixture of PLGA, PEG-bis-amine and FA dissolved in DMSO and dialyzed against distilled water for 48 h and freeze dried) or polymer (PLGA-PEG-FOL) was placed on the horizontal face of the internal reflectance crystal. A diamond crystal with a transmission range of 4000-650 cm^{-1} was used in the experiment.

7.2.8. Development of folate conjugated nanoparticles

7.2.8.1. Double emulsion solvent evaporation method (DESE method): Briefly, 2 mg of DOX was dissolved in 400 µL of distilled deionized water and added to 3 mL of dichloromethane consisting of PLGA (25 mg). A primary W/O emulsion was obtained by sonication (Fisher 100 Sonic Dismembrator, Fisher Scientific) at a constant power output of 55 W for 2 min. The primary emulsion was further mixed with 2 mL of dichloromethane consisting of 75 mg PLGA-PEG-FOL and vortexed vigorously for 2.5 min. The organic phase was slowly mixed with an aqueous solution containing 2.5% PVA under continuous stirring. A W/O/W emulsion was obtained by sonication at a constant power output of 55 W for 5 min. The sample was kept in an ice bath during sonication to prevent any overheating of the emulsion. It was stirred gently at room temperature for 12 h. Subsequently, the nanoparticle suspension was exposed to vacuum for 1 h to ensure complete removal of organic solvents. PVA residue was removed by washing nanoparticles three times with distilled water. The resulting solution was centrifuged at 22,000 g for 60 minutes. The nanoparticles were freeze-dried for 48 h in the presence of 2 % trehalose.

7.2.8.2. Single emulsion solvent evaporation method (SESE method): DOX extraction in methylene chloride was carried out per the previously published method with minor modification (Tewes et al., 2007) . Two milligrams of DOX was dissolved in 5 mL of 0.1 M sodium carbonate and sodium bicarbonate buffer (pH adjusted to 8.6). The aqueous phase was shaken with 50 mL of methylene chloride for 24 h at 25^{o}C. Methylene

chloride solution was evaporated under vacuum until the final volume of 5 mL was reached. One hundred milligrams of PLGA-PEG-FOL was added to the methylene chloride solution. The organic phase was slowly mixed with an aqueous solution containing 2.5% PVA under continuous stirring. An O/W type emulsion was obtained by sonication at a constant power output of 55W for 5 min (Boddu et al., 2010). The sample was kept in an ice bath during sonication to prevent any overheating of the emulsion and stirred gently at room temperature for 12 h. Subsequently, nanoparticle suspension was exposed to vacuum for 1 h to ensure complete removal of organic solvents. PVA residue was removed by washing nanoparticles thrice with distilled water. The resulting solution was centrifuged at 22,000 g for 60 minutes. The nanoparticles formed were freeze-dried for 48 h in the presence of 2% trehalose. Unmodified nanoparticles were also prepared in the similar manner using PLGA 65:35 and used as control as needed.

7.2.8.3. Dialysis method: PLGA-PEG-FOL nanoparticles were prepared by dialysis method without the incorporation of any surfactants. DOX was neutralized with a 2 mol excess of triethylamine (TEA) in 2 mL of DMSO. Briefly, 2 mg of DOX (after TEA treatment) and 100 mg of PLGA-PEG-FOL were dissolved in 3 mL of DMSO and vortexed for 10 min. The solution was introduced into a dialysis bag (MWCO: 6.5 kDa) and dialyzed against distilled water with continuous stirring at room temperature for 24 h. With the water rplaced every 3 h. The resulting solution was centrifuged at 22,000 g for 60 minutes. Nanoparticles were freeze-dried for 48 h in the presence of 2 % trehalose.

7.2.9. Entrapment efficiency

Two milligrams of freeze dried nanoparticles were dissolved in DMSO and their DOX content analyzed using a microplate reader (DTX 880 Series Multimode Detector, Multimode Detection Software, Beckman Coulter, Inc, CA) at 485 nm (excitation wavelength) and 595 nm (emission wavelength). Entrapment efficiency was calculated using equation 1 (Boddu et al., 2010). All experiments were conducted in triplicate.

7.2.10. Morphology

TEM (Philips CM12 STEM, Hillsboro, OR) was utilized for examining the morphology of nanoparticles. A drop of solution containing nanoparticles was placed on a carbon-coated copper grid and excess fluid removed with a piece of filter paper. The sample was stained with a 2% phosphotungstic acid solution and excess solution removed using a filter paper. TEM images were taken after the sample was completely dried.

7.2.11. Particle size and zeta-potential measurement

Particle size and surface charge analysis of nanoparticles was performed using a Zeta Phase Analysis Light Scattering (PALS) UltraSensitive Zeta Potential Analyzer instrument (Brookhaven Instruments, Holtsville, NY). Nanoparticles were suspended in double distilled deionized water to give optimum signal intensity. The particle size and zeta-potential of each sample was determined using 3 independent measurements.

7.2.12. Characterization of folate linked nanoparticles by NMR

The presence of folate in PLGA-PEG-FOL nanoparticles was confirmed by ^{1}H NMR spectroscopy (Varian-400 MHz NMR spectrometer). Ghost nanoparticles made up of the

DESE method, the SESE method and the dialysis method were dissolved in d_6-DMSO. Chemical shifts (δ) were expressed in parts per million (ppm) relative to the NMR solvent signal (d_6-DMSO) or tetramethylsilane as an internal standard.

7.2.13. Characterization of folate linked nanoparticles by TEM

The functional presence of folate ligand on the nanoparticle surface was determined by TEM as per the previously published method with minor modifications (Debotton et al., 2008). Folate conjugated nanoparticles were initially incubated with 10% bovine serum albumin solution in PBS for 1 h and then incubated with mouse anti-FA monoclonal antibody for 1 h. Unbound mouse anti-folic acid monoclonal antibody was removed by washing the nanoparticles with PBS. Nanoparticles were then incubated with goat anti-mouse IgG labeled with 10 nm gold particles. Unbound gold particles were removed by washing the nanoparticles with PBS solution. A drop of solution containing nanoparticles was placed on a carbon-coated copper grid and excess fluid was removed with a piece of filter paper. TEM images were taken after the sample was completely dried.

7.2.14. Determination of folate content on the surface of nanoparticles

The amount of folate present on the surface of the nanoparticles prepared by SESE, DESE or dialysis methods was determined by UV spectrophotometer. Analysis was carried out in CH_2Cl_2/DMSO (1:4) solvent. The nanoparticles were evaluated by measuring the absorbance of the sample at 358 nm (folic acid $\varepsilon = 15{,}760\ M^{-1}\ cm^{-1}$) (Stella et al., 2000).

7.2.15. *In vitro* drug release

Drug loaded nanoparticles (5 mg) were dispersed in 1mL of isotonic phosphate buffer saline (IPBS) at pH 7.4 and subsequently introduced into dialysis bags (MWCO - 6275 g/mole) (Duvvuri et al., 2005). The dialysis bags were introduced into vials containing 10 mL IPBS and 0.025% w/v sodium azide to avoid microbial growth and 0.02% (w/v) Tween 80 to maintain sink conditions (Choi and Park, 2000; Duvvuri et al., 2006). The vials were placed in a shaker bath at 37 ± 0.5 °C and 60 oscillations per minute. At regular time intervals 200 µL of samples were withdrawn and replaced with equal volumes of fresh buffer. Samples were analyzed as mentioned above. Experiments were conducted in triplicate.

7.2.16. Cell culture studies

FOL-receptor-positive human ovarian cancer cells (SKOV3) were obtained from ATCC (American Type Culture Collection, Manassas, VA, USA). These cells were grown in T-75 flasks with DMEM medium supplemented with 10% fetal bovine serum and 1% penicillin–streptomycin at 37 ^{o}C in a humidified incubator with 5% CO_2. The medium was changed every alternate day. Trypsinization procedure was carried out for cell harvesting and sub-cultivation after 80 to 90% confluence.

7.2.17. Qualitative uptake studies

SKOV3 cells were seeded in a chambered cover glass system (Lab-Tek, Nunc International Co., Naperville, IL, USA) and incubated with DOX, DOXNP, FDOXNP, and FDOXNP in presence of excess folic acid (~1 mM) for 30 min in DPBS. A DOX

concentration equivalent to 10 µg/mL was maintained in solutions. Following incubation, the cells were washed 3 times to remove un-internalized DOX and then exposed to 4% buffered paraformaldehyde for 20 min at 4 ^{o}C, rinsed thrice with DPBS and mounted on glass slides using mounting gel. Slides were observed under confocal laser fluorescence microscope (Olympus FV300 confocal laser scanning unit coupled to an Olympus BX61 upright microscope (Center Valley, PA)). Pictures were processed using Fluoview™ software and edited with Adobe Photoshop CS3 (Adobe Systems Inc., San Jose, CA, USA).

7.2.18. Quantitative uptake studies

SKOV3 cells were washed three times with Dulbecco's phosphate-buffered saline (DPBS), pH 7.4, containing 0.03 mM KCl, 130 mM NaCl, 1 mM $CaCl_2$, 7.5 mM Na_2HPO_4, 1.5 mM KH_2PO_4, 0.5 mM $MgSO_4$, and 5 mM glucose to remove endogenous folates bound to folate receptors on the cell surface. Uptake studies were carried out in DPBS, pH 7.4. Uptake was initiated by the addition of 100 µg/mL of pure DOX, DOX loaded unmodified nanoparticles (DOXNP), and DOX loaded PLGA-PEG-FOL nanoparticles (FDOXNP) or FDOXNP in presence of excess FA (~ 1 mM) for 1 h. After incubation, cells were rinsed 3 times with 1mL of ice-cold stop solution (210 mM KCl, 2 mM HEPES), to arrest uptake. After each wash cells were centrifuged and separated. Cells were then solubilized in 0.5 mL of 1% Triton-X solution. DOX concentration was measured with the help of fluorescence spectrophotometer at 485 nm (excitation

wavelength) and 595 nm (emission wavelength) (Chittasupho et al., 2009; Davda and Labhasetwar, 2002).

7.2.19. Cell viability studies

Cells were harvested and seeded on 96 well plates (Costar, Chicago, IL) at a density of 10,000 cells/100 μL of medium. The plates were incubated at 37 ºC for 24 h to allow the exponential growth of cells. The medium was replaced on alternate days. The cells were incubated with pure DOX, DOX loaded unmodified nanoparticles (DOXNP) or DOX-loaded PLGA-PEG-FOL nanoparticles (FDOXNP) in concentrations ranging from 0-10 μM. Vehicle without drug or blank nanoparticles were used as control (Esmaeili et al., 2008). Cells were incubated for 48 h and drug solutions were aspirated and then 100 μL of resazurin dye solution was added to each well. The plate was incubated for 1 h at 37 ^{o}C and the amount of absorbance in each well was measured at 600 nm. Resazurin is a blue colored compound and turns pink upon oxidation in presence of viable cells. The absorbance of the sample reflects the number of viable cells (Yeung et al., 2004). Statistical significance was tested using the student t-test at (* $p < 0.05$).

7.3. Results

The biodegradable copolymer, PLGA-PEG-FOL, was successfully synthesized according to a previously published procedure with minor modifications (Yoo and Park, 2004). On a molar ratio basis, the conjugation of folate to PLGA-PEG was found to be 8.2 μmol of folate/gm of polymer. Two different strategies were employed to increase the folate conjugation to diblock copolymer PLGA-PEG. In the first strategy, the reaction time of

step 3 was increased from 0.5 to 4.0 days. However, no significant difference in the folate conjugation was observed after 4.0 days (Fig. 37). In the second strategy, the reaction in step III was terminated after 12 h and the PLGA-PEG-folate polymer was purified and freeze dried. The freeze dried polymer was reused in the conjugation of FA to unreacted PEG groups. After 12 h the reaction was terminated and the polymer sample was purified, freeze dried and analyzed for folate content. Surprisingly, the conjugation percentage of folate was increased by 3.5 fold (Fig. 38). On a molar ratio basis, the conjugation of folate to PLGA-PEG was found to be 28 μmol of folate/g of polymer.

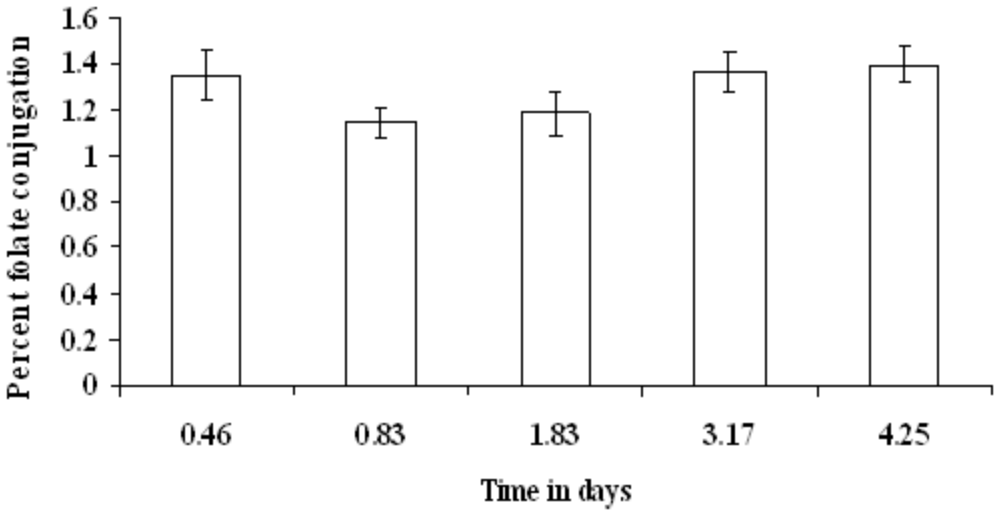

Fig. 37. Conjugation percentage of folate with time using strategy I

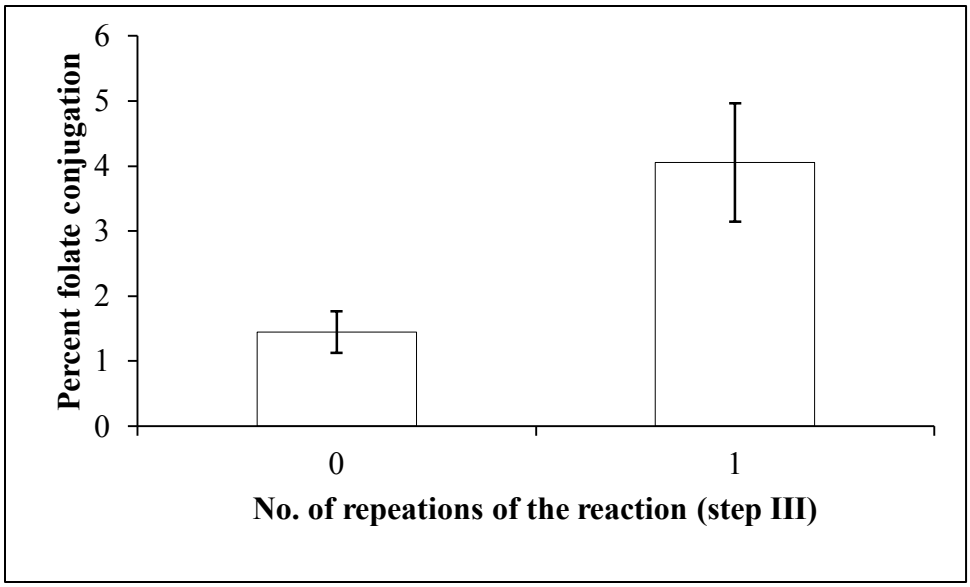

Fig. 38. Conjugation percentage of folate with time using strategy II

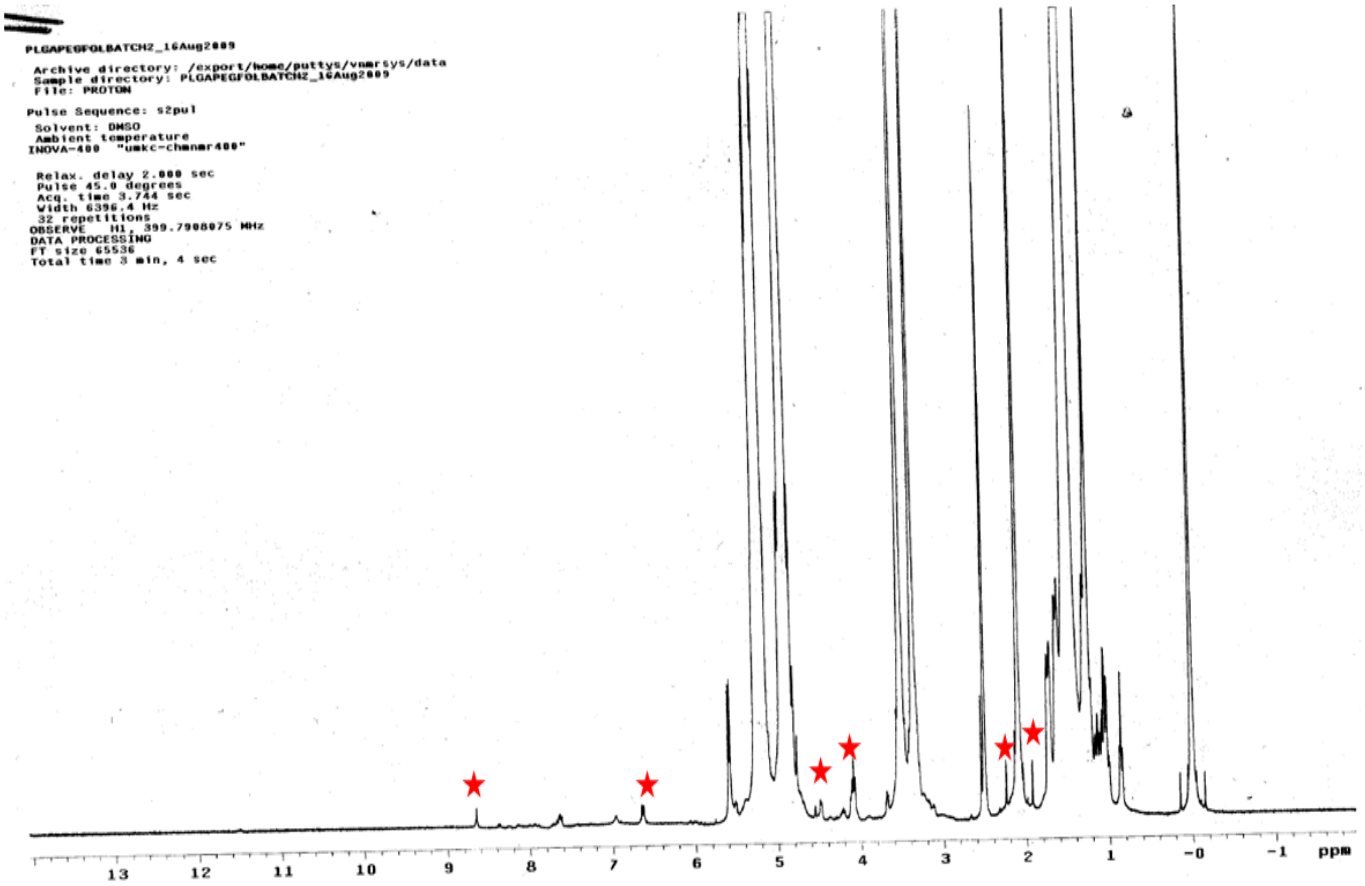

Fig. 39. ^{1}H NMR spectrum of PLGA-PEG-FOL

PLGA-PEG-FOL polymer was characterized by NMR, FTIR and gel permeation chromatography. Chemical shifts (δ) were expressed in parts per million (ppm) relative to the NMR solvent signal (d_6-DMSO) or tetramethylsilane as an internal standard. Figure 39 demonstrates various proton peaks associated with PLGA-PEG-FOL polymer. Small peaks at 6.6, 7.6 and 8.7 ppm; indicate the presence of aromatic protons associated with folate. This reveals the coupling of folate to PLGA-PEG via the NHS/DCC mediated reaction (Dube et al., 2002). The peak at 3.6 ppm indicates the presence of -CH_2- protons associated with PEG block. Peaks at 1.6 and 5.2 ppm are due to -CH_3 and -CH- protons of PLA block. Peak at 4.8 ppm belongs to the -CH_2- protons of PGA block. PLGA-PEG-FOL polymer was further characterized for the number average molecular weight (M_n), weight average molecular weight (M_w) and polydispersity values using GPC. The M_n and M_w of PLGA-PEG-folate were found to be 18,500 and 37,150 Da respectively with a polydispersity of 2. The GPC curve exhibited a single peak that was eluted at a retention time of 7.4 min (Fig. 40). FTIR studies were carried out to confirm the presence of the amide linkage in the polymer. Characteristic IR bands of folate in control or polymer were observed at 1453 and 1605 cm^{-1} (Fig. 41). In the control or polymer, the bands at 1453 and 1606 cm^{-1} are due to the stretching vibrations of -C=C- in the backbone of the aromatic ring present in FA (Choy et al., 2004). The most significant FTIR absorption peak (1606 cm^{-1}) in PLGA-PEG-FOL polymer was due to the presence of the -CONH- linkage.

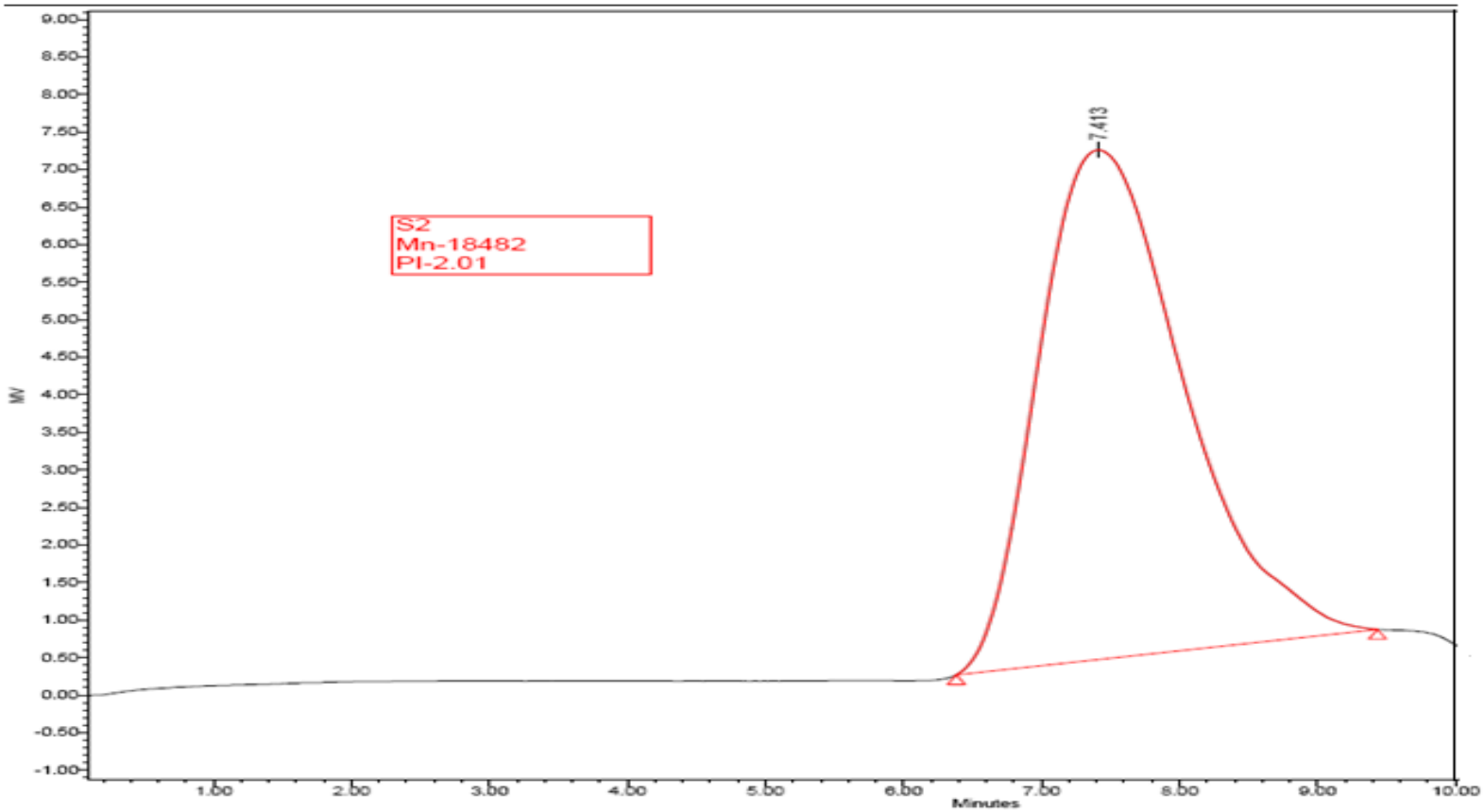

Fig. 40. Gel permeation chromatography of PLGA-PEG-FOL

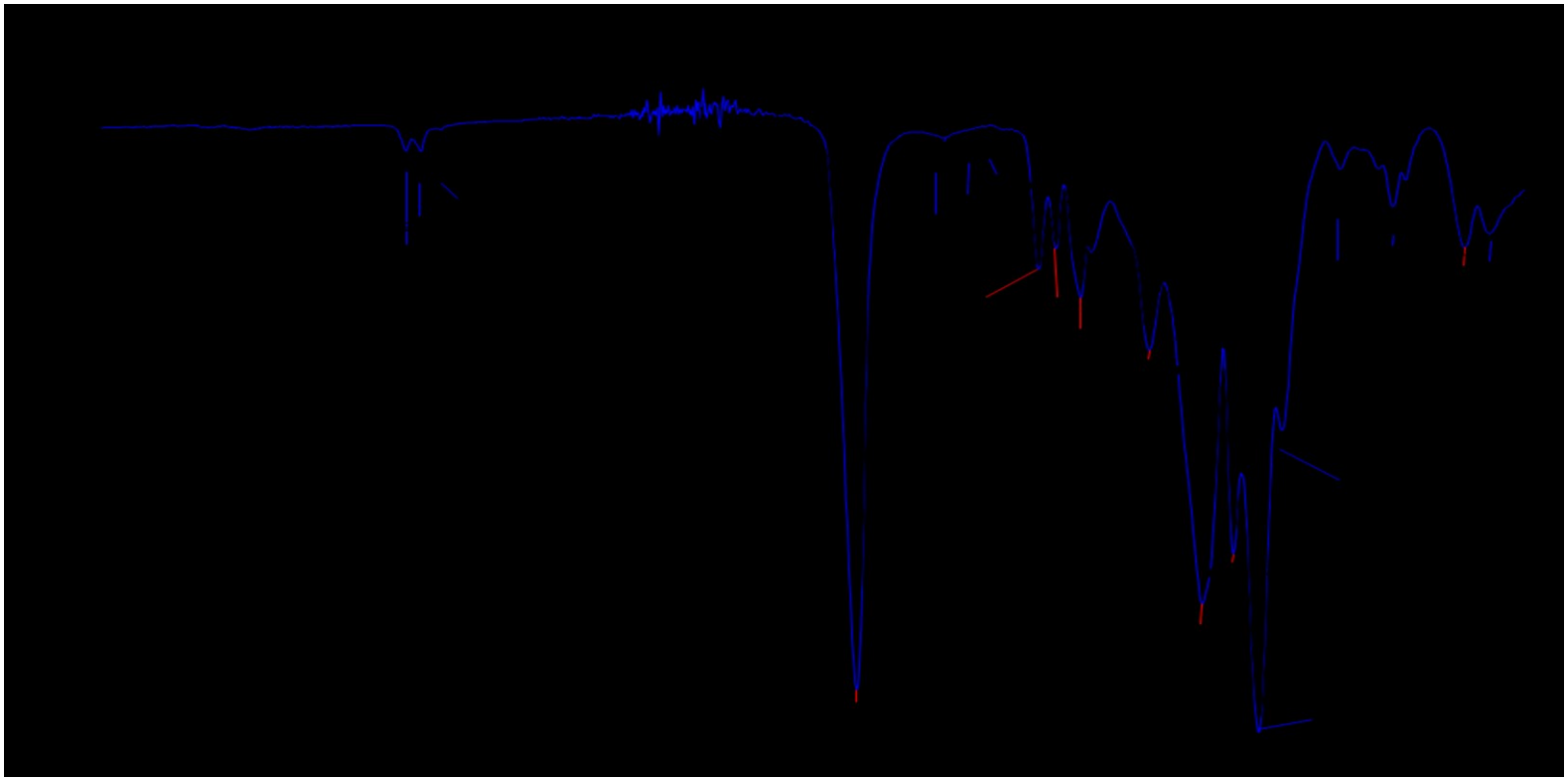

Fig. 41. FTIR absorption peaks of control (Blue) and polymer (Black)

The carbonyl (C═O) and amine (N−H) groups present in the amide linkage also exhibit bands at 1621 and 1568cm^{-1} respectively (Akasaka et al., 2005; Yang et al.). However, these bands for amide linkage were absent in the control sample.

PLGA-PEG-FOL polymer was utilized in the preparation of nanoparticles using DESE, SESE or dialysis methods. DOX HCl was used for the preparation of nanoparticles by the DESE method. The neutral form of DOX was utilized in the preparation of nanoparticles by SESE and dialysis methods. The DOX molecule contains three ionizable groups at the C_6 (phenol group), C_{11} (phenol group) and $C_{5'}$ (amine group) (Fig. 42). Tewes and his colleagues have concluded that at pH 8.6, DOX exists in its neutral form and can be extracted into the organic phase (Tewes et al., 2007). DOX concentration in the organic phase was measured using a fluorescence spectrophotometer. Approximately 96.8% of DOX is extracted into methylene chloride from aqueous phase consisting of 0.1 M sodium carbonate and sodium bicarbonate buffer (pH adjusted to 8.6). DOX nanoparticles of ~200 nm were successfully prepared by single and double emulsion solvent evaporation methods. However, the dialysis method resulted in the formation of microparticles of ~2.5 μm. The experimental values of particle size, polydispersity and zeta-potential values of nanoparticles are shown in Table 14. The size and morphology of nanoparticles was confirmed by TEM (Figs. 43 and 44). Both unmodified as well as folate conjugated nanoparticles exhibit negative zeta potential due to the presence of terminal carboxylic groups in the polymer (Esmaeili et al., 2008).

Table 14. Particle size of nanoparticles prepared by various methods using PLGA-PEG-FOL polymer

Polymer used	Preparation Method	Particle size (nm)	Polydispersity	Zeta potential (mV)
PLGA	O/W emulsion solvent evaporation method	209.1±1.0	0.050	-23.96±1.2
PLGA-PEG-FOL	O/W emulsion solvent evaporation method	200.9±0.1	0.180	-8.96±1.1
	W/O/W double emulsion solvent evaporation method	192.5±4.1	0.108	-15.2± 2.7
	Dialysis method	2504.9±208.5	0.249	-14.46±1.3

PLGA-PEG-FOL:poly(lactide-co-glycolide)-b-poly(ethyleneglycol)-folate

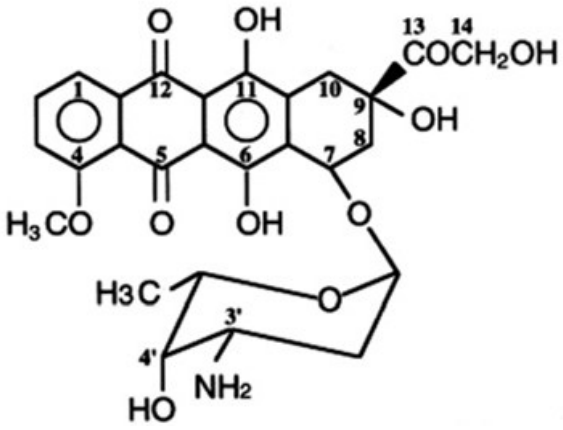

Fig. 42. The structure of doxorubicin

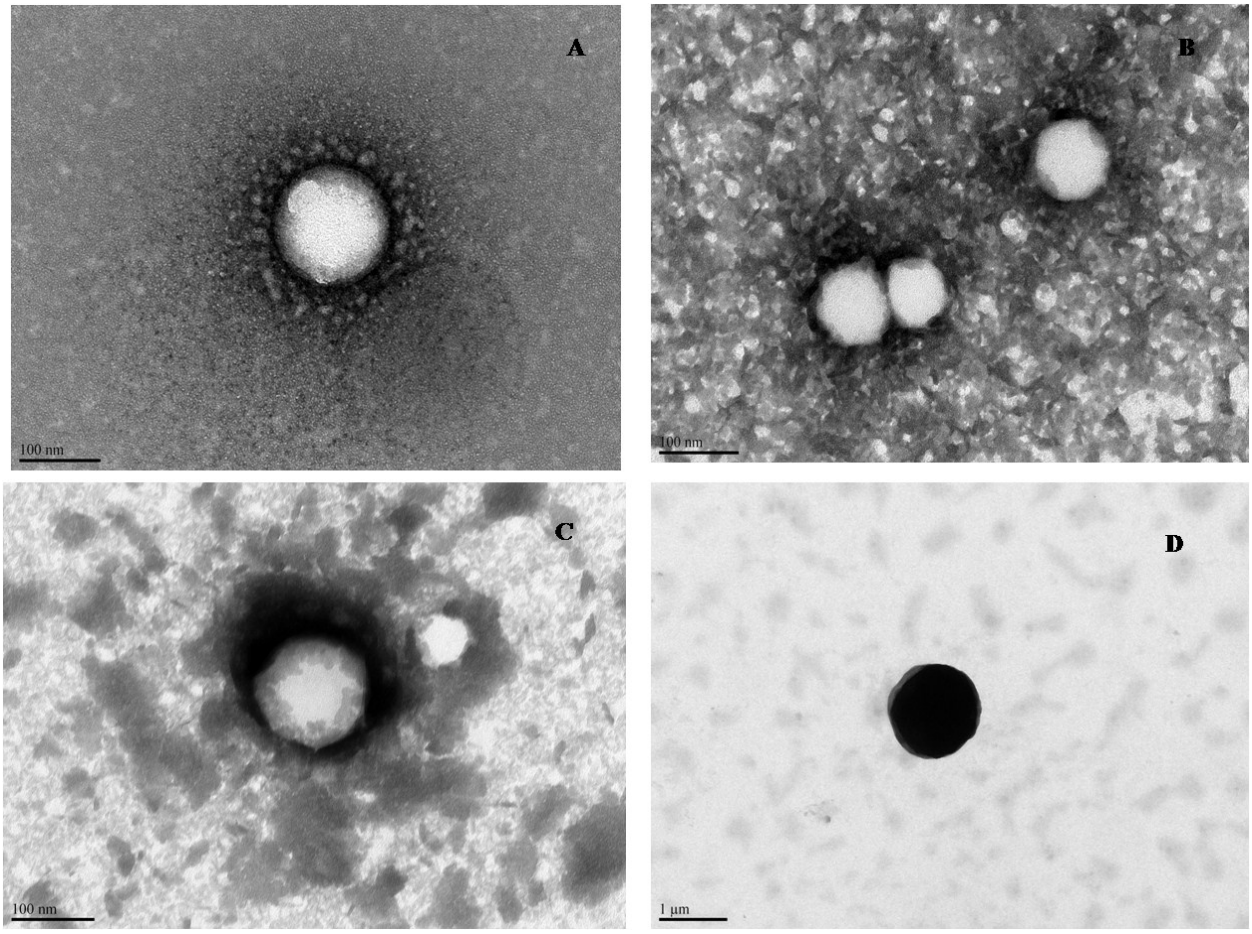

Fig. 43. Transmission electron microscopy image of nanoparticles (A) PLGA nanoparticles, (B) PLGA-PEG-FOL nanoparticles prepared by W/O/W double emulsion solvent evaporation method, (C) PLGA-PEG-FOL nanoparticles prepared by O/W emulsion method, (D) PLGA-PEG-FOL nanoparticles prepared by dialysis method.

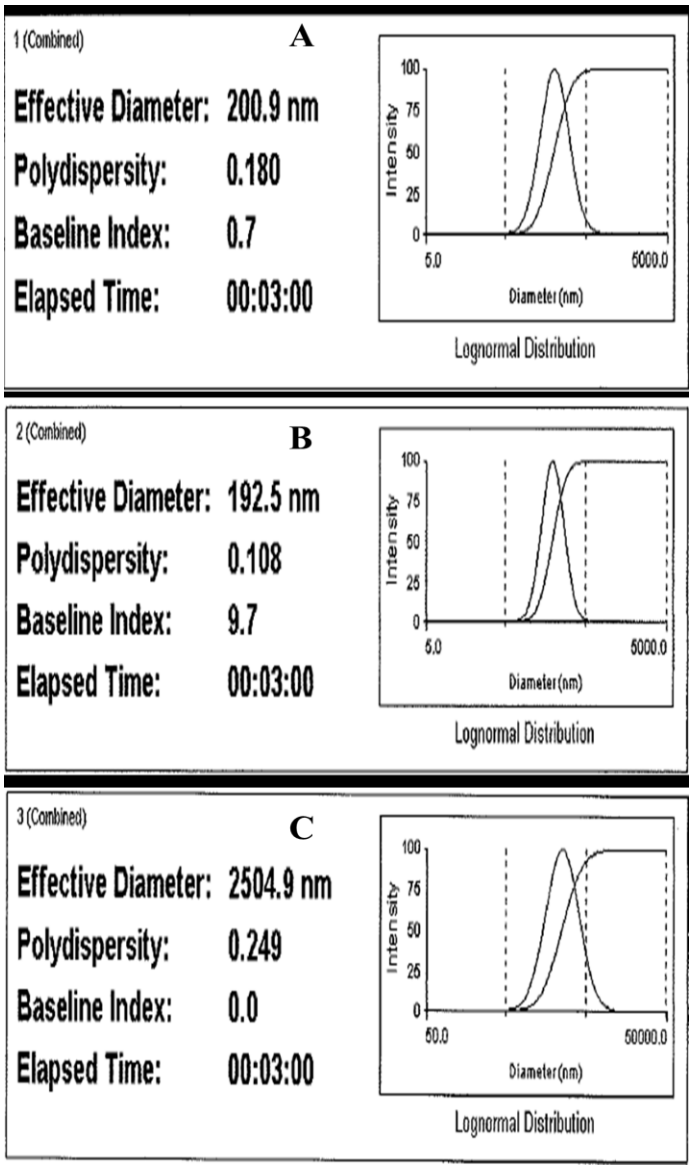

Fig. 44. Particle size distribution curves of nanoparticles (A) PLGA-PEG-FOL nanoparticles prepared by W/O/W double emulsion solvent evaporation method, (B) PLGA-PEG-FOL nanoparticles prepared by O/W emulsion method, (C) PLGA-PEG-FOL nanoparticles prepared by dialysis method.

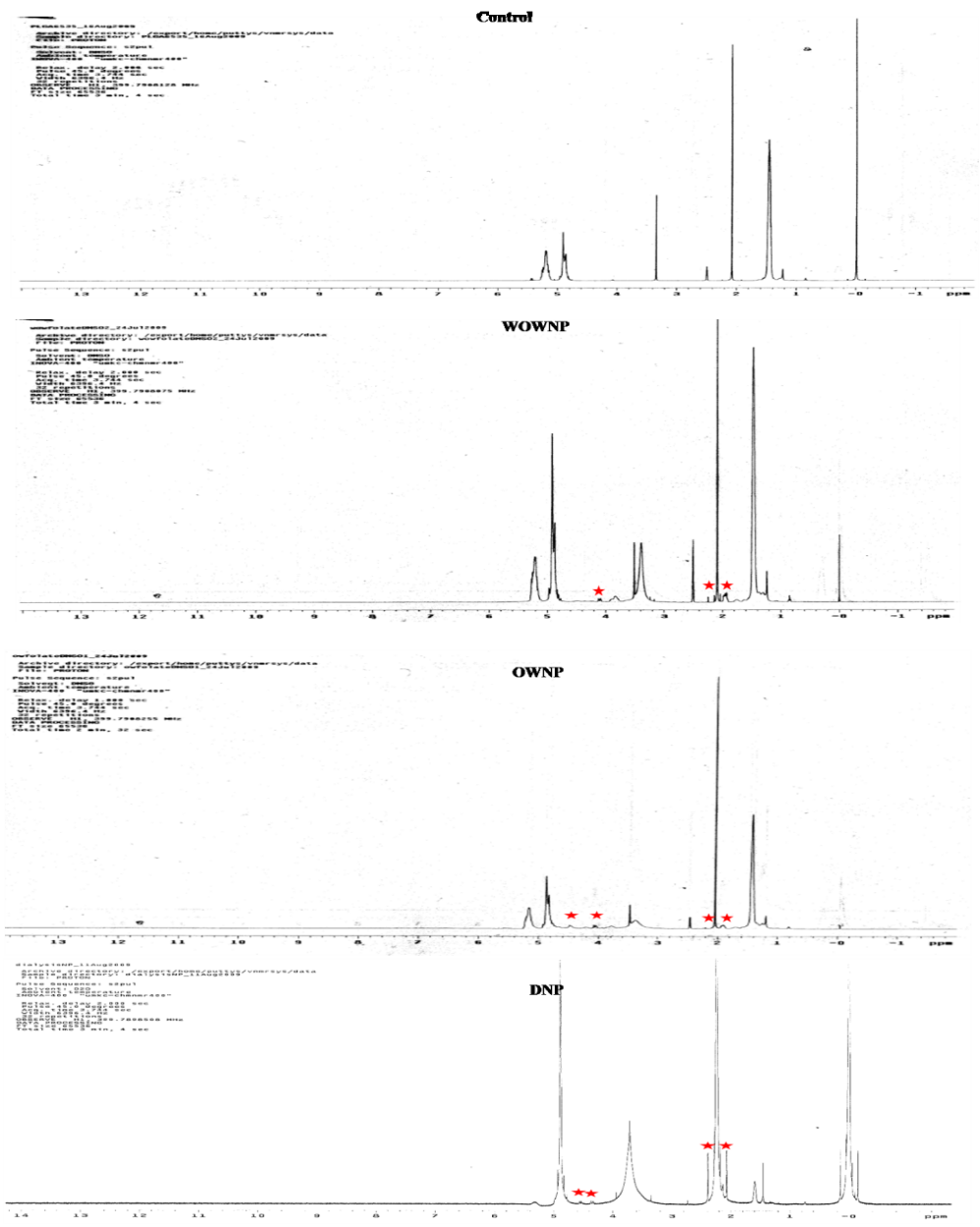

Fig. 45. Proton NMR of PLGA nanoparticles surface functionalized with folic acid (A) PLGA nanoparticles; (B) PLGA-PEG-FOL nanoparticles prepared by O/W emulsion/solvent evaporation method, (C) PLGA-PEG-FOL nanoparticles prepared by W/O/W double emulsion solvent evaporation method (D) PLGA-PEG-FOL nanoparticles prepared by dialysis method. FA proton peaks (★).

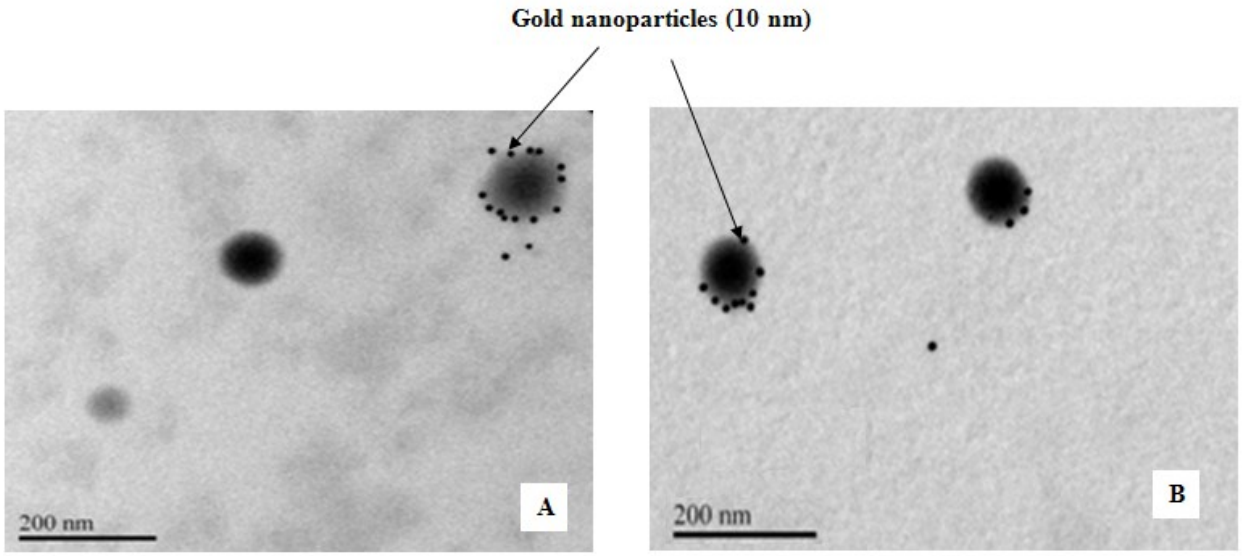

Fig. 46. Transmission electron microscopy studies demonstrating the functional presence of folic acid on nanoparticles (A) PLGA-PEG-FOL nanoparticles prepared by O/W emulsion/solvent evaporation method, (B) PLGA-PEG-FOL nanoparticles prepared by W/O/W double emulsion solvent evaporation method.

Folate conjugated nanoparticles exhibited smaller negative zeta potential values which may be due to the presence of the positively charged ammonium groups in FA. The SESE method resulted in higher DOX entrapment as compared to DESE and dialysis methods. Entrapment efficiencies of DOX using DESE, SESE and dialysis methods were found to be 24.5, 51.9, and 32.6% respectively (Table 15). A decrease in affinity of neutral DOX molecule towards external aqueous phase during emulsification step may have resulted in higher entrapment efficiency by the SESE method. Folate present on the surface of nanoparticles was qualitatively and quantitatively estimated using NMR and UV spectroscopy. Ghost nanoparticles were used for the qualitative analysis of folate using NMR spectroscopy. Small peaks at 2.10, 2.18, 4.32 and 4.46 ppm indicate the presence of specific methylene groups in folic acid (Fig. 45). The amount of folate on the surface of nanoparticles prepared by DESE, SESE and dialysis methods were found to be 3.57, 4.08 and 7.0 μmol of folate/gm of nanoparticles respectively (Table 15). The microparticles resulting from dialysis method were not further characterized. The functional presence of folic acid on the surface of the nanoparticles was studied using transmission electron microscopy. Folate conjugated nanoparticles were incubated with anti-folic acid antibody and then with gold-labeled secondary antibody (10 nm). As seen in Fig. 46, gold probes were found to bind to folate conjugated nanoparticles. Moreover the folate conjugated nanoparticles were ~200 nm.

In vitro release studies were carried out for the nanoparticles prepared form SESE and DESE methods. Irrespective of the preparation method, a biphasic release pattern of DOX was observed from the nanoparticles. However, the nanoparticles prepared by using SESE method showed a significantly lower burst release. The duration of drug release from nanoparticles prepared by SESE and DESE methods was found to be 144 and 96 h, respectively (Fig. 47). The lower burst release of drug from nanoparticles prepared by SESE method may be attributed to the better arrangement of DOX inside the PLGA matrix as a free base. Nanoparticles prepared by the SESE method were further used for assessing quantitative DOX uptake and cytotoxicity in SKOV3 cells.

Table 15. Entrapment efficiency and folate content of nanoparticles prepared by various methods using PLGA-PEG-FOL polymer

Preparation Method	**Entrapment efficiency (mean±SEM)**	**Amount of folate on the surface of nanoparticles (µmol folic acid/g of nanoparticles)**
O/W emulsion solvent evaporation method	51.9±2.1	4.08±0.9
W/O/W double emulsion solvent evaporation method	24.5±1.4	3.57± 0.5
Dialysis method	32.6±2.4	7.0±1.6

S.E.M: Standard error of Mean

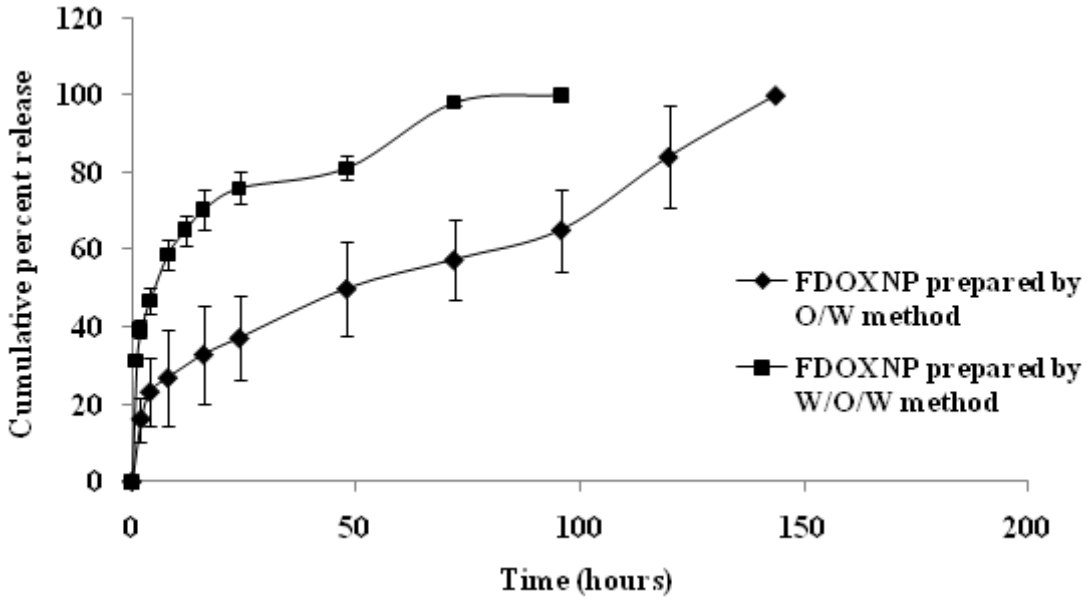

Fig. 47. Percent cumulative release profiles of DOX from PLGA-PEG-FOL nanoparticles prepared by O/W emulsion/solvent evaporation method (n=3) and W/O/W double emulsion solvent evaporation method (n=3). Error bars represent the standard error of mean (S.E.M).

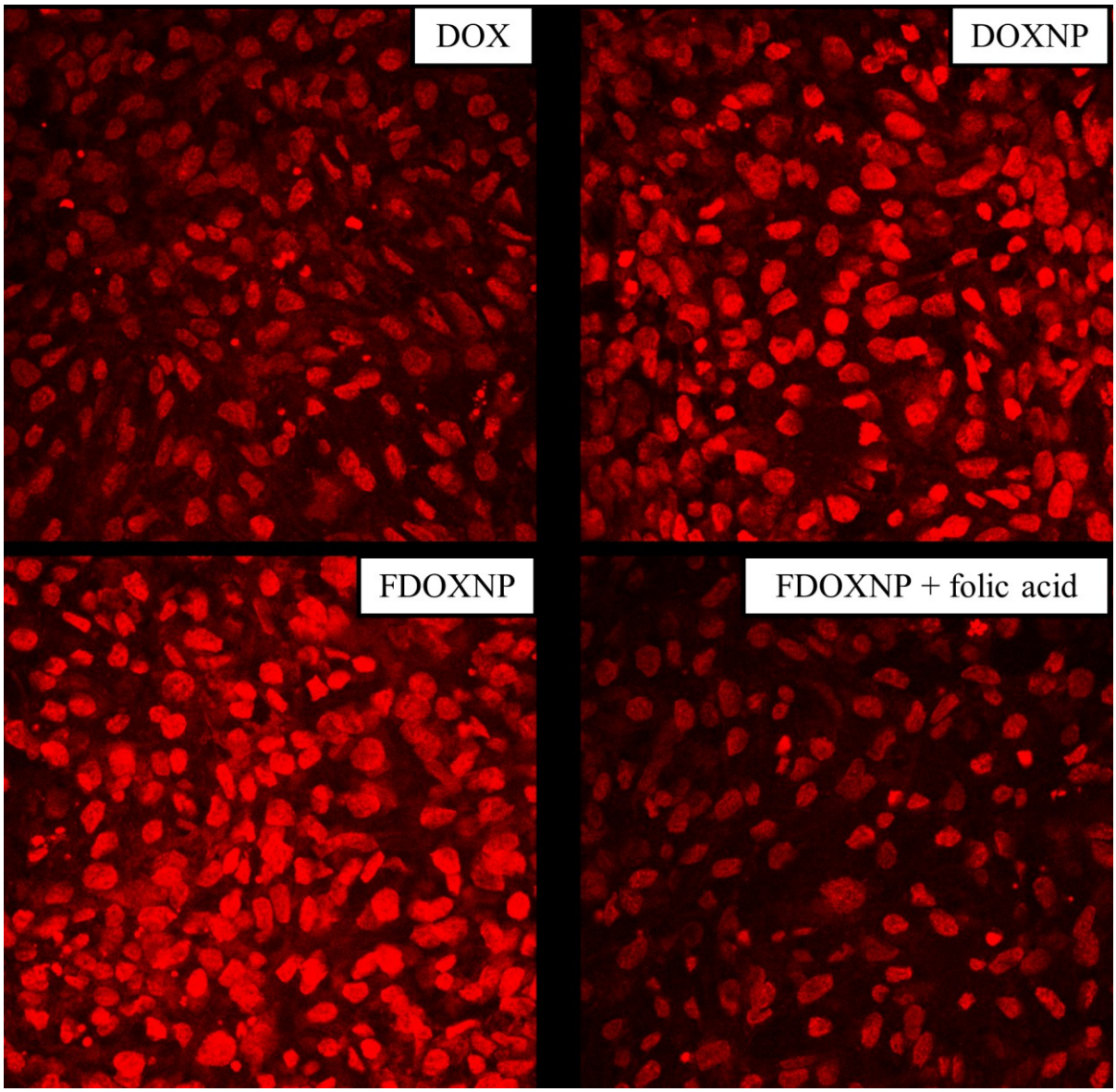

Fig. 48. Qualitative uptake of DOX in SKOV3 cells using pure DOX, DOXNP (doxorubicin loaded unmodified nanoparticles), FDOXNP (doxorubicin loaded folate conjugated nanoparticles) and FDOXNP in presence of folic acid.

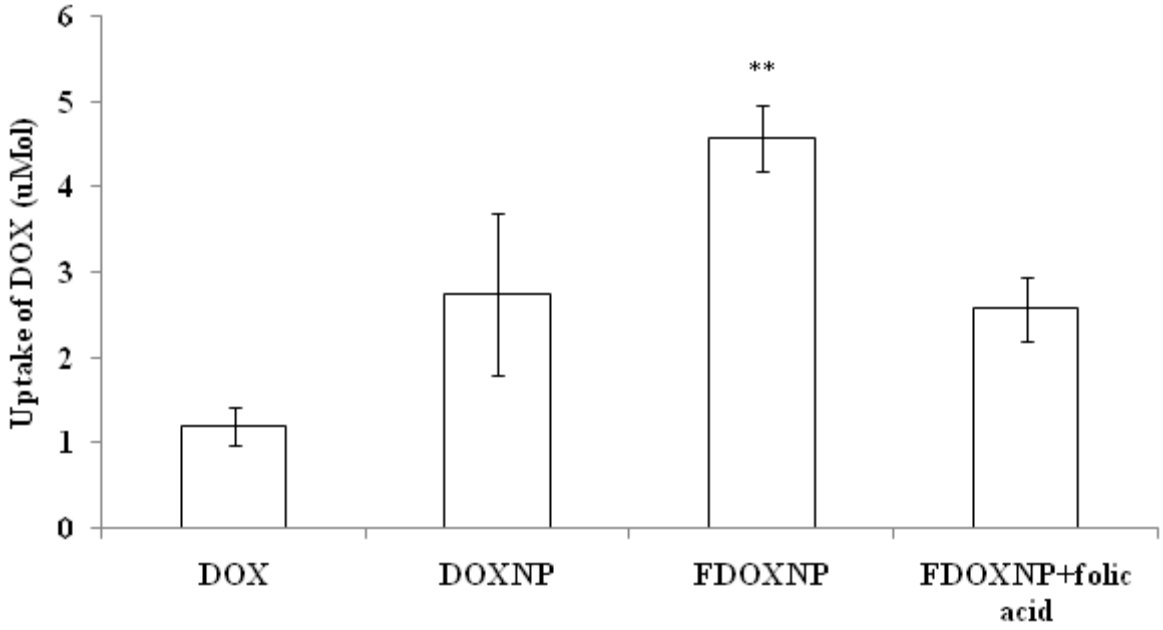

Fig. 49. Quantitative uptake of DOX in SKOV3 cells using pure DOX, DOXNP, FDOXNP micelles/non-targeted micelles (DOXMC), DOX-loaded PLGA-PEG-FOL micelles (DOXM) and DOXM in presence of folic acid. ** $p < 0.05$

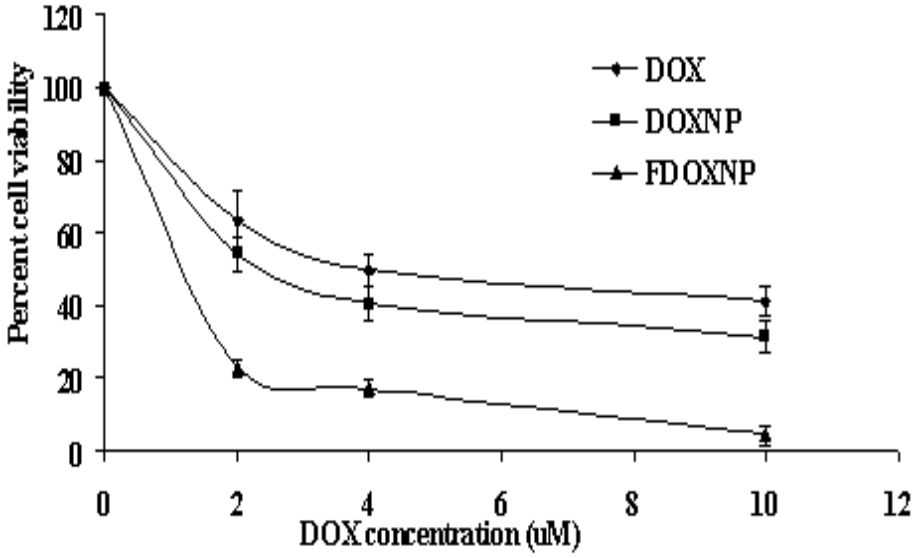

Fig. 50. Cell viability studies of DOX in SKOV3 cells following treatment with DOX and DOX-loaded PLGA-PEG-FOL micelles (DOXM).

Uptake of DOX from pure drug solution, unconjugated nanoparticles (DOXNP), folate conjugated nanoparticles (FDOXNP) and FDOXNP in presence of FA was measured using a fluorescence spectrophotometer. FDOXNP exhibited higher uptake relative to free DOX and DOXNP (Fig. 49). Uptake of DOX from FDOXNP was reduced in the presence of excess FA suggesting the uptake of nanoparticles is mediated via folate receptor. FDOXNP exhibited approximately four times higher uptake compared to pure DOX. Cytotoxicity studies of DOX formulations (DOX in solution, DOXNP and FDOXNP) were carried out in SKOV3 cells. At concentrations ranging from 0-10 μM, FDOXNP exhibited higher cytotoxicity in SKOV3 cells expressing folate receptor as compared to free DOX or DOXNP (Fig. 50).

7.4. Discussion

The use of intravenously administered antineoplastic agents presents the possibility of severe side-effects and toxicity. Moreover, cancer cells express high levels efflux proteins including P-gp and MRP which further restrict the permeation of chemotherapeutic agents. Active targeting helps in delivering the toxic anticancer agents to the site of action and minimizes its exposure to non-target regions. Active targeting of nanoparticles can potentially increase the efficacy and reduce the toxicity of therapeutic agents (Zhao et al., 2008). Several targeting ligands such as folate, biotin, galactose, glucose, mannose, and RGD peptide have been reported in literature (Gao et al., 2004; Jain, 2005; Park et al., 1997). Folic acid (FA) has been widely used in the delivery of anticancer agents due to its small size, low cost, high tumor tissue specificity and non-immunogenic nature (Lu and

Low, 2002). In the present study we have proposed a relatively easy strategy for the preparation of folate conjugated PLGA nanoparticles for both hydrophilic and hydrophobic drug molecules. The conjugation of folate was found to be 28 μmol of folate/g of polymer (strategy II). The PLGA-PEG-FOL polymer was characterized by NMR, FTIR and gel permeation chromatography. Peaks at 6.6, 7.6 and 8.7 ppm indicate the presence of aromatic protons associated with folate. This confirms the coupling of folic acid to PLGA-PEG via NHS/DCC mediated reaction. The M_w of PLGA-PEG-FOL was found to be 37,150 Da with a polydispersity of 2. The total molecular weight of PLGA-PEG-FOL was found to be slightly less than the molecular weight of individual blocks (PLGA, PEG, and folic acid). This may be due to the degradation of PLGA during the dialysis process for purification. FTIR studies were carried out to confirm the presence of amide linkage in polymer. Characteristic FTIR absorption peaks at 1621 and 1568 cm^{-1} confirm the presence of amide linkages in PLGA-PEG-FOL polymer (Akasaka et al., 2005; Yang et al.).

PLGA-PEG-FOL polymer was utilized in the preparation of nanoparticles using DESE, SESE and dialysis methods. DOX HCl was used for the preparation of nanoparticles by DESE method. Tewes and his co-workers have concluded that at pH 8.6, DOX exists in its neutral form and can be extracted into the organic phase (Tewes et al., 2007). Neutral form of DOX was utilized in the preparation of nanoparticles by SESE and dialysis methods. DOX nanoparticles of size ~200 nm were successfully prepared by single and double emulsion solvent evaporation methods. However, the dialysis method resulted in

the formation of microparticles of size ~2.5 μm. This may be due to the absence of surfactants and sonication process which play an important role in controlling the particles size. Folate conjugated nanoparticles exhibited lower negative zeta potential values. It may be attributed to the presence of positively charged amine groups in FA. SESE method resulted in higher DOX entrapment as compared to DESE and dialysis methods. A decrease in affinity of neutral DOX molecule towards external aqueous phase during emulsification step might have resulted in higher entrapment efficiency by SESE method. *In vitro* release studies showed that nanoparticles exhibited a biphasic release pattern irrespective of preparation method. However, the nanoparticles prepared by using SESE method showed a significantly lower burst release. This may be attributed to the better arrangement of DOX inside the PLGA matrix as a free base. Nanoparticles prepared from SESE method were further used for assessing the quantitative uptake and cytotoxicity studies in SKOV3 cells.

FDOXNP exhibited higher uptake relative to free DOX and DOXNP. Uptake of DOX from FDOXNP was reduced in presence of excess FA. This indicates that FDOXNP enter the cells via folate receptor. FDOXNP exhibited higher cytotoxicity in SKOV3 cells as compared to free DOX and DOXNP. DOX is a well known substrate for multidrug resistant (MDR1) efflux pumps which are highly expressed on SKOV3 cells (Pan et al., 2001). These efflux pumps lower the entry of DOX into SKOV3 cells (Kartner et al., 1985). However, FDOXNP enter the cells via folate receptors on the surface of SKOV3

cells. PEG acts as a linker between PLGA and folate moiety and helps in the binding of FA to folate receptors highly expressed on the surface of SKOV3 cells.

7.5.Conclusion

In summary, we have synthesized a PLGA-PEG-FOL polymer. Further, this polymer has been successfully employed in the preparation of folate conjugated DOX loaded nanoparticles (size ~ 200nm) using SESE and DESE methods. Quantitative uptake and cell viability studies revealed that FDOXNP exhibited higher cellular uptake compared to pure DOX and DOXNP in SKOV3 cells overexpressing FRs. The PLGA-PEG-FOL polymer can be used to target chemotherapeutic agents to cancer cells and may help in reducing systemic toxicity.

CHAPTER 8

SUMMARY AND RECOMMENDATIONS

8.1. Summary

Drug delivery to the retina is a clinically significant issue that challenges ophthalmologists and drug delivery scientists. The treatment of retinal diseases is relatively more challenging compared to anterior segment diseases. Posterior segment diseases are generally treated via systemic or intravitreal administration. However, most drugs fail to achieve required therapeutic concentrations in the eye following systemic administration. This is mainly attributed to the presence of blood ocular barriers (BOB) such as the blood aqueous barrier (BAB) and the blood retinal barrier (BRB).

The BRB which comprises of inner and outer BRB's prevent the entry of drugs from blood into the vitreous and retina.The inner BRB consists of endothelial membrane of retinal vessels and the outer BRB consists of retinal pigment epithelium. Intravitreal injection delivers the compound directly to the retina. However, intravitreal delivery is associated with potential side effects such as increased intraocular pressure, hemorrhage, retinal detachment, cataract, and endophthalmitis, limiting long term therapy.

There is an unmet need for the development of novel therapeutic strategies for the delivery of ophthalmic drugs without compromising patient comfort. For instance, the treatment of diabetic macular edema requires administration of a wide variety of molecules (for small molecule steroids to large monoclonal antibodies). Each molecule exhibits a unique behavior with respect to its delivery. Following intravitreal administration, drug

molecules may exhibit varying vitreal retention times depending on their molecular weight. Large linear (>40 kDa) and globular (>70 kDa) molecules tend to have longer retention times, while small molecules exhibit shorter retention times and require frequent administration.

In this dissertation project, a novel injectable and controlled-release formulation of DEX, HA and PA which can be used in the treatment of macular edema was prepared. Steroid nanoparticles suspendend in thermosensitve gels can serve as an alternative to current therapies including implants and intravitreal injections. From the *in vitro* release studies a clear zero order release pattern of steroids from the formulations was observed. Further, this was corroborated from the *ex vivo* permeability studies. Using the formulations, DEX concentrations can be maintained well above the minimum effective concentrations for a duration of several months following single episcleral administration. Depending on the severity of inflammation, various combinations of nanoparticles and thermosensitive gels (with varying molecular weights) loaded with steroids can be tailor made to match the dosing requirements of a particular patient.

Similarly, the treatment of the retinoblastoma (RB) requires intravitreal administration of anticancer agents. However intravitreal delivery is associated with patient noncompliance and has potential side-effects involving healthy retinal cells. In this dissertation project, a folate conjugated polymeric micellar system suspended in thermosensitive gels for the treatment of RB was developed. Release of DOX from DOXM was successfully retarded by PLGA-PEG-PLGA gel system. Qualitative uptake studies

revealed that DOXM exhibited higher cellular uptake than pure DOX in Y-79 cells over-expressing folate receptors. Polymeric micellar systems suspended in thermosensitive gels may provide sustained and targeted delivery of anticancer agents (topotecan, etoposide, carboplatin and vincristine) to RB cells following intravitreal injection.

8.2. Recommendations

During the last decade, polymeric nanoparticles have gained lot of attention due to their versatile properties including: long shelf stability, high drug loading capacity, and ability to deliver both hydrophilic and hydrophobic drug molecules via peroral, transmucosal and inhalation routes. They have been successfully utilized for passive and active targeting of drugs. Active targeting helps in delivering the drug molecules to the site of action and hence minimizing its exposure to non-target regions. Active targeting of nanoparticles can potentially increase the efficacy and reduce the toxicity of therapeutic agents. This is achieved by decorating the surface of nanoparticles using specific cell ligands. Functional and molecular evidence of folate receptor α was studied on cultured human RPE cells (ARPE-19 cells) and basal membrane of the mouse retina (Bridges et al., 2002; Smith et al., 1999). Recently, Kansara et al. from our laboratory has established the presence of folate receptor on the basolateral side of the rabbit retina (Kansara and Mitra, 2006).

In this dissertation project, PLGA-PEG-FOL polymer was successfully synthesized and characterized. Further this polymer was sucessfully employed in the preparation of folate conjugated nanoparticles (size ~ 200nm) using O/W single emulsion and W/O/W double emulsion solvent evaporation methods. Quantitative uptake and cell viability studies revealed

that FDOXNP exhibited higher cellular uptake compared to pure DOX or DOXNP in SKOV3 cells overexpressing FRs. In the future, the PLGA-PEG-FOL polymer can be utilized in the preparation of folate conjugated nanoparticles for cortisteroids (dexamethasone, hydrocortisone and prednisolone) and antibodies (Avastin™ and Lucentis™). Following subconjunctival administration, folate conjugated nanoparticles may be recognized by folate receptors present on the basolateral side of the RPE and on the neural retina. However, the size of the nanoparticles should be optimized (size ~50-75 nm) to prevent the retention of the particles in the sclera. Size optimization can be carried out by increasing the sonication time during the preparation of the nanoparticles. Futher similar studies can be carried out by using biotin as a targeting ligand. The mechanism of biotin uptake has recently been studied in various mammalian cells (human, rat, and rabbit). Studies from our laboratory have shown evidence that the sodium-dependent multivitamin transporter (SMVT) mediates biotin uptake into human retinal cells (Kansara et al., 2006). PLGA (poly lactic co-glycolic acid) nanoparticles functionalized with biotin may result in enhanced cellular uptake of steroids and antibodies into the retina. Therefore, surface modified nanoparticles targeted to folate or biotin receptor/transporters on the RPE may be utilized for retinal delivery.

FW: Liebert Online feedback

Ballen, Karen [KBallen@liebertpub.com]
Sent: Tuesday, June 29, 2010 9:40 AM
To: sboddu@umkc.edu

Dear Dr. Boddu:
Copyright permission is granted for this request.
Kind regards,
Karen Ballen
Manager, Reprint Department

System information:

User: not logged in
Institution(s): MILLER NICHOLS LIBRARY - UMKC University of Missouri,
Date/time: Mon Jun 28 16:10:02 PDT 2010
Previous page: http://www.liebertonline.com/doi/abs/10.1089/jop.2009.0074
Browser/OS: Mozilla/5.0 (Windows; U; Windows NT 5.1; en-US; rv:1.8.1.12) Gecko/20080201 Firefox/2.0.0.12 (.NET CLR 3.5.30729)
IP Address: 134.193.244.195

User entered information:

Name: Sai HS Boddu
Institution/affiliation: University of Missouri -Kansas city
Department: Pharmaceutical sciences

City/town:
Country: United States
ZIP/postal code: 64112

Customer number:
Email: sboddu@umkc.edu

Question regarding: Other
Journal:
Question:

Hello, I am graduate student in Dept. Of Pharmaceutical Sciences, at University of Missouri-Kansas City. I am the author of the work Boddu SH, Jwala J, Vaishya R, Earla R, Karla PK, Pal D, Mitra AK. Novel nanoparticulate gel formulations of steroids for the treatment of macular edema.J Ocul Pharmacol Ther. 2010 Feb;26(1):37-48; published in your journal. I request your permission to put this work in my dissertation.

Send copy: yes

Title: Development and validation of a fast and sensitive bioanalytical method for the quantitative determination of glucocorticoids—Quantitative measurement of dexamethasone in rabbit ocular matrices by liquid chromatography tandem mass spectrometry

Author: Ravinder Earla, Sai H.S. Boddu, Kishore Cholkar, Sudharshan Hariharan, Jwala Jwala, Ashim K. Mitra

Publication: Journal of Pharmaceutical and Biomedical Analysis

Publisher: Elsevier

Date: 1 August 2010

Order Completed

Thank you very much for your order.

This is a License Agreement between Sai HS Boddu ("You") and Elsevier ("Elsevier"). The license consists of your order details, the terms and conditions provided by Elsevier, and the payment terms and conditions.

Get the printable license.

License Number	2458311238683
License date	Jun 29, 2010
Licensed content publisher	Elsevier
Licensed content publication	Journal of Pharmaceutical and Biomedical Analysis
Licensed content title	Development and validation of a fast and sensitive bioanalytical method for the quantitative determination of glucocorticoids—Quantitative measurement of dexamethasone in rabbit ocular matrices by liquid chromatography tandem mass spectrometry
Licensed content author	Ravinder Earla, Sai H.S. Boddu, Kishore Cholkar, Sudharshan Hariharan, Jwala Jwala, Ashim K. Mitra
Licensed content date	1 August 2010
Licensed content volume number	52
Licensed content issue number	4
Number of pages	9
Type of Use	reuse in a thesis/dissertation
Requestor type	Not specified
Intended publisher of new work	other
Portion	excerpt
Number of excerpts	4
Format	both print and electronic
Are you the author of this Elsevier article?	Yes
Will you be translating?	No
Order reference number	

Title of your thesis/dissertation	FORMULATION AND DELIVERY OF DRUGS FOR THE TREATMENT OF MACULAR EDEMA AND RETINOBLASTOMA
Expected completion date	Aug 2010
Estimated size (number of pages)	200
Elsevier VAT number	GB 494 6272 12
Permissions price	0.00 USD
Value added tax 0.0%	0.00 USD
Total	0.00 USD

ORDER MORE... CLOSE WINDOW

Title:	Development and validation of a fast and sensitive bioanalytical method for the quantitative determination of glucocorticoids—Quantitative measurement of dexamethasone in rabbit ocular matrices by liquid chromatography tandem mass spectrometry
Author:	Ravinder Earla, Sai H.S. Boddu, Kishore Cholkar, Sudharshan Hariharan, Jwala Jwala, Ashim K. Mitra
Publication:	Journal of Pharmaceutical and Biomedical Analysis
Publisher:	Elsevier
Date:	1 August 2010

Order Completed

Thank you very much for your order.

This is a License Agreement between Sai HS Boddu ("You") and Elsevier ("Elsevier"). The license consists of your order details, the terms and conditions provided by Elsevier, and the payment terms and conditions.

Get the printable license.

License Number	2458311493448
License date	Jun 29, 2010
Licensed content publisher	Elsevier
Licensed content publication	Journal of Pharmaceutical and Biomedical Analysis
Licensed content title	Development and validation of a fast and sensitive bioanalytical method for the quantitative determination of glucocorticoids—Quantitative measurement of dexamethasone in rabbit ocular matrices by liquid chromatography tandem mass spectrometry
Licensed content author	Ravinder Earla, Sai H.S. Boddu, Kishore Cholkar, Sudharshan Hariharan, Jwala Jwala, Ashim K. Mitra
Licensed content date	1 August 2010
Licensed content volume number	52
Licensed content issue number	4
Number of pages	9
Type of Use	reuse in a thesis/dissertation
Requestor type	Not specified
Intended publisher of new work	other
Portion	figures/tables/illustrations
Number of figures/tables/illustrations	4
Format	both print and electronic
Are you the author of this Elsevier article?	Yes
Will you be translating?	No
Order reference number	

Title of your thesis/dissertation	FORMULATION AND DELIVERY OF DRUGS FOR THE TREATMENT OF MACULAR EDEMA AND RETINOBLASTOMA
Expected completion date	Aug 2010
Estimated size (number of pages)	200
Elsevier VAT number	GB 494 6272 12
Permissions price	0.00 USD
Value added tax 0.0%	0.00 USD
Total	0.00 USD

ORDER MORE... CLOSE WINDOW

Title:	In Vitro Evaluation of a Targeted and Sustained Release System for Retinoblastoma Cells Using Doxorubicin as a Model Drug
Author:	Sai H.S. Boddu et al.
Publication:	Journal of Ocular Pharmacology and Therapeutics
Publisher:	Mary Ann Liebert, Inc. publishers
Date:	Oct 1, 2010

Author Reuse of Chart/Graph/Table or Text Excerpt

Please note Mary Ann Liebert, Inc. publishers does not require authors of the content being reused to obtain a license for their personal reuse of a figure, table, chart, or text excerpt.

RE: Permission to reuse my research article in dissertation

Ballen, Karen [KBallen@liebertpub.com]
Sent: Monday, October 18, 2010 2:35 PM
To: Boddu, Sai Hanuman Sagar (UMKC-Student)

Dear Sai:
Copyright permission is granted for this request.
Kind regards,
Karen Ballen
Manager, Reprints and Permissions

-----Original Message-----
From: Boddu, Sai Hanuman Sagar (UMKC-Student) [mailto:sboddu@mail.umkc.edu]
Sent: Saturday, October 16, 2010 11:36 AM
To: Ballen, Karen
Subject: Permission to reuse my research article in dissertation

Hello Ballen,
I am graduate student in Dept. Of Pharmaceutical Sciences, at University of Missouri-Kansas City. I am the author of the work Sai H.S. Boddu, Jwala Jwala, Monica R. Chowdhury, Ashim K. Mitra. In Vitro Evaluation of a Targeted and Sustained Release System for Retinoblastoma Cells Using Doxorubicin as a Model Drug. Journal of Ocular Pharmacology and Therapeutics. October 2010, 26(5): 459-468. published in your journal. I request your permission to put this work in my dissertation.

Thanks & Regards
==========
Sai Hanuman Sagar Boddu
PhD Candidate & Doctoral Fellow
School of Pharmacy
University of Missouri-Kansas City
5211 Health Sciences Building
2464 Charlotte Street
Kansas City, MO 64108-2718
Ph No.1-816-235-2423 (Lab)
Mobile. 314 258 3513

REFERENCES

Abraham, S.A., Waterhouse, D.N., Mayer, L.D., Cullis, P.R., Madden, T.D., and Bally, M.B. (2005). The liposomal formulation of doxorubicin. Methods in enzymology *391*, 71-97.

Aerts, I., Lumbroso-Le Rouic, L., Gauthier-Villars, M., Brisse, H., Doz, F., and Desjardins, L. (2006). Retinoblastoma. Orphanet J Rare Dis *1*, 31.

Aggarwal, D., and Kaur, I.P. (2005). Improved pharmacodynamics of timolol maleate from a mucoadhesive niosomal ophthalmic drug delivery system. Int J Pharm *290*, 155-159.

Ahmed, I., and Patton, T.F. (1985). Importance of the noncorneal absorption route in topical ophthalmic drug delivery. Invest Ophthalmol Vis Sci *26*, 584-587.

Aiello, L.P., Bursell, S.E., Clermont, A., Duh, E., Ishii, H., Takagi, C., Mori, F., Ciulla, T.A., Ways, K., Jirousek, M.*, et al.* (1997). Vascular endothelial growth factor-induced retinal permeability is mediated by protein kinase C in vivo and suppressed by an orally effective beta-isoform-selective inhibitor. Diabetes *46*, 1473-1480.

Akasaka, K., Gyimesi-Forras, K., Lammerhofer, M., Fujita, T., Watanabe, M., Harada, N., and Lindner, W. (2005). Investigations of molecular recognition aspects related to the enantiomer separation of 2-methoxy-2-(1-naphthyl)propionic acid using quinine carbamate as chiral selector: An NMR and FT-IR spectroscopic as well as X-ray crystallographic study. Chirality *17*, 544-555.

Albert, D.M. (1987). Historic review of retinoblastoma. Ophthalmology *94*, 654-662.

Alghadyan, A.A., Peyman, G.A., Khoobehi, B., and Liu, K.R. (1988a). Liposome-bound cyclosporine: retinal toxicity after intravitreal injection. Int Ophthalmol *12*, 105-107.

Alghadyan, A.A., Peyman, G.A., Khoobehi, B., Milner, S., and Liu, K.R. (1988b). Liposome-bound cyclosporine: clearance after intravitreal injection. Int Ophthalmol *12*, 109-112.

Ambati, J., Gragoudas, E.S., Miller, J.W., You, T.T., Miyamoto, K., Delori, F.C., and Adamis, A.P. (2000). Transscleral delivery of bioactive protein to the choroid and retina. Investigative ophthalmology & visual science *41*, 1186-1191.

Amrite, A.C., and Kompella, U.B. (2005). Size-dependent disposition of nanoparticles and microparticles following subconjunctival administration. The Journal of pharmacy and pharmacology *57*, 1555-1563.

Anumolu, S.S., Singh, Y., Gao, D., Stein, S., and Sinko, P.J. (2009). Design and evaluation of novel fast forming pilocarpine-loaded ocular hydrogels for sustained pharmacological response. J Control Release *137*, 152-159.

Arendt, D., and Wittbrodt, J. (2001). Reconstructing the eyes of Urbilateria. Philos Trans R Soc Lond B Biol Sci *356*, 1545-1563.

Asaria, R.H., Kon, C.H., Bunce, C., Charteris, D.G., Wong, D., Khaw, P.T., and Aylward, G.W. (2001). Adjuvant 5-fluorouracil and heparin prevents proliferative vitreoretinopathy : Results from a randomized, double-blind, controlled clinical trial. Ophthalmology *108*, 1179-1183.

Aukunuru, J.V., Sunkara, G., Bandi, N., Thoreson, W.B., and Kompella, U.B. (2001). Expression of multidrug resistance-associated protein (MRP) in human retinal pigment epithelial cells and its interaction with BAPSG, a novel aldose reductase inhibitor. Pharm Res *18*, 565-572.
Ausayakhun, S., Yuvaves, P., Ngamtiphakom, S., and Prasitsilp, J. (2005). Treatment of cytomegalovirus retinitis in AIDS patients with intravitreal ganciclovir. J Med Assoc Thai *88 Suppl 9*, S15-20.
Bae, Y.H., and Yin, H. (2008). Stability issues of polymeric micelles. J Control Release *131*, 2-4.
Bandello, F., Pognuz, R., Polito, A., Pirracchio, A., Menchini, F., and Ambesi, M. (2003). Diabetic macular edema: classification, medical and laser therapy. Seminars in ophthalmology *18*, 251-258.
Barar, J., Javadzadeh, A.R., and Omidi, Y. (2008). Ocular novel drug delivery: impacts of membranes and barriers. Expert Opin Drug Deliv *5*, 567-581.
Barratt, G.M. (2000). Therapeutic applications of colloidal drug carriers. Pharm Sci Technolo Today *3*, 163-171.
Baum, J., Peyman, G.A., and Barza, M. (1982). Intravitreal administration of antibiotic in the treatment of bacterial endophthalmitis. III. Consensus. Survey of ophthalmology *26*, 204-206.
Beck, M.N., Balmer, A., Dessing, C., Pica, A., and Munier, F. (2000). First-line chemotherapy with local treatment can prevent external-beam irradiation and enucleation in low-stage intraocular retinoblastoma. J Clin Oncol *18*, 2881-2887.
Bishop, J.O., and Madson, E.C. (1975). Retinoblastoma. Review of the current status. Surv Ophthalmol *19*, 342-366.
Bito, L.Z., and Baroody, R.A. (1981). The penetration of exogenous prostaglandin and arachidonic acid into, and their distribution within, the mammalian eye. Current eye research *1*, 659-669.
Boddu, S.H., Jwala, J., Vaishya, R., Earla, R., Karla, P.K., Pal, D., and Mitra, A.K. (2010). Novel nanoparticulate gel formulations of steroids for the treatment of macular edema. J Ocul Pharmacol Ther *26*, 37-48.
Bourlais, C.L., Acar, L., Zia, H., Sado, P.A., Needham, T., and Leverge, R. (1998). Ophthalmic drug delivery systems--recent advances. Progress in retinal and eye research *17*, 33-58.
Bridges, C.C., El-Sherbeny, A., Ola, M.S., Ganapathy, V., and Smith, S.B. (2002). Transcellular transfer of folate across the retinal pigment epithelium. Current eye research *24*, 129-138.
Brubaker, R.F. (1991). Flow of aqueous humor in humans [The Friedenwald Lecture]. Invest Ophthalmol Vis Sci *32*, 3145-3166.
Budhian, A., Siegel, S.J., and Winey, K.I. (2007). Haloperidol-loaded PLGA nanoparticles: systematic study of particle size and drug content. International journal of pharmaceutics *336*, 367-375.

Canavan, K.S., Dark, A., and Garrioch, M.A. (2003). Sub-Tenon's administration of local anaesthetic: a review of the technique. British journal of anaesthesia *90*, 787-793.
Carvalho, C., Santos, R.X., Cardoso, S., Correia, S., Oliveira, P.J., Santos, M.S., and Moreira, P.I. (2009). Doxorubicin: the good, the bad and the ugly effect. Current medicinal chemistry *16*, 3267-3285.
Castellarin, A., and Pieramici, D.J. (2004). Anterior segment complications following periocular and intraocular injections. Ophthalmol Clin North Am *17*, 583-590, vii.
Chan, H.S., Canton, M.D., and Gallie, B.L. (1989). Chemosensitivity and multidrug resistance to antineoplastic drugs in retinoblastoma cell lines. Anticancer Res *9*, 469-474.
Chan, H.S., Gallie, B.L., Munier, F.L., and Beck Popovic, M. (2005). Chemotherapy for retinoblastoma. Ophthalmol Clin North Am *18*, 55-63, viii.
Chen, E., Kaiser, R.S., and Vander, J.F. (2007). Intravitreal bevacizumab for refractory pigment epithelial detachment with occult choroidal neovascularization in age-related macular degeneration. Retina (Philadelphia, Pa *27*, 445-450.
Chen, H., Kim, S., He, W., Wang, H., Low, P.S., Park, K., and Cheng, J.X. (2008). Fast release of lipophilic agents from circulating PEG-PDLLA micelles revealed by in vivo forster resonance energy transfer imaging. Langmuir *24*, 5213-5217.
Cheng, Y., Xu, Z., Ma, M., and Xu, T. (2008). Dendrimers as drug carriers: applications in different routes of drug administration. J Pharm Sci *97*, 123-143.
Cherkasov, I.S., Marmur, R.K., Radkovskaia, A., and Loskova, L.M. (1974). [Phonophoresis of hypotensive agents in the treatment of simple glaucoma]. Oftalmol Zh *29*, 114-118.
Chin, K.V., and Liu, B. (1994). Regulation of the multidrug resistance (MDR1) gene expression. In vivo (Athens, Greece) *8*, 835-841.
Chintagumpala, M., Chevez-Barrios, P., Paysse, E.A., Plon, S.E., and Hurwitz, R. (2007). Retinoblastoma: review of current management. Oncologist *12*, 1237-1246.
Chittasupho, C., Xie, S.X., Baoum, A., Yakovleva, T., Siahaan, T.J., and Berkland, C.J. (2009). ICAM-1 targeting of doxorubicin-loaded PLGA nanoparticles to lung epithelial cells. Eur J Pharm Sci *37*, 141-150.
Choi, S.H., and Park, T.G. (2000). Hydrophobic ion pair formation between leuprolide and sodium oleate for sustained release from biodegradable polymeric microspheres. International journal of pharmaceutics *203*, 193-202.
Choy, J.H., Jung, J.S., Oh, J.M., Park, M., Jeong, J., Kang, Y.K., and Han, O.J. (2004). Layered double hydroxide as an efficient drug reservoir for folate derivatives. Biomaterials *25*, 3059-3064.
Ciulla, T.A., Walker, J.D., Fong, D.S., and Criswell, M.H. (2004). Corticosteroids in posterior segment disease: an update on new delivery systems and new indications. Current opinion in ophthalmology *15*, 211-220.
Civan, M.M., and Macknight, A.D. (2004). The ins and outs of aqueous humour secretion. Exp Eye Res *78*, 625-631.

Conrad, J.M., and Robinson, J.R. (1980). Mechanisms of anterior segment absorption of pilocarpine following subconjunctival injection in albino rabbits. Journal of pharmaceutical sciences *69*, 875-884.
Costa, R.A., Jorge, R., Calucci, D., Cardillo, J.A., Melo, L.A., Jr., and Scott, I.U. (2006). Intravitreal bevacizumab for choroidal neovascularization caused by AMD (IBeNA Study): results of a phase 1 dose-escalation study. Invest Ophthalmol Vis Sci *47*, 4569-4578.
Cunha-Vaz, J. (1979). The blood-ocular barriers. Surv Ophthalmol *23*, 279-296.
Cunha-Vaz, J.G. (1976). The blood-retinal barriers. Documenta ophthalmologica *41*, 287-327.
Cunha-Vaz, J.G. (1997). The blood-ocular barriers: past, present, and future. Documenta ophthalmologica *93*, 149-157.
Cunha-Vaz, J.G. (2004). The blood-retinal barriers system. Basic concepts and clinical evaluation. Exp Eye Res *78*, 715-721.
Davda, J., and Labhasetwar, V. (2002). Characterization of nanoparticle uptake by endothelial cells. International journal of pharmaceutics *233*, 51-59.
Davis, D.B., 2nd, and Mandel, M.R. (1994). Efficacy and complication rate of 16,224 consecutive peribulbar blocks. A prospective multicenter study. Journal of cataract and refractive surgery *20*, 327-337.
De Potter, P. (2002). Current treatment of retinoblastoma. Curr Opin Ophthalmol *13*, 331-336.
Debotton, N., Parnes, M., Kadouche, J., and Benita, S. (2008). Overcoming the formulation obstacles towards targeted chemotherapy: in vitro and in vivo evaluation of cytotoxic drug loaded immunonanoparticles. J Control Release *127*, 219-230.
Dey, S., and Mitra, A.K. (2005). Transporters and receptors in ocular drug delivery: opportunities and challenges. Expert Opin Drug Deliv *2*, 201-204.
Dingeldein, S.A., and Klyce, S.D. (1988). Imaging of the cornea. Cornea *7*, 170-182.
Doane, M.G., Jensen, A.D., and Dohlman, C.H. (1978). Penetration routes of topically applied eye medications. American journal of ophthalmology *85*, 383-386.
Doolittle, R.F. (1988). Lens proteins. More molecular opportunism. Nature *336*, 18.
Dube, D., Francis, M., Leroux, J.C., and Winnik, F.M. (2002). Preparation and tumor cell uptake of poly(N-isopropylacrylamide) folate conjugates. Bioconjugate chemistry *13*, 685-692.
Duvvuri, S., Gaurav Janoria, K., and Mitra, A.K. (2006). Effect of polymer blending on the release of ganciclovir from PLGA microspheres. Pharmaceutical research *23*, 215-223.
Duvvuri, S., Janoria, K.G., and Mitra, A.K. (2005). Development of a novel formulation containing poly(d,l-lactide-co-glycolide) microspheres dispersed in PLGA-PEG-PLGA gel for sustained delivery of ganciclovir. J Control Release *108*, 282-293.
Duvvuri, S., Janoria, K.G., Pal, D., and Mitra, A.K. (2007). Controlled delivery of ganciclovir to the retina with drug-loaded Poly(d,L-lactide-co-glycolide) (PLGA) microspheres dispersed in PLGA-PEG-PLGA Gel: a novel intravitreal delivery system for the treatment of cytomegalovirus retinitis. J Ocul Pharmacol Ther *23*, 264-274.

Duvvuri, S., Majumdar, S., and Mitra, A.K. (2003). Drug delivery to the retina: challenges and opportunities. Expert opinion on biological therapy *3*, 45-56.
Ebner, R., Devoto, M.H., Weil, D., Bordaberry, M., Mir, C., Martinez, H., Bonelli, L., and Niepomniszcze, H. (2004). Treatment of thyroid associated ophthalmopathy with periocular injections of triamcinolone. The British journal of ophthalmology *88*, 1380-1386.
Eljarrat-Binstock, E., and Domb, A.J. (2006). Iontophoresis: a non-invasive ocular drug delivery. J Control Release *110*, 479-489.
Eng, C., Li, F.P., Abramson, D.H., Ellsworth, R.M., Wong, F.L., Goldman, M.B., Seddon, J., Tarbell, N., and Boice, J.D., Jr. (1993). Mortality from second tumors among long-term survivors of retinoblastoma. J Natl Cancer Inst *85*, 1121-1128.
Esmaeili, F., Ghahremani, M.H., Ostad, S.N., Atyabi, F., Seyedabadi, M., Malekshahi, M.R., Amini, M., and Dinarvand, R. (2008). Folate-receptor-targeted delivery of docetaxel nanoparticles prepared by PLGA-PEG-folate conjugate. Journal of drug targeting *16*, 415-423.
Fernald, R.D. (1997). The evolution of eyes. Brain Behav Evol *50*, 253-259.
Fernald, R.D. (2004). Eyes: variety, development and evolution. Brain Behav Evol *64*, 141-147.
Fernald, R.D. (2006). Casting a genetic light on the evolution of eyes. Science *313*, 1914-1918.
Ferris, F.L., 3rd, and Patz, A. (1983). Macular edema: a major complication of diabetic retinopathy. Trans New Orleans Acad Ophthalmol *31*, 307-316.
Ferry, L.L. (1995). Theoretical model of iontophoresis utilized in transdermal drug delivery. Pharmaceutica acta Helvetiae *70*, 279-287.
Fialho, S.L., Behar-Cohen, F., and Silva-Cunha, A. (2008). Dexamethasone-loaded poly(epsilon-caprolactone) intravitreal implants: a pilot study. Eur J Pharm Biopharm *68*, 637-646.
Fielding, J.A. (1996). Ocular ultrasound. Clin Radiol *51*, 533-544.
Filippenko, V.I., and Tret'iak, V.V. (1989). [The treatment of eye diseases using the Gamma-G ultrasonic apparatus]. Voen Med Zh, 30-31.
Fishman, P.H., Peyman, G.A., and Lesar, T. (1986). Intravitreal liposome-encapsulated gentamicin in a rabbit model. Prolonged therapeutic levels. Invest Ophthalmol Vis Sci *27*, 1103-1106.
Forrester, J.V. (1990). Endogenous posterior uveitis. Br J Ophthalmol *74*, 620-623.
Forrester, J.V. (2007). Intermediate and posterior uveitis. Chem Immunol Allergy *92*, 228-243.
Frerichs, V.A., and Tornatore, K.M. (2004). Determination of the glucocorticoids prednisone, prednisolone, dexamethasone, and cortisol in human serum using liquid chromatography coupled to tandem mass spectrometry. J Chromatogr B Analyt Technol Biomed Life Sci *802*, 329-338.

Gallie, B.L., Budning, A., DeBoer, G., Thiessen, J.J., Koren, G., Verjee, Z., Ling, V., and Chan, H.S. (1996). Chemotherapy with focal therapy can cure intraocular retinoblastoma without radiotherapy. Arch Ophthalmol *114*, 1321-1328.
Gao, X., Cui, Y., Levenson, R.M., Chung, L.W., and Nie, S. (2004). In vivo cancer targeting and imaging with semiconductor quantum dots. Nature biotechnology *22*, 969-976.
Gaudana, R., Jwala, J., Boddu, S.H., and Mitra, A.K. (2009). Recent perspectives in ocular drug delivery. Pharm Res *26*, 1197-1216.
Gehring, W.J., and Ikeo, K. (1999). Pax 6: mastering eye morphogenesis and eye evolution. Trends Genet *15*, 371-377.
Geroski, D.H., and Edelhauser, H.F. (2000). Drug delivery for posterior segment eye disease. Investigative ophthalmology & visual science *41*, 961-964.
Geroski, D.H., and Edelhauser, H.F. (2001). Transscleral drug delivery for posterior segment disease. Advanced drug delivery reviews *52*, 37-48.
Ghate, D., Brooks, W., McCarey, B.E., and Edelhauser, H.F. (2007). Pharmacokinetics of intraocular drug delivery by periocular injections using ocular fluorophotometry. Invest Ophthalmol Vis Sci *48*, 2230-2237.
Giordano, G.G., Chevez-Barrios, P., Refojo, M.F., and Garcia, C.A. (1995). Biodegradation and tissue reaction to intravitreous biodegradable poly(D,L-lactic-co-glycolic)acid microspheres. Curr Eye Res *14*, 761-768.
Glowka, F.K., Karazniewicz, M., and Lipnicka, E. (2006). RP-HPLC method with fluorescence detection for determination of small quantities of triamcinolone in plasma in presence of endogenous steroids after derivatization with 9-anthroyl nitrile; pharmacokinetic studies. J Chromatogr B Analyt Technol Biomed Life Sci *839*, 54-61.
Goren, D., Horowitz, A.T., Tzemach, D., Tarshish, M., Zalipsky, S., and Gabizon, A. (2000). Nuclear delivery of doxorubicin via folate-targeted liposomes with bypass of multidrug-resistance efflux pump. Clin Cancer Res *6*, 1949-1957.
Grass, G.M., Wood, R.W., and Robinson, J.R. (1985). Effects of calcium chelating agents on corneal permeability. Invest Ophthalmol Vis Sci *26*, 110-113.
Gray, H., and Carter, H.V. (1991). Anatomy, descriptive and surgical (St. Louis, Mosby Year Book).
Green, K., and Tonjum, A. (1971). Influence of various agents on corneal permeability. American journal of ophthalmology *72*, 897-905.
Gupta, J., Felner, E.I., and Prausnitz, M.R. (2009). Minimally invasive insulin delivery in subjects with type 1 diabetes using hollow microneedles. Diabetes technology & therapeutics *11*, 329-337.
Gupta, P., Chawla, G., and Bansal, A.K. (2004). Physical stability and solubility advantage from amorphous celecoxib: the role of thermodynamic quantities and molecular mobility. Molecular pharmaceutics *1*, 406-413.
Gurny, R., Kaltsatos, V.V., Deshpande, A.A., Zignani, M., Percicot, C., and Baeyens, V.V. (1997). Ocular drug delivery in veterinary medicine. Advanced drug delivery reviews *28*, 335-361.

Gvarishvili, E.P., and Dushin, N.V. (1999). [Effect of superphonoelectrophoresis on chorioretinal dystrophy]. Vestn Oftalmol *115*, 19-21.
Halhal, M., Renard, G., Courtois, Y., BenEzra, D., and Behar-Cohen, F. (2004). Iontophoresis: from the lab to the bed side. Experimental eye research *78*, 751-757.
Haller, J.A., Bandello, F., Belfort, R., Jr., Blumenkranz, M.S., Gillies, M., Heier, J., Loewenstein, A., Yoon, Y.H., Jacques, M.L., Jiao, J.*, et al.* Randomized, sham-controlled trial of dexamethasone intravitreal implant in patients with macular edema due to retinal vein occlusion. Ophthalmology *117*, 1134-1146 e1133.
Hariharan, S., Gunda, S., Mishra, G.P., Pal, D., and Mitra, A.K. (2009). Enhanced corneal absorption of erythromycin by modulating P-glycoprotein and MRP mediated efflux with corticosteroids. Pharmaceutical research *26*, 1270-1282.
Hashizoe, M., Ogura, Y., Takanashi, T., Kunou, N., Honda, Y., and Ikada, Y. (1997). Biodegradable polymeric device for sustained intravitreal release of ganciclovir in rabbits. Current eye research *16*, 633-639.
Hawkins, B.S., Bird, A., Klein, R., and West, S.K. (1999). Epidemiology of age-related macular degeneration. Mol Vis *5*, 26.
Henkes, H.E., Henkes, H.E., and Oosterhuis, J.A. (1977). Tumors of the eye. Documenta Ophthalmologica *43*, 341-342.
Henkind , P., Hansen, R.I., and Szalay, J. (1979). Physiology of the human eye and visual system. In, R.E. Records, ed. (Hagerstown, Md., Harper & Row), pp. 98-155.
Honavar, S.G., and Singh, A.D. (2005). Management of advanced retinoblastoma. Ophthalmol Clin North Am *18*, 65-73, viii.
Huang, H.S., Schoenwald, R.D., and Lach, J.L. (1983). Corneal penetration behavior of beta-blocking agents II: Assessment of barrier contributions. Journal of pharmaceutical sciences *72*, 1272-1279.
Huang, W., Prasad, P.D., Kekuda, R., Leibach, F.H., and Ganapathy, V. (1997). Characterization of N5-methyltetrahydrofolate uptake in cultured human retinal pigment epithelial cells. Invest Ophthalmol Vis Sci *38*, 1578-1587.
Hughes, P.M., Olejnik, O., Chang-Lin, J.E., and Wilson, C.G. (2005). Topical and systemic drug delivery to the posterior segments. Advanced drug delivery reviews *57*, 2010-2032.
Hyndiuk, R.A., and Reagan, M.G. (1968). Radioactive depot-corticosteroid penetration into monkey ocular tissue. I. Retrobulbar and systemic administration. Archives of ophthalmology *80*, 499-503.
Imesch, P.D., Wallow, I.H., and Albert, D.M. (1997). The color of the human eye: a review of morphologic correlates and of some conditions that affect iridial pigmentation. Surv Ophthalmol *41 Suppl 2*, S117-123.
Ionita, I.A., Fast, D.M., and Akhlaghi, F. (2009). Development of a sensitive and selective method for the quantitative analysis of cortisol, cortisone, prednisolone and prednisone in human plasma. J Chromatogr B Analyt Technol Biomed Life Sci *877*, 765-772.
Ismaiel, O.A., Halquist, M.S., Elmamly, M.Y., Shalaby, A., and Karnes, H.T. (2007). Monitoring phospholipids for assessment of matrix effects in a liquid chromatography-

tandem mass spectrometry method for hydrocodone and pseudoephedrine in human plasma. J Chromatogr B Analyt Technol Biomed Life Sci *859*, 84-93.
Iu, L.P., and Kwok, A.K. (2007). An update of treatment options for neovascular age-related macular degeneration. Hong Kong Med J *13*, 460-470.
Jain, K.K. (2005). Editorial: targeted drug delivery for cancer. Technology in cancer research & treatment *4*, 311-313.
Janoria, K.G., Gunda, S., Boddu, S.H., and Mitra, A.K. (2007). Novel approaches to retinal drug delivery. Expert opinion on drug delivery *4*, 371-388.
Jeon, H.J., Jeong, Y.I., Jang, M.K., Park, Y.H., and Nah, J.W. (2000). Effect of solvent on the preparation of surfactant-free poly(DL-lactide-co-glycolide) nanoparticles and norfloxacin release characteristics. Int J Pharm *207*, 99-108.
Johnston, M.C., Noden, D.M., Hazelton, R.D., Coulombre, J.L., and Coulombre, A.J. (1979). Origins of avian ocular and periocular tissues. Exp Eye Res *29*, 27-43.
Jonas, J.B. (2006). Intravitreal triamcinolone acetonide: a change in a paradigm. Ophthalmic research *38*, 218-245.
Jones, M., and Leroux, J. (1999). Polymeric micelles - a new generation of colloidal drug carriers. Eur J Pharm Biopharm *48*, 101-111.
Judd, D.B., and Wyszecki, G. (1975). Color in business, science, and industry, 3d edn (New York, Wiley).
Kansara, V., Luo, S., Balasubrahmanyam, B., Pal, D., and Mitra, A.K. (2006). Biotin uptake and cellular translocation in human derived retinoblastoma cell line (Y-79): a role of hSMVT system. International journal of pharmaceutics *312*, 43-52.
Kansara, V., and Mitra, A.K. (2006). Evaluation of an ex vivo model implication for carrier-mediated retinal drug delivery. Current eye research *31*, 415-426.
Kansara, V., Paturi, D., Luo, S., Gaudana, R., and Mitra, A.K. (2008). Folic acid transport via high affinity carrier-mediated system in human retinoblastoma cells. Int J Pharm *355*, 210-219.
Kaplan, H.J. (2007). Anatomy and function of the eye. Chemical immunology and allergy *92*, 4-10.
Karla, P.K., Earla, R., Boddu, S.H., Johnston, T.P., Pal, D., and Mitra, A. (2009a). Molecular expression and functional evidence of a drug efflux pump (BCRP) in human corneal epithelial cells. Current eye research *34*, 1-9.
Karla, P.K., Pal, D., Quinn, T., and Mitra, A.K. (2007). Molecular evidence and functional expression of a novel drug efflux pump (ABCC2) in human corneal epithelium and rabbit cornea and its role in ocular drug efflux. International journal of pharmaceutics *336*, 12-21.
Karla, P.K., Quinn, T.L., Herndon, B.L., Thomas, P., Pal, D., and Mitra, A. (2009b). Expression of multidrug resistance associated protein 5 (MRP5) on cornea and its role in drug efflux. J Ocul Pharmacol Ther *25*, 121-132.
Kartner, N., Evernden-Porelle, D., Bradley, G., and Ling, V. (1985). Detection of P-glycoprotein in multidrug-resistant cell lines by monoclonal antibodies. Nature *316*, 820-823.

Kaufman, P.L., Alm, A., and Adler, F.H. (2003). Adler's physiology of the eye : clinical application, 10th edn (St. Louis, Mosby).
Kaur, I.P., Garg, A., Singla, A.K., and Aggarwal, D. (2004). Vesicular systems in ocular drug delivery: an overview. Int J Pharm *269*, 1-14.
Kaur, I.P., and Smitha, R. (2002). Penetration enhancers and ocular bioadhesives: two new avenues for ophthalmic drug delivery. Drug development and industrial pharmacy *28*, 353-369.
Kawazu, K., Yamada, K., Nakamura, M., and Ota, A. (1999). Characterization of cyclosporin A transport in cultured rabbit corneal epithelial cells: P-glycoprotein transport activity and binding to cyclophilin. Invest Ophthalmol Vis Sci *40*, 1738-1744.
Kearns, V.R., and Williams, R.L. (2009). Drug delivery systems for the eye. Expert review of medical devices *6*, 277-290.
Kim, D.H., and Martin, D.C. (2006). Sustained release of dexamethasone from hydrophilic matrices using PLGA nanoparticles for neural drug delivery. Biomaterials *27*, 3031-3037.
Kim, S.H., Jeong, J.H., Chun, K.W., and Park, T.G. (2005). Target-specific cellular uptake of PLGA nanoparticles coated with poly(L-lysine)-poly(ethylene glycol)-folate conjugate. Langmuir *21*, 8852-8857.
Kim, T.W., Lindsey, J.D., Aihara, M., Anthony, T.L., and Weinreb, R.N. (2002). Intraocular distribution of 70-kDa dextran after subconjunctival injection in mice. Investigative ophthalmology & visual science *43*, 1809-1816.
Kimura, H., Ogura, Y., Hashizoe, M., Nishiwaki, H., Honda, Y., and Ikada, Y. (1994). A new vitreal drug delivery system using an implantable biodegradable polymeric device. Investigative ophthalmology & visual science *35*, 2815-2819.
Kirsch, R.E. (1975). The lens. Arch Ophthalmol *93*, 284-314.
Klein, M.L., Jampol, L.M., Condon, P.I., Rice, T.A., and Serjeant, G.R. (1982). Central retinal artery occlusion without retrobulbar hemorrhage after retrobulbar anesthesia. American journal of ophthalmology *93*, 573-577.
Klein, R., Knudtson, M.D., Lee, K.E., Gangnon, R., and Klein, B.E. (2009). The Wisconsin Epidemiologic Study of Diabetic Retinopathy XXIII: the twenty-five-year incidence of macular edema in persons with type 1 diabetes. Ophthalmology *116*, 497-503.
Komai, Y., and Ushiki, T. (1991). The three-dimensional organization of collagen fibrils in the human cornea and sclera. Invest Ophthalmol Vis Sci *32*, 2244-2258.
Kompella, U.B., Bandi, N., and Ayalasomayajula, S.P. (2003). Subconjunctival nano- and microparticles sustain retinal delivery of budesonide, a corticosteroid capable of inhibiting VEGF expression. Investigative ophthalmology & visual science *44*, 1192-1201.
Kristinsson, J.K., Fridriksdottir, H., Thorisdottir, S., Sigurdardottir, A.M., Stefansson, E., and Loftsson, T. (1996). Dexamethasone-cyclodextrin-polymer co-complexes in aqueous eye drops. Aqueous humor pharmacokinetics in humans. Investigative ophthalmology & visual science *37*, 1199-1203.
Kumar, S. (2009). Vernal keratoconjunctivitis: a major review. Acta Ophthalmol *87*, 133-147.

Kuo, M.T. (2007). Roles of multidrug resistance genes in breast cancer chemoresistance. Advances in experimental medicine and biology *608*, 23-30.
Kuppermann, B.D., Blumenkranz, M.S., Haller, J.A., Williams, G.A., Weinberg, D.V., Chou, C., and Whitcup, S.M. (2007). Randomized controlled study of an intravitreous dexamethasone drug delivery system in patients with persistent macular edema. Archives of ophthalmology *125*, 309-317.
Labhasetwar, V., Song, C., Humphrey, W., Shebuski, R., and Levy, R.J. (1998). Arterial uptake of biodegradable nanoparticles: effect of surface modifications. Journal of pharmaceutical sciences *87*, 1229-1234.
Land, M.F., and Fernald, R.D. (1992). The evolution of eyes. Annu Rev Neurosci *15*, 1-29.
Langer, R. (2000). Biomaterials in drug delivery and tissue engineering: one laboratory's experience. Accounts of chemical research *33*, 94-101.
Lee, S.S., and Robinson, M.R. (2009). Novel drug delivery systems for retinal diseases. A review. Ophthalmic research *41*, 124-135.
Lee, V.H., and Robinson, J.R. (1979). Mechanistic and quantitative evaluation of precorneal pilocarpine disposition in albino rabbits. Journal of pharmaceutical sciences *68*, 673-684.
Lee, V.H., and Robinson, J.R. (1986). Topical ocular drug delivery: recent developments and future challenges. Journal of ocular pharmacology *2*, 67-108.
Leibowitz, H.M., Krueger, D.E., Maunder, L.R., Milton, R.C., Kini, M.M., Kahn, H.A., Nickerson, R.J., Pool, J., Colton, T.L., Ganley, J.P.*, et al.* (1980). The Framingham Eye Study monograph: An ophthalmological and epidemiological study of cataract, glaucoma, diabetic retinopathy, macular degeneration, and visual acuity in a general population of 2631 adults, 1973-1975. Surv Ophthalmol *24*, 335-610.
Lemus Gallego, J.M., and Perez Arroyo, J. (2003). Determination of prednisolone and the most important associated compounds in ocular and cutaneous pharmaceutical preparations by micellar electrokinetic capillary chromatography. J Chromatogr B Analyt Technol Biomed Life Sci *784*, 39-47.
Li, B., Gao, R., Zhang, H., Li, L.Q., Gao, F., and Ren, R.J. (2009). [Studies on multidrug resistance associated protein in retinoblastoma]. Zhonghua Yan Ke Za Zhi *45*, 314-317.
Lightman, S. (1991). Use of steroids and immunosuppressive drugs in the management of posterior uveitis. Eye (Lond) *5 (Pt 3)*, 294-298.
Liu, K.R., Peyman, G.A., Khoobehi, B., Alkan, H., and Fiscella, R. (1987). Intravitreal liposome-encapsulated trifluorothymidine in a rabbit model. Ophthalmology *94*, 1155-1159.
Liu, S.Q., Tong, Y.W., and Yang, Y.Y. (2005). Incorporation and in vitro release of doxorubicin in thermally sensitive micelles made from poly(N-isopropylacrylamide-co-N,N-dimethylacrylamide)-b-poly(D,L-lactide-c o-glycolide) with varying compositions. Biomaterials *26*, 5064-5074.
Lu, Y., and Low, P.S. (2002). Folate-mediated delivery of macromolecular anticancer therapeutic agents. Advanced drug delivery reviews *54*, 675-693.
Mainardes, R.M., and Silva, L.P. (2004). Drug delivery systems: past, present, and future. Curr Drug Targets *5*, 449-455.

Malaekeh-Nikouei, B., Sajadi Tabassi, S.A., and Jaafari, M.R. (2006). The effect of different grades of PLGA on characteristics of microspheres encapsulated with cyclosporine A. Current drug delivery *3*, 343-349.
Mannermaa, E., Vellonen, K.S., and Urtti, A. (2006). Drug transport in corneal epithelium and blood-retina barrier: emerging role of transporters in ocular pharmacokinetics. Advanced drug delivery reviews *58*, 1136-1163.
Marmor, M.F., Negi, A., and Maurice, D.M. (1985). Kinetics of macromolecules injected into the subretinal space. Exp Eye Res *40*, 687-696.
Marshall, G.E. (1995). Human scleral elastic system: an immunoelectron microscopic study. Br J Ophthalmol *79*, 57-64.
Marshall, G.E., Konstas, A.G., and Lee, W.R. (1993). Collagens in the aged human macular sclera. Current eye research *12*, 143-153.
Martini, F., Timmons, M.J., and Tallitsch, R.B. (2003). Human anatomy, 6th edn (San Francisco, Pearson Benjamin Cummings).
Maurice, D. (2001). Review: practical issues in intravitreal drug delivery. J Ocul Pharmacol Ther *17*, 393-401.
Maurice, D.M., and Mishima, S. (1984). Pharmacology of the eye. In Pharmacology of the eye, G. Chader, and M.L. Sears, eds. (Berlin ; New York, Springer-Verlag), pp. 19–116.
Meyer, C.H. (2007). Current treatment approaches in diabetic macular edema. Ophthalmologica *221*, 118-131.
Miller, D.L. (1987). A review of the ultrasonic bioeffects of microsonation, gas-body activation, and related cavitation-like phenomena. Ultrasound Med Biol *13*, 443-470.
Molokhia, S.A., Jeong, E.K., Higuchi, W.I., and Li, S.K. (2009). Transscleral iontophoretic and intravitreal delivery of a macromolecule: study of ocular distribution in vivo and postmortem with MRI. Experimental eye research *88*, 418-425.
Morgan, J.P., and Clearkin, L.G. (2001). Rapid onset of ptosis indicates accurate intraconal placement during retrobulbar anaesthetic injection. The British journal of ophthalmology *85*, 363-365.
Murphree, A.L., Villablanca, J.G., Deegan, W.F., 3rd, Sato, J.K., Malogolowkin, M., Fisher, A., Parker, R., Reed, E., and Gomer, C.J. (1996). Chemotherapy plus local treatment in the management of intraocular retinoblastoma. Arch Ophthalmol *114*, 1348-1356.
Musch, D.C., Martin, D.F., Gordon, J.F., Davis, M.D., and Kuppermann, B.D. (1997). Treatment of cytomegalovirus retinitis with a sustained-release ganciclovir implant. The Ganciclovir Implant Study Group. The New England journal of medicine *337*, 83-90.
Musumeci, T., Ventura, C.A., Giannone, I., Ruozi, B., Montenegro, L., Pignatello, R., and Puglisi, G. (2006). PLA/PLGA nanoparticles for sustained release of docetaxel. International journal of pharmaceutics *325*, 172-179.
Myles, M.E., Neumann, D.M., and Hill, J.M. (2005). Recent progress in ocular drug delivery for posterior segment disease: emphasis on transscleral iontophoresis. Advanced drug delivery reviews *57*, 2063-2079.

Nah, J.W., Paek, Y.W., Jeong, Y.I., Kim, D.W., Cho, C.S., Kim, S.H., and Kim, M.Y. (1998). Clonazepam release from poly(DL-lactide-co-glycolide) nanoparticles prepared by dialysis method. Archives of pharmacal research *21*, 418-422.
Nauck, M., Karakiulakis, G., Perruchoud, A.P., Papakonstantinou, E., and Roth, M. (1998). Corticosteroids inhibit the expression of the vascular endothelial growth factor gene in human vascular smooth muscle cells. European journal of pharmacology *341*, 309-315.
Nauck, M., Roth, M., Tamm, M., Eickelberg, O., Wieland, H., Stulz, P., and Perruchoud, A.P. (1997). Induction of vascular endothelial growth factor by platelet-activating factor and platelet-derived growth factor is downregulated by corticosteroids. Am J Respir Cell Mol Biol *16*, 398-406.
Newell, F.W. (1982). Ophthalmology, principles and concepts, 5th edn (St. Louis, Mosby).
Nicoli, S., Ferrari, G., Quarta, M., Macaluso, C., and Santi, P. (2009). In vitro transscleral iontophoresis of high molecular weight neutral compounds. Eur J Pharm Sci *36*, 486-492.
Noe, S., Bohler, J., Keller, E., and Frahm, A.W. (1998). Determination of prednisolone in serum: method development using solid-phase extraction and micellar electrokinetic chromatography. Journal of pharmaceutical and biomedical analysis *18*, 471-476.
Norton, T.T., and Rada, J.A. (1995). Reduced extracellular matrix in mammalian sclera with induced myopia. Vision research *35*, 1271-1281.
Ozkiris, A., and Erkilic, K. (2005). Complications of intravitreal injection of triamcinolone acetonide. Canadian journal of ophthalmology *40*, 63-68.
Pan, L., Tong, Y., Jin, Y., Zhou, S., Zhang, Y., Yang, X., and Mao, N. (2001). Reversing drug resistance in the ovarian carcinoma cell line SKOV3/mdr1 in vitro by antisense oligodeoxynucleotides. Chinese medical journal *114*, 929-932.
Pandey, R., and Khuller, G.K. (2005). Antitubercular inhaled therapy: opportunities, progress and challenges. The Journal of antimicrobial chemotherapy *55*, 430-435.
Panyam, J., Williams, D., Dash, A., Leslie-Pelecky, D., and Labhasetwar, V. (2004). Solid-state solubility influences encapsulation and release of hydrophobic drugs from PLGA/PLA nanoparticles. Journal of pharmaceutical sciences *93*, 1804-1814.
Park, E.K., Kim, S.Y., Lee, S.B., and Lee, Y.M. (2005). Folate-conjugated methoxy poly(ethylene glycol)/poly(epsilon-caprolactone) amphiphilic block copolymeric micelles for tumor-targeted drug delivery. J Control Release *109*, 158-168.
Park, J.W., Hong, K., Kirpotin, D.B., Papahadjopoulos, D., and Benz, C.C. (1997). Immunoliposomes for cancer treatment. Advances in pharmacology (San Diego, Calif *40*, 399-435.
Parkinson, T.M., Ferguson, E., Febbraro, S., Bakhtyari, A., King, M., and Mundasad, M. (2003). Tolerance of ocular iontophoresis in healthy volunteers. J Ocul Pharmacol Ther *19*, 145-151.
Patil, Y.B., Toti, U.S., Khdair, A., Ma, L., and Panyam, J. (2009). Single-step surface functionalization of polymeric nanoparticles for targeted drug delivery. Biomaterials *30*, 859-866.

Patravale, V.B., Date, A.A., and Kulkarni, R.M. (2004). Nanosuspensions: a promising drug delivery strategy. J Pharm Pharmacol *56*, 827-840.
Patton, T.F., and Robinson, J.R. (1976). Quantitative precorneal disposition of topically applied pilocarpine nitrate in rabbit eyes. Journal of pharmaceutical sciences *65*, 1295-1301.
Pesin, S.R., and Shields, J.A. (1989). Seven cases of trilateral retinoblastoma. Am J Ophthalmol *107*, 121-126.
Peyman, G.A., and Ganiban, G.J. (1995). Delivery systems for intraocular routes. Adv Drug Deliv Rev *16*.
Peyman, G.A., Khoobehi, B., Tawakol, M., Schulman, J.A., Mortada, H.A., Alkan, H., and Fiscella, R. (1987). Intravitreal injection of liposome-encapsulated ganciclovir in a rabbit model. Retina *7*, 227-229.
Phylactos, A.C., and Unger, W.G. (1998). Biochemical changes induced by intravitreally-injected doxorubicin in the iris-ciliary body and lens of the rabbit eye. Doc Ophthalmol *95*, 145-155.
Pignatello, R., Ricupero, N., Bucolo, C., Maugeri, F., Maltese, A., and Puglisi, G. (2006). Preparation and characterization of eudragit retard nanosuspensions for the ocular delivery of cloricromene. AAPS PharmSciTech *7*, E27.
Plachetzki, D.C., Serb, J.M., and Oakley, T.H. (2005). New insights into the evolutionary history of photoreceptor cells. Trends Ecol Evol *20*, 465-467.
Prausnitz, M.R., Mikszta, J.A., Cormier, M., and Andrianov, A.K. (2009). Microneedle-based vaccines. Current topics in microbiology and immunology *333*, 369-393.
Prausnitz, M.R., and Noonan, J.S. (1998). Permeability of cornea, sclera, and conjunctiva: a literature analysis for drug delivery to the eye. Journal of pharmaceutical sciences *87*, 1479-1488.
Qiao, M., Chen, D., Ma, X., and Liu, Y. (2005). Injectable biodegradable temperature-responsive PLGA-PEG-PLGA copolymers: synthesis and effect of copolymer composition on the drug release from the copolymer-based hydrogels. International journal of pharmaceutics *294*, 103-112.
Rada, J.A., Shelton, S., and Norton, T.T. (2006). The sclera and myopia. Exp Eye Res *82*, 185-200.
Ragab, A.H., Sutow, W.W., Komp, D.M., Starling, K.A., Lyon, G.M., Jr., and George, S. (1975). Adriamycin in the treatment of childhood solid tumors. A Southwest Oncology Group study. Cancer *36*, 1567-1576.
Ranta, V.P., and Urtti, A. (2006). Transscleral drug delivery to the posterior eye: prospects of pharmacokinetic modeling. Advanced drug delivery reviews *58*, 1164-1181.
Reddy, J.A., Allagadda, V.M., and Leamon, C.P. (2005). Targeting therapeutic and imaging agents to folate receptor positive tumors. Current pharmaceutical biotechnology *6*, 131-150.
Rhee, D.J., Peck, R.E., Belmont, J., Martidis, A., Liu, M., Chang, J., Fontanarosa, J., and Moster, M.R. (2006). Intraocular pressure alterations following intravitreal triamcinolone acetonide. The British journal of ophthalmology *90*, 999-1003.

Ripart, J., Lefrant, J.Y., de La Coussaye, J.E., Prat-Pradal, D., Vivien, B., and Eledjam, J.J. (2001). Peribulbar versus retrobulbar anesthesia for ophthalmic surgery: an anatomical comparison of extraconal and intraconal injections. Anesthesiology *94*, 56-62.
Riva, C., Perlino, P., Valpreda, A., Ricotti, E., Castagneri, G., Balbo, L., and Musso, A. (1992). [Long lasting conjunctivitis: research of etiological factors]. Minerva Pediatr *44*, 595-600.
Rivero-Marabe, J.J., Maynar-Marino, J.I., Garcia-de-Tiedra, M.P., Galan-Martin, A.M., Caballero-Loscos, M.J., and Maynar-Marino, M. (2001). Determination of natural corticosteroids in urine samples from sportsmen. Journal of chromatography *761*, 77-84.
Rizzolo, L.J. (1997). Polarity and the development of the outer blood-retinal barrier. Histol Histopathol *12*, 1057-1067.
Rizzolo, L.J. (2007). Development and role of tight junctions in the retinal pigment epithelium. Int Rev Cytol *258*, 195-234.
Rizzuti, A.E., Dunkel, I.J., and Abramson, D.H. (2008). The adverse events of chemotherapy for retinoblastoma: what are they? Do we know? Arch Ophthalmol *126*, 862-865.
Roman, S.J., Chong Sit, D.A., Boureau, C.M., Auclin, F.X., and Ullern, M.M. (1997). Sub-Tenon's anaesthesia: an efficient and safe technique. The British journal of ophthalmology *81*, 673-676.
Roy, P. (2007). Drug administration with ocular iontophoresis: reaching maturity. Archivos de la Sociedad Espanola de Oftalmologia *82*, 601-605.
Saha, P., Yang, J.J., and Lee, V.H. (1998). Existence of a p-glycoprotein drug efflux pump in cultured rabbit conjunctival epithelial cells. Investigative ophthalmology & visual science *39*, 1221-1226.
Sahoo, S.K., Ma, W., and Labhasetwar, V. (2004). Efficacy of transferrin-conjugated paclitaxel-loaded nanoparticles in a murine model of prostate cancer. International journal of cancer *112*, 335-340.
Sanborn, G.E., Anand, R., Torti, R.E., Nightingale, S.D., Cal, S.X., Yates, B., Ashton, P., and Smith, T. (1992). Sustained-release ganciclovir therapy for treatment of cytomegalovirus retinitis. Use of an intravitreal device. Archives of ophthalmology *110*, 188-195.
Sanchez de Toledo, J. (2008). Retinoblastoma. Can we do more? Clin Transl Oncol *10*, 525-526.
Sandberg-Lall, M., Hagg, P.O., Wahlstrom, I., and Pihlajaniemi, T. (2000). Type XIII collagen is widely expressed in the adult and developing human eye and accentuated in the ciliary muscle, the optic nerve and the neural retina. Exp Eye Res *70*, 401-410.
Sawada, H., Konomi, H., and Hirosawa, K. (1990). Characterization of the collagen in the hexagonal lattice of Descemet's membrane: its relation to type VIII collagen. The Journal of cell biology *110*, 219-227.
Scheer, S., Morel, C., Touzeau, O., Sahel, J.A., and Laroche, L. (2004). [Pharmacological adjuvants for surgical treatment of proliferative vitreoretinopathy]. J Fr Ophtalmol *27*, 1051-1059.

Schmidt-Erfurth, U., Laqua, H., Schlotzer-Schrehard, U., Viestenz, A., and Naumann, G.O. (2002). Histopathological changes following photodynamic therapy in human eyes. Arch Ophthalmol *120*, 835-844.
Schoenwald, R.D. (1993). Ocular pharmacokinetics/pharmacodynamics. In Ophthalmic drug delivery systems, A.K. Mitra, ed. (New York, Dekker), pp. 83–110.
Schoenwald, R.W. (1997). Ocular pharmakokinetics. In Textbook of ocular pharmacology, T.J. Zimmerman, ed. (Philadelphia, Lippincott - Raven), pp. 119-138.
Sebag, J. (1989). The vitreous : structure, function, and pathobiology (New York, Springer-Verlag).
Shakesheff, K.M., Evora, C., Soriano, I.I., and Langer, R. (1997). The Adsorption of Poly(vinyl alcohol) to Biodegradable Microparticles Studied by X-Ray Photoelectron Spectroscopy (XPS). Journal of colloid and interface science *185*, 538-547.
Shaw, L.M., and Olsen, B.R. (1991). FACIT collagens: diverse molecular bridges in extracellular matrices. Trends in biochemical sciences *16*, 191-194.
Sheikh, A., and Hurwitz, B. (2001). Topical antibiotics for acute bacterial conjunctivitis: a systematic review. Br J Gen Pract *51*, 473-477.
Shibasaki, H., Nakayama, H., Furuta, T., Kasuya, Y., Tsuchiya, M., Soejima, A., Yamada, A., and Nagasawa, T. (2008). Simultaneous determination of prednisolone, prednisone, cortisol, and cortisone in plasma by GC-MS: estimating unbound prednisolone concentration in patients with nephrotic syndrome during oral prednisolone therapy. J Chromatogr B Analyt Technol Biomed Life Sci *870*, 164-169.
Shibata, N., Hayakawa, T., Takada, K., Hoshino, N., Minouchi, T., and Yamaji, A. (1998). Simultaneous determination of glucocorticoids in plasma or urine by high-performance liquid chromatography with precolumn fluorimetric derivatization by 9-anthroyl nitrile. Journal of chromatography *706*, 191-199.
Shiokawa, T., Hattori, Y., Kawano, K., Ohguchi, Y., Kawakami, H., Toma, K., and Maitani, Y. (2005). Effect of polyethylene glycol linker chain length of folate-linked microemulsions loading aclacinomycin A on targeting ability and antitumor effect in vitro and in vivo. Clin Cancer Res *11*, 2018-2025.
Siepmann, J., and Peppas, N.A. (2001). Modeling of drug release from delivery systems based on hydroxypropyl methylcellulose (HPMC). Adv Drug Deliv Rev *48*, 139-157.
Sigurdsson, R., and Begg, I.S. (1980). Organised macular plaques in exudative diabetic maculopathy. Br J Ophthalmol *64*, 392-397.
Silverman, R.H. (2009). High-resolution ultrasound imaging of the eye - a review. Clin Experiment Ophthalmol *37*, 54-67.
Singh, P., and Maibach, H.I. (1994). Iontophoresis in drug delivery: basic principles and applications. Critical reviews in therapeutic drug carrier systems *11*, 161-213.
Smith, S.B., Kekuda, R., Gu, X., Chancy, C., Conway, S.J., and Ganapathy, V. (1999). Expression of folate receptor alpha in the mammalian retinol pigmented epithelium and retina. Invest Ophthalmol Vis Sci *40*, 840-848.

Snell, R.S., and Lemp, M.A. (1989). Clinical anatomy of the eye (Cambridge, MA, Blackwell Scientific Publications).
Sonvico, F., Mornet, S., Vasseur, S., Dubernet, C., Jaillard, D., Degrouard, J., Hoebeke, J., Duguet, E., Colombo, P., and Couvreur, P. (2005). Folate-conjugated iron oxide nanoparticles for solid tumor targeting as potential specific magnetic hyperthermia mediators: synthesis, physicochemical characterization, and in vitro experiments. Bioconjugate chemistry *16*, 1181-1188.
Soppimath, K.S., Aminabhavi, T.M., Kulkarni, A.R., and Rudzinski, W.E. (2001). Biodegradable polymeric nanoparticles as drug delivery devices. J Control Release *70*, 1-20.
Spilsbury, K., Garrett, K.L., Shen, W.Y., Constable, I.J., and Rakoczy, P.E. (2000). Overexpression of vascular endothelial growth factor (VEGF) in the retinal pigment epithelium leads to the development of choroidal neovascularization. Am J Pathol *157*, 135-144.
Stella, B., Arpicco, S., Peracchia, M.T., Desmaele, D., Hoebeke, J., Renoir, M., D'Angelo, J., Cattel, L., and Couvreur, P. (2000). Design of folic acid-conjugated nanoparticles for drug targeting. Journal of pharmaceutical sciences *89*, 1452-1464.
Sudimack, J., and Lee, R.J. (2000). Targeted drug delivery via the folate receptor. Advanced drug delivery reviews *41*, 147-162.
Sunness, J.S., Rubin, G.S., Applegate, C.A., Bressler, N.M., Marsh, M.J., Hawkins, B.S., and Haselwood, D. (1997). Visual function abnormalities and prognosis in eyes with age-related geographic atrophy of the macula and good visual acuity. Ophthalmology *104*, 1677-1691.
Tachibana, K., and Tachibana, S. (2001). The use of ultrasound for drug delivery. Echocardiography *18*, 323-328.
Tang, H., Mitragotri, S., Blankschtein, D., and Langer, R. (2001). Theoretical description of transdermal transport of hydrophilic permeants: application to low-frequency sonophoresis. Journal of pharmaceutical sciences *90*, 545-568.
Tewes, F., Munnier, E., Antoon, B., Ngaboni Okassa, L., Cohen-Jonathan, S., Marchais, H., Douziech-Eyrolles, L., Souce, M., Dubois, P., and Chourpa, I. (2007). Comparative study of doxorubicin-loaded poly(lactide-co-glycolide) nanoparticles prepared by single and double emulsion methods. Eur J Pharm Biopharm *66*, 488-492.
Thomas, O.E. (1989). Retina. In, S.J. Ryan, ed. (St. Louis, Mosby).
Thompson, J.T. (2006). Cataract formation and other complications of intravitreal triamcinolone for macular edema. American journal of ophthalmology *141*, 629-637.
Tolentino, F.I. (1974). The vitreous. Arch Ophthalmol *92*, 350-358.
Tortora, G.J., and Derrickson, B. (2009). Principles of anatomy and physiology, 12th edn (Hoboken John Wiley & Sons).
Treupel, L., Poupon, M.F., Couvreur, P., and Puisieux, F. (1991). [Vectorisation of doxorubicin in nanospheres and reversion of pleiotropic resistance of tumor cells]. C R Acad Sci III *313*, 171-174.
Trivedi, H., Todkar, H., Arbhave, V., and Bhatia, P. (2003). Ocular anaesthesia for cataract surgery. Lancet *3*, 1312, 1313, 1319.

Trotter, R.R. (1968). Cornea and sclera. Arch Ophthalmol *79*, 338-348.
Tsok, R.M., Gereliuk, I.P., Tsok, O.B., and Kaminskii Iu, M. (1990). [The effect of ultrasonic oscillations of different frequencies on radionuclide accumulation in the eye tissues]. Oftalmol Zh, 46-49.
Tunn, S., Pappert, G., Willnow, P., and Krieg, M. (1990). Multicentre evaluation of an enzyme-immunoassay for cortisol determination. Journal of clinical chemistry and clinical biochemistry *28*, 929-935.
van den Berg, A.A. (2004). An audit of peribulbar blockade using 15 mm, 25 mm and 37.5 mm needles, and sub-Tenon's injection. Anaesthesia *59*, 775-780.
Vandervoort, J., and Ludwig, A. (2002). Biocompatible stabilizers in the preparation of PLGA nanoparticles: a factorial design study. International journal of pharmaceutics *238*, 77-92.
Velez, G., and Whitcup, S.M. (1999). New developments in sustained release drug delivery for the treatment of intraocular disease. The British journal of ophthalmology *83*, 1225-1229.
Venkateswarlu, V., and Manjunath, K. (2004). Preparation, characterization and in vitro release kinetics of clozapine solid lipid nanoparticles. J Control Release *95*, 627-638.
Vinores, S.A. (1995). Assessment of blood-retinal barrier integrity. Histol Histopathol *10*, 141-154.
Virgili, G., and Bini, A. (2007). Laser photocoagulation for neovascular age-related macular degeneration. Cochrane Database Syst Rev, CD004763.
Wadhwa, S., Paliwal, R., Paliwal, S.R., and Vyas, S.P. (2009). Nanocarriers in ocular drug delivery: an update review. Curr Pharm Des *15*, 2724-2750.
Wang, P.C., Wester, B.A., Rajaraman, S., Paik, S.J., Kim, S.H., and Allen, M.G. (2009). Hollow polymer microneedle array fabricated by photolithography process combined with micromolding technique. Conf Proc IEEE Eng Med Biol Soc *1*, 7026-7029.
Watkins, R., Beigi, B., Yates, M., Chang, B., and Linardos, E. (2001). Intraocular pressure and pulsatile ocular blood flow after retrobulbar and peribulbar anaesthesia. The British journal of ophthalmology *85*, 796-798.
Watson, P.G., and Young, R.D. (2004). Scleral structure, organisation and disease. A review. Exp Eye Res *78*, 609-623.
Weijtens, O., Schoemaker, R.C., Lentjes, E.G., Romijn, F.P., Cohen, A.F., and van Meurs, J.C. (2000). Dexamethasone concentration in the subretinal fluid after a subconjunctival injection, a peribulbar injection, or an oral dose. Ophthalmology *107*, 1932-1938.
Weijtens, O., Schoemaker, R.C., Romijn, F.P., Cohen, A.F., Lentjes, E.G., and van Meurs, J.C. (2002). Intraocular penetration and systemic absorption after topical application of dexamethasone disodium phosphate. Ophthalmology *109*, 1887-1891.
Weitman, S.D., Lark, R.H., Coney, L.R., Fort, D.W., Frasca, V., Zurawski, V.R., Jr., and Kamen, B.A. (1992). Distribution of the folate receptor GP38 in normal and malignant cell lines and tissues. Cancer Res *52*, 3396-3401.
White, L. (1991). Chemotherapy in retinoblastoma: current status and future directions. Am J Pediatr Hematol Oncol *13*, 189-201.

Wickstrom, K. (2008). Acute bacterial conjunctivitis--benefits versus risks with antibiotic treatment. Acta Ophthalmol *86*, 2-4.
Williams, C.D., and Rizzolo, L.J. (1997). Remodeling of junctional complexes during the development of the outer blood-retinal barrier. Anat Rec *249*, 380-388.
Wimmer, N., Marano, R.J., Kearns, P.S., Rakoczy, E.P., and Toth, I. (2002). Syntheses of polycationic dendrimers on lipophilic peptide core for complexation and transport of oligonucleotides. Bioorg Med Chem Lett *12*, 2635-2637.
Wylie, J., Henderson, M., Doyle, M., and Hickey-Dwyer, M. (1994). Persistent binocular diplopia following cataract surgery: aetiology and management. Eye (London, England) *8 (Pt 5)*, 543-546.
Yang, S.J., Lin, F.H., Tsai, K.C., Wei, M.F., Tsai, H.M., Wong, J.M., and Shieh, M.J. Folic acid-conjugated chitosan nanoparticles enhanced protoporphyrin IX accumulation in colorectal cancer cells. Bioconjugate chemistry *21*, 679-689.
Yeung, C.K., Chan, K.P., Chan, C.K., Pang, C.P., and Lam, D.S. (2004). Cytotoxicity of triamcinolone on cultured human retinal pigment epithelial cells: comparison with dexamethasone and hydrocortisone. Japanese journal of ophthalmology *48*, 236-242.
Yoo, H.S., and Park, T.G. (2001). Biodegradable polymeric micelles composed of doxorubicin conjugated PLGA-PEG block copolymer. J Control Release *70*, 63-70.
Yoo, H.S., and Park, T.G. (2004). Folate receptor targeted biodegradable polymeric doxorubicin micelles. J Control Release *96*, 273-283.
Zderic, V., Clark, J.I., and Vaezy, S. (2004). Drug delivery into the eye with the use of ultrasound. J Ultrasound Med *23*, 1349-1359.
Zeng, S., Hu, C., Wei, H., Lu, Y., Zhang, Y., Yang, J., Yun, G., Zou, W., and Song, B. (1993). Intravitreal pharmacokinetics of liposome-encapsulated amikacin in a rabbit model. Ophthalmology *100*, 1640-1644.
Zhang, L., Li, Y., Zhang, C., Wang, Y., and Song, C. (2009). Pharmacokinetics and tolerance study of intravitreal injection of dexamethasone-loaded nanoparticles in rabbits. Int J Nanomedicine *4*, 175-183.
Zhao, H., and Yung, L.Y. (2008). Selectivity of folate conjugated polymer micelles against different tumor cells. International journal of pharmaceutics *349*, 256-268.
Zhao, X., Li, H., and Lee, R.J. (2008). Targeted drug delivery via folate receptors. Expert opinion on drug delivery *5*, 309-319.
Zignani, M., Einmahl, S., Baeyens, V., Varesio, E., Veuthey, J.L., Anderson, J., Heller, J., Tabatabay, C., and Gurny, R. (2000). A poly(ortho ester) designed for combined ocular delivery of dexamethasone sodium phosphate and 5-fluorouracil: subconjunctival tolerance and in vitro release. Eur J Pharm Biopharm *50*, 251-255.

VITA

Sai Hanuman Sagar Boddu was born on June 5th 1981, in Machilipatnam, Andhra Pradesh, India. He completed his secondary education from Sainik School Korukonda, located at Vijayanagaram District, Andhra Pradesh, India. He later obtained his Bachelor of Pharmacy degree from Bapatla College of Pharmacy, Bapatla, which is affiliated to Jawaharlal Nehru Technological Institute, in July 2003. He secured 97.04 percentile in GATE-2003, All India Rank-191. On the basis of merit he got admission into N.D.M.V. P Samaj's College of Pharmacy, in 2003 (August) and obtained a Master's degree in Pharmaceutics, in July 2005.

Boddu joined University of Missouri-Kansas City, Department of Pharmaceutical Sciences in August 2006 in pursuit of a doctorate degree. He has been awarded Chancellor's Doctoral Fellowship award for academic excellence during 2008-10.

Mr. Boddu is a member of American Association of Pharmaceutical Scientists (AAPS) and Association of Research in Vision and Ophthalmology (ARVO). He has authored/co-authored 10 peer reviewed research and review articles in reputed international journals.